Doctoral Dissertation

博士論文

Concrete Models and Phenomenologies of Composite Asymmetric Dark Matter

（複合的非対称暗黒物質の具体的模型とその現象論）

A Dissertation Submitted for the Degree of Doctor of Philosophy

December 2021

令和３年１２月博士（理学）申請

Department of Physics, Graduate School of Science,

The University of Tokyo

東京大学大学院理学系研究科

物理学専攻

Shin Kobayashi

小林　伸

Abstract

Asymmetric dark matter (ADM) is a framework relating the observed baryon asymmetry of the Universe to the dark matter number density by generating an asymmetry component in DM via baryogenesis. Thus ADM naturally explains the coincidence of the baryon and DM density for DM with an $\mathcal{O}(1)\,\mathrm{GeV}$ mass and a large annihilation cross section.

In order to construct the ADM model with mass in the GeV range and with a large annihilation cross section, a composite particle in a new strong dynamics is a possible and simple candidate for two reasons. First, the strong dynamics naturally explains the ADM mass in the GeV range. Second, its large annihilation cross section due to the strong dynamics leaves the asymmetric component to be dominant over the symmetric component. In such composite ADM scenarios, the dark sector, which contains the DM, has a relatively large number of particles emerging from the confinement of the strong dynamics. The large degrees of freedom in the dark sector results in the overclosure of the Universe or contradicts the observations of the cosmic microwave background (CMB) and the successful Big-Bang Nucleosynthesis. Thus, in order to construct a cosmologically safe composite ADM model, we need a portal to transfer the excessive energy in the dark sector to the Standard Model (SM) sector.

In this thesis, we consider composite ADM models with a dark photon portal, which has a sub-GeV mass and kinetic mixing with the SM photon. We investigate the viable parameter space of the dark photon in detail, considering the constraints from the CMB observation of the effective number of neutrinos and direct detection experiments. We also discuss the testability of the model in indirect detection experiments. Finally, we construct a chiral composite ADM model which dynamically generates $\mathcal{O}(100)\,\mathrm{MeV}$ mass of the dark photon. The contents of this thesis is based on Refs. [1, 2, 3].

Contents

Chapter 1

Introduction

1.1 Overview

The Standard Model (SM) of particle physics has achieved a great success in describing the interacting nature of the visible particle contents of the Universe. Despite this successful construction of the SM, there remain unsolved problems such as the nature of the dark matter (DM), the origin of the tiny neutrino mass, the strong CP problem, etc. Among these physics beyond the SM, DM is one of the most attractive subjects of cosmology, astrophysics, and particle physics. Since the discovery by Zwicky [4], there have been many observations that support the existence of DM (see [5, 6] for reviews). Although a vast amount of theoretical and experimental researches has been carried out to unveil the detail of the DM, its nature remains elusive apart from several properties: its electromagnetic interaction is feeble; it is cold enough to cluster along with the primordial gravitational potential; it is stable at least over the age of the Universe.

One of the theoretical goals is to reveal the DM production mechanism. A simple and realistic candidate is the thermal freeze-out mechanism [7]: Starting from an equilibrium state with a hot and dense SM plasma, the DM particle gradually decreases its interaction rate with SM particles as the Universe expands and cools down, and eventually decouples from the thermal bath with its abundance fixed near the decoupling temperature. The most prominent feature of this mechanism is a so-called "WIMP miracle". Because the abundance of a thermally produced massive particle is determined only by its interacting cross section with the Standard Model (SM) particles, but not depending on its mass, we can reproduce the observed abundance of the DM by setting its annihilation cross section as $\langle \sigma v \rangle \sim 10^{-26}\,\mathrm{cm^3/s}$, which is comparable to the weak interaction cross section. Due to this simple and miraculous feature, the weakly interacting massive particle (WIMP) has been one of the most promising candidates for DM [8, 9].

However, there are known problems that are difficult to solve within the WIMP paradigm, which motivate to construct other DM scenario than WIMP. One of such problems is the so-called "coincidence problem of the Universe", which means the close matching between the abundances of baryons and of DM; $\Omega_{\mathrm{DM}}/\Omega_b \sim 5$ [10]. Because there is a 10-orders-of-magnitude discrepancy between the observed baryon number density and theoretically predicted value of thermally produced baryon abundance without asymmetry, we need baryon asymmetry generation mechanism, *baryogenesis*, to compensate for this discrepancy. Thus, after the recovery of the $\mathcal{O}(10^{-10})$ discrepancy in the baryon sector, the coincidence of baryon and DM abundance seems unnatural. Within the WIMP paradigm, because of the difference in the production mechanism between baryons and DM, it is difficult to solve this coincidence problem. Although the coincidence problem is often overlooked, it can lead to a breakthrough to identify the origin of the DM. Therefore, it is worth considering concrete models which can solve this problem and their phenomenologies.

To solve this problem, a paradigm called asymmetric DM (ADM) is suggested [11]. The ADM is based on the simple idea that the abundance of the DM and baryons have the same origin, i.e., the baryogenesis. With this scenario, the asymmetries in SM and dark sector are related to each other, thus for the DM with $\mathcal{O}(1)\,\mathrm{GeV}$ mass, the coincidences of the baryon and DM are naturally related.

When building models within the ADM scenario, there are some requirements. The first is that the DM has a mass of $\mathcal{O}(1)\,\mathrm{GeV}$. The second is that the DM annihilation cross section is large enough to eliminate the symmetric component in DM. The third is that we need a portal operator which relates the asymmetries in SM and dark sectors. Among ADM models, a composite ADM can dynamically realize the first two requirements [12, 13]. The DM mass in the GeV range naturally arises from the strong dynamics. A large annihilation cross section of composite DM into lighter degrees of freedom (e.g., dark meson) makes the symmetric component of the relic DM density negligible.

By construction, however, the effective number of massless degrees of freedom in the composite dark sector is sizable in the early Universe. If those particles are also stable, their energy density overcloses the Universe, or contributes to the effective number of neutrino degrees of freedom, N_{eff}, too much, depending on their masses [14]. Thus, some light portal particle is needed to transfer the excessive entropy of the dark sector into the SM sector.

A simple possibility for such a portal is a light dark photon. It has a mass in the sub-GeV range and decays into the SM particles (mainly into the leptons) through kinetic mixing with the SM photon. In this thesis, we construct minimal ADM models with a QCD-like SU(3) strong interaction, a QED-like U(1) gauge interaction, and global $B - L$ symmetry.

We also adopt thermal leptogenesis [15] for $B - L$ asymmetry generation mechanism. Added with massive right-handed neutrinos, this model also naturally explains the observed tiny neutrino masses via the seesaw mechanism [16, 17, 18, 19, 20]. With this model, we investigate the impact of decaying dark photon on N_{eff} and identify the viable parameter space.

Based on the model above, we also consider the impact of a Majorana mass in DM. The Majorana mass violates $B - L$ symmetry, thus can lead to late time oscillation of the DM. By taking into account the derived constraints, we show that such a model can be tested by direct detection experiments of DM through the coupling to the dark photon.

In the ADM model above, the dark photon plays an important role to transfer the excessive energy of the dark sector into the SM. However, for this scenario to be successful, the dark photon should be lighter than DM. This requirement invokes another coincidence problem.

A natural solution for the mass coincidence of DM and the dark photon is to generate the dark photon mass in the same dynamics which produces dark baryons. Therefore, we construct a chiral ADM model with a similar charge assignment as in Refs. [21, 22], in which the dark photon mass is dynamically produced.

1.2   Outline of this thesis

The construction of this thesis is as follows.

Cahpters 2 and 3 are devoted to review of DM theory and experimental bounds on DM. In chapter 2, we review the thermal production mechanism of the DM and baryogenesis. After that, we review the motivation of ADM and key ingredients in constructing ADM models. In chapter 3, we review the experimental constraints on general DM such as direct detection and indirect detection experiments.

From chapter 4 to chapter 6, we investigate concrete models of composite ADM and estimate experimental constraints on the models. The contents of these chapters are based on Refs. [1, 2, 3] respectively. In chapter 4, we construct a composite ADM model with a dark photon portal based on $\text{SU}(3)_D \times \text{U}(1)_D$ gauge group. We also investigate the cosmological and direct detection constraints on this model. In chapter 5, we discuss the impact of a Majorana mass term on the ADM model and testability in the indirect detection experiments. In chapter 6, we construct a chiral composite ADM model which dynamically induces $\mathcal{O}(100)\,\text{MeV}$ dark photon mass.

We devote the final chapter of discussions and conclusions.

1.3   Notations

We adapt the natural unit $\hbar = \mathrm{c} = \mathrm{k_B} = 1$ unless otherwise noted. We take the convention for the metric signature as $\eta_{\mu\nu} = (+, -, -, -)$, where $\eta_{\mu\nu}$ is the Minkowski metric. For the flat and expanding Universe, we work in the Friedmann-Lemaitre-Robertson-Walker metric

$$ds^2 \equiv g_{\mu\nu}dx^\mu dx^\nu = dt^2 - a(t)^2[dx^2 + dy^2 + dz^2]\,,$$

where $a(t)$ is the scale factor of the Universe. The reduced Planck mass is

$$M_{\mathrm{Pl}} \equiv \frac{1}{\sqrt{8\pi G}} = 2.435 \times 10^{18}\,\mathrm{GeV}\,,$$

where G is the gravitational constant, $G = 6.674^{-11}\,\mathrm{m^3 kg^{-1} s^{-2}}$.

Chapter 2

Review of Asymmetric Dark Matter

There has been a wide variety of DM models proposed. Among them, the WIMP scenario has long been considered as the most promising candidate for the DM motivated by the so-called "WIMP miracle", which means that thermally produced DM abundance is determined only by the weak scale annihilation cross section. However, within the WIMP paradigm, it is obviously difficult to solve the "coincidence problem", which mentions that there is a miraculous match between the DM and the baryon abundances. This is because the DM abundance and the baryon abundance are produced from different mechanisms from each other. This deficit of the ability to explain the coincidence problem leads to the asymmetric dark matter (ADM) scenario.

In this chapter, we first review the thermal production mechanism of DM and baryon asymmetry generation called baryogenesis. Next, we review the motivation of the ADM scenario and finally review the key ingredients required to construct a concrete model for this paradigm.

2.1   Thermal DM Production

In the early stage of the evolution process, the Universe was a hot and dense plasma consisting of the SM particles and the DM. At first, in this plasma, particles scatter each other frequently enough that they are in thermal equilibrium. However, as the Universe expands, the plasma temperature and the interaction rates decrease and some particles decouple from the thermal bath, eventually. The DM, which is a stable particle, reaches a constant number density after decoupling from the SM thermal bath. In this section, we see how the relic abundances of particles are determined by thermal freeze-out [23, 24].

Generally, a particle obeying a momentum distribution, $f(\mathbf{p})$, has a num-

ber density

$$n = \int \frac{g\,\mathrm{d}^3 p}{(2\pi)^3} f(\mathbf{p}), \qquad (2.1.1)$$

where g represents spin degrees of freedom of the particle. Especially, a particle in thermal equilibrium with a thermal bath has a distribution

$$f_{\text{eq}}(\mathbf{p}) = \frac{1}{e^{E_\mathbf{p}/T} \mp 1}, \quad E_\mathbf{p} = \sqrt{|\mathbf{p}|^2 + m^2} \qquad (2.1.2)$$

where T is the temperature of the thermal bath, m is the mass of the particle, and the minus (plus) sign in the denominator corresponds to a bosonic (fermionic) statistics.

To describe a departure from the thermal equilibrium, the Boltzmann equation with collision terms is frequently used. The distribution function of the i-th particle obeys the equation

$$\frac{\partial}{\partial t} f_\psi(t, \boldsymbol{x}, \boldsymbol{p}) + \frac{\mathrm{d}\boldsymbol{x}}{\mathrm{d}t} \cdot \frac{\partial}{\partial \boldsymbol{x}} f_\psi(t, \boldsymbol{x}, \boldsymbol{p}) + \frac{\mathrm{d}\boldsymbol{p}}{\mathrm{d}t} \cdot \frac{\partial}{\partial \boldsymbol{p}} f_\psi(t, \boldsymbol{x}, \boldsymbol{p}) = \mathcal{C}[f_\psi], \quad (2.1.3)$$

where $f_\psi(t, \boldsymbol{x}, \boldsymbol{p})$ is the distribution function of the particle and ψ and $\mathcal{C}[f_\psi]$ stands for the collision terms of ψ. More specifically, for the process $\psi + X \leftrightarrow Y$ the collision term is given by

$$\mathcal{C}_{\psi+X\leftrightarrow Y}[f_\psi] = -\frac{1}{2E_\psi} \int d\Pi_X d\Pi_Y (2\pi)^4 \delta\left(p_\psi + \sum_i p_{X_i} - \sum_j p_{Y_j}\right) S |\bar{\mathcal{M}}_{\psi+X\to Y}|^2$$

$$\times \left[f_\psi \prod_i f_{X_i} \prod_j (1 \pm f_{Y_j}) - (1 \pm f_\psi) \prod_i (1 \pm f_{X_i}) \prod_j f_{Y_j} \right].$$

$$(2.1.4)$$

$$d\Pi_i d\Pi_f = \prod_i \frac{g_{X_i} d^3 p_{X_i}}{(2\pi)^3 2E_{X_i}} \prod_j \frac{g_{Y_j} d^3 p_{Y_j}}{(2\pi)^3 2E_{Y_j}}, \qquad (2.1.5)$$

where X and Y can be multi-particle states, g's are spin degrees of freedom of particles, $\bar{\mathcal{M}}_{\psi+X\to Y}$ is a spin-averaged amplitude for the process and S counts the symmetry factor. The factor $1 \pm f$ indicates the Bose enhancement for the plus sign and the Pauli blocking for the minus sign. $E_\psi = \sqrt{p_\psi^2 + m^2}$ is the energy of the particle ψ with mass m. Since the Universe is homogeneous and isotropic[1], we ignore the position and angular dependence of the distribution function. Because of the expanding Universe,

---

[1]This assumption is valid since the observed density fluctuations and anisotropies are small enough [25, 26].

momenta of the particle redshift as the inverse of the scale factor, $\boldsymbol{p} \propto 1/a(t)$, thus Eq.(2.1.3) is rewritten as

$$\frac{\partial}{\partial t} f_\psi(t, p) - H \frac{\partial}{\partial p} f_\psi(t, p) = \mathcal{C}[f_\psi], \qquad (2.1.6)$$

where H is the Hubble parameter. By integrating over the momentum space, we can rewrite the Boltzmann equation of two-body scattering, $\psi + \psi \leftrightarrow$ (any final state), in terms of number density,

$$\dot{n}_\psi + 3H n_\psi = -\langle \sigma v \rangle (n_\psi^2 - n_{\psi,\mathrm{eq}}^2), \qquad (2.1.7)$$

where $n_{\psi,\mathrm{eq}}$ denotes the equilibrium density of the particle and $\langle \sigma v \rangle$ is a thermally averaged cross section of the annihilation process. Here we assume that the distribution of ψ is proportional to the equilibrium distribution function, $f_\psi \propto f_{\psi,\mathrm{eq}}$. Let us define a yield as $Y = n_\psi/T^3$ and introduce a dimensionless variable $x = m/T$. Then the equation above is rewritten as

$$\frac{\mathrm{d}Y}{\mathrm{d}x} = -\frac{m^3 \langle \sigma v \rangle}{x^2 H(m)} (Y^2 - Y_{\mathrm{EQ}}^2). \qquad (2.1.8)$$

To get more intuition, we deform this equation as

$$\frac{x}{Y_{\mathrm{EQ}}} \frac{\mathrm{d}Y}{\mathrm{d}x} = -\frac{\Gamma}{H(m)} \left[\left(\frac{Y}{Y_{\mathrm{EQ}}} \right)^2 - 1 \right], \qquad (2.1.9)$$

where $\Gamma = \langle \sigma v \rangle n_{\mathrm{EQ}}$ is the interaction rate and we use the x dependence of the Hubble parameter, $H \propto x^{-2}$ [2]. We see that the Boltzmann equation describes the feature of thermal equilibrium and decoupling; if the interaction is strong enough ($\Gamma \gg H$) particle ψ is in thermal equilibrium with SM particles ($Y \simeq Y_{\mathrm{EQ}}$), and if the interaction becomes inefficient ($\Gamma \ll H$) the particle ψ decouples from SM thermal bath.

When we think about the relic density of DM, we mostly care about freeze-out temperature, x_f, and relic yield, Y_∞. To estimate these quantities, we consider the evolution of the departure from the equilibrium density, $\Delta = Y - Y_{\mathrm{EQ}}$ by solving the equation,

$$\frac{\mathrm{d}}{\mathrm{d}x} \Delta = -\frac{\mathrm{d}}{\mathrm{d}x} Y_{\mathrm{EQ}} - \frac{m^3 \sigma_0}{x^2 H(m)} \Delta (2 Y_{\mathrm{EQ}} + \Delta). \qquad (2.1.10)$$

Here we assume that the annihilation process is s-wave, thus the thermal average of the cross section is independent of the temperature, and we parameterize it as $\langle \sigma v \rangle = \sigma_0$. For early times, Y is close to its equilibrium value, therefore we can approximate $\Delta \simeq 0$ and $d\Delta/dx \simeq 0$. This yields,

$$\Delta \simeq -\frac{x^2}{2\lambda} \frac{\mathrm{d} \ln Y_{\mathrm{EQ}}}{\mathrm{d}x} \sim \frac{x^2}{2\lambda}, \qquad (2.1.11)$$

---

[2] We neglected the temperature dependence of the degrees of freedom, g_* for simplicity. However, this does not change the discussion significantly.

where $\lambda = m^3 \sigma_0 / H(m)$. At the freeze-out temperature, x_f, the difference from the equilibrium value is not negligible. Thus, we define x_f as $\Delta(x_f) = c Y_{\rm EQ}(x_f)$, where $c = \mathcal{O}(1)$. Even at the temperature around freeze-out, Δ varies slowly, therefore the approximation $d\Delta/dx \simeq 0$ is valid. Then, near the freeze-out, Δ behaves as

$$\Delta \simeq -\frac{x^2}{\lambda(2Y_{\rm EQ}+\Delta)}\frac{\mathrm{d}}{\mathrm{d}x}Y_{\rm EQ} \simeq -\frac{x^2}{\lambda(c+2)}\frac{\mathrm{d}\ln Y_{\rm EQ}}{\mathrm{d}x} \sim \frac{x^2}{\lambda(c+2)}\,, \quad (2.1.12)$$

thus $\Delta(x_f) \simeq x_f^2/(\lambda(2+c))$. Combining with $Y_{\rm EQ} \sim x^{3/2}\exp(-x)$ we see that x_f depends only on $\ln\lambda$ and is almost independent of the mass of DM.

After freeze-out, $Y_{\rm EQ}$ is much smaller than Y, thus Y obeys

$$\frac{\mathrm{d}}{\mathrm{d}x}\Delta = -\lambda x^{-2} Y^2 \qquad (2.1.13)$$

Integrating this equation from $x = x_f$ to $x = \infty$, we obtain

$$\frac{1}{Y_\infty} - \frac{1}{Y_f} \simeq \frac{1}{Y_\infty} = \frac{\lambda}{x_f}, \qquad (2.1.14)$$

where Y_f is the yield at the freeze-out and we ignore $1/Y_f$ since Y_f is larger than Y_∞.

Finally, we can estimate the DM mass dependence of the energy density of the DM at today's Universe, $\rho_{\rm DM,0}$. It can be written in terms of m, Y_∞,

$$\rho_{\rm DM,0} \propto m Y_\infty = \frac{H(m)x_f}{m^2\sigma_0}. \qquad (2.1.15)$$

In the radiation-dominated era, $H(m) \propto m^2$, thus $\rho_{\rm DM,0}$ is determined only by the annihilation cross section. More specifically, we write the cosmological parameter of the matter content,

$$\begin{aligned}
\Omega_{\rm DM} &\simeq \frac{H(m)x_f T_{\gamma,0}^3}{30 m^2 \langle\sigma\rangle \rho_{\rm cr}} \\
&\sim 0.1 h^{-2} \left(\frac{x_f}{10}\right)\left(\frac{g_*(m)}{100}\right)^{1/2}\left(\frac{10^{-26}\,{\rm cm^3/s}}{\langle\sigma v\rangle}\right)
\end{aligned} \qquad (2.1.16)$$

where the factor $1/30$ accounts for the change of degrees of freedom in SM thermal bath [27]. h is a dimensionless parameter defined by $H_0 = 100h\,{\rm km\,s^{-1}Mpc^{-1}}$, where H_0 is the Hubble constant of the present Universe. If we consider the weak interaction, $\Omega_{\rm DM}h^2 \simeq 0.3$ is miraculously explained. Thus, this coincidence is called "the WIMP miracle".

2.2 Baryogenesis

In the last section, we see that the DM density is explained by the weak scale annihilation cross section. This thermal freeze-out mechanism seems to be able to explain any other particle abundances. However, the freeze-out scenario lacks the ability to explain the SM baryons relic abundance. If we naively apply the freeze-out relic abundance formula Eq.(2.1.14), we obtain $Y_b \sim 10^{-20}$, where Y_b is the yield of baryons [24]. On the other hand, from observations, we know that today's universe has the baryon number as

$$\eta_B = \frac{n_b - n_{\bar{b}}}{s} \sim 10^{-10}, \tag{2.2.1}$$

where s represents the entropy density of the Universe. Thus, to compensate for this difference, we need the baryon asymmetry generation mechanism called *baryogenesis*. In this section, we first briefly review the overview of baryogenesis and next review the dynamics of leptogenesis.

2.2.1 Sakharov's conditions and baryogenesis

The baryogenesis, literally, generates a baryon asymmetry dynamically even if the Universe starts from a baryon symmetric state. For the general charge asymmetry generating mechanism to work, we need three basic conditions.

(i) *Charge number violation*
   If all processes do not violate the charge, the resultant products are also charge symmetric. In the case of baryogenesis, we consider baryon number violating processes.

(ii) *C and CP violation*
   Even under the existence of a charge violating process, if either C/CP is conserved, we find that the C/CP conjugated process cancels the charge number produced from the original process.

(iii) *Out of Equilibrium*
   If the process takes place in equilibrium the chemical potentials of baryons and anti-baryons are equal to zero, $\mu_b = \mu_{\bar{b}} = 0$. Together with $m_b = m_{\bar{b}}$, it means that the net produced baryon number density is equal to that of anti-baryons, $n_b = n_{\bar{b}}$.

These conditions are called Sakharov's conditions [28]. Thus, for successful baryogenesis, we must have a process that violates baryon number conservation.

   Even within the SM, the baryon number and the lepton number are not conserved independently at the quantum level, and the strictly conserved

charge is $B - L$ number. For classical theory, the baryon current and the lepton current are conserved;

$$\partial_\mu j_B^\mu = \partial_\mu j_L^\mu = 0. \tag{2.2.2}$$

However, in quantum field theory, these conservation laws are violated because of the $U(1)_{B/L}$ -$SU(2)_L$ -$SU(2)_L$ anomaly;

$$\partial_\mu j_B^\mu = \partial_\mu j_L^\mu = \frac{N_f}{16\pi^2} \frac{1}{2} g_2^2 F_{\mu\nu}^a \tilde{F}^{a\mu\nu}, \tag{2.2.3}$$

where N_f is the flavor, g_2 is the gauge coupling of weak interaction and $F_{\mu\nu}^a$, $\tilde{F}_{\mu\nu}^a$ are gauge field strength and the dual one. The factor $1/2$ accounts for that only left-handed fermions are charged under weak interaction. Thus, we see that only $B - L$ charge is conserved but $B + L$ is not;

$$\partial_\mu j_{B-L}^\mu = 0, \quad \partial_\mu j_{B+L}^\mu = \frac{N_f}{16\pi^2} g_2^2 F_{\mu\nu}^a \tilde{F}^{a\mu\nu}. \tag{2.2.4}$$

The integration over spacetime of the right-hand side of the second equation is characterized by an integer called instanton number depending on the configuration of the gauge field. This suggests that the electroweak (EW) theory has distinct vacua labeled by $B + L$ charge, of which displacement is integers. At zero temperature an instanton, a classical configuration connecting the distinct EW vacua, causes a $B + L$ changing process. The probability of this process is highly suppressed by a factor

$$e^{-S_{\text{instanton}}} \sim e^{-\frac{16\pi^2}{g_2^2}} \sim e^{-170} \tag{2.2.5}$$

The very small exponential suppression represents that this process arises from the quantum tunneling effect. However, by considering the finite temperature effect, the transition rate becomes a different form due to the classical configuration which connects adjacent vacua. This configuration is called the sphaleron [29, 30]. In this case, the transition is caused by the thermal excitation process, thus the suppression comes from the Boltzmann factor,

$$\exp\left(-\frac{E_{\text{sph}}}{T}\right), \tag{2.2.6}$$

where E_{sph} represents the height of the potential barrier between adjacent vacua. As we can see, for high temperatures the sphaleron process is not suppressed and is expected to frequently occur. The baryogenesis mechanism called EW baryogenesis utilizes the sphaleron process to invoke the baryon asymmetry within the realm of the SM. For the EW baryogenesis to occur in a non-equilibrium way, the EW phase transition must be first order, which requires the Higgs mass is $m_H \lesssim 80\,\text{GeV}$ [31, 32] and contradicts with the observation.

A simple realization of baryogenesis is to utilize an out-of-equilibrium decay of a heavy particle which violates $B - L$, C, and CP conservation. This satisfies the Sakharov's conditions. With the out-of-equilibrium decay, we can realize the baryogenesis from the decay of a heavy Majorana neutrino. The massive Majorana mass of the right-handed neutrino is motivated from the aspect of the seesaw mechanism [16, 17, 18, 19, 20], which explains the tiny mass of the left-handed neutrinos. The Yukawa coupling terms with right-handed neutrinos can be written as

$$\mathcal{L}_{N_R \, \text{Yukawa}} = \tilde{y}_{ij} H L^i \bar{N}_R^j + \frac{1}{2} M_{R,ij} \bar{N}_R^i \bar{N}_R^j + \text{h.c.} \,, \qquad (2.2.7)$$

where i, j is the flavor indices, H denotes the EW Higgs doublet. We use H for both Hubble expansion rate and the electroweak Higgs boson, but we can easily distinguish one from the other from the context. $\tilde{y}_{ij}$ is the Yukawa coupling and $M_{R,ij}$ is the right-handed Majorana mass that realizes the seesaw mechanism. The Majorana mass explicitly violates the lepton number, thus the heavy neutrino, N_R, has a lepton number violating processes, $N_R \to L + H$ and $N_R \to \bar{L} + H^\dagger$. Therefore, if the Yukawa coupling, $\tilde{y}_{ij}$, has a complex phase, it violates C and CP. Thus, we again realize the Sakharov's conditions. A lepton asymmetry generated via right-handed neutrino decay is converted into baryon asymmetry through the sphaleron process described above [15] (see also Refs. [33, 34, 35] for reviews).

Though we do not review in detail, it is worth noting that there are other types of baryogenesis such as the spontaneous baryogenesis [36] and Affleck–Dine mechanism [37], which utilize a circular motion of a scalar field charged under $B - L$ symmetry to invoke a $B - L$ breaking process.

2.2.2 Dynamics of leptogenesis

We have seen the necessary condition for asymmetry generation and several types of baryogenesis. Next, we see how the dynamics of leptogenesis generate the asymmetry [38, 39, 40]. Hereafter, we assume that the first generation is the lightest among right-handed neutrinos; $M_{R,1} \ll M_{R,2}, M_{R,3}$. We also suppress the flavor indices for simplicity.

To describe the out-of-equilibrium processes, the Boltzmann equation is used again. We must pay attention to that the amplitudes for the decay and the inverse decay are not equal to each other because of the CP-violation in neutrino Yukawa couplings. Thus, we parameterize the CP-violation effect as

$$\left| \mathcal{M}_{N_R \to L + H} \right|^2 = \left| \mathcal{M}_{\bar{L} + H^\dagger \to N_R} \right|^2 = \frac{1}{2}(1 + \varepsilon) |\mathcal{M}_D|^2 \qquad (2.2.8)$$

$$\left| \mathcal{M}_{N_R \to \bar{L} + H^\dagger} \right|^2 = \left| \mathcal{M}_{L + H \to N_R} \right|^2 = \frac{1}{2}(1 - \varepsilon) |\mathcal{M}_D|^2 \,. \qquad (2.2.9)$$

11

In the collision term of N_R decay and inverse decay, we find that the effect of CP-violation cancels between $N_R \rightarrow L + H$ and $N_R \rightarrow \bar{L} + H^\dagger$, thus the collision term is written as

$$\int \mathrm{d}^3 p_{N_R} \, \mathcal{C}_{N_R \, \mathrm{decay}}[f_{N_R}] = \int d\Pi_{N_R} d\Pi_L d\Pi_H (2\pi)^4 \delta(p_{N_R} - p_L - p_H)$$
$$\times \, (-f_{N_R}(p_{N_R}) + f_{N_R}^{\mathrm{eq}}(p_{N_R})) \big| \bar{\mathcal{M}}_D \big|^2$$
$$= -\langle \Gamma_D \rangle (n_{N_R} - n_{N_R}^{\mathrm{eq}}). \tag{2.2.10}$$

In the same way, scattering processes, $N_R + L(\bar{L}) \leftrightarrow \bar{t} + Q(t + \bar{Q})$ and $N_R + t(\bar{t}) \leftrightarrow \bar{L} + Q(L + Q)$, produce and reduce the number of N_R. Thus, the Boltzmann equation for N_R is

$$\frac{\mathrm{d}n_{N_R}}{\mathrm{d}t} + 3H n_{N_R} = -(\langle \Gamma_D \rangle + \langle \Gamma_S \rangle)(n_{N_R} - n_{N_R}^{\mathrm{eq}}), \tag{2.2.11}$$

where $n_{N_R}^{(\mathrm{eq})}$ is the (equilibrium) number density of N_R, $\langle \Gamma_{D(S)} \rangle$ is a thermally averaged interaction rate for decay (scattering) process. By taking the time variable as $z = M_R/T$ and rewriting the Boltzmann equation with comoving number of right-handed neutrino, $N_{N_R} = n_{N_R} a^3$, we obtain

$$\frac{\mathrm{d}N_{N_R}}{\mathrm{d}z} = -(D + S)(N_{N_R} - N_{N_R}^{\mathrm{eq}}), \tag{2.2.12}$$

where $D = \langle \Gamma_D \rangle / (Hz)$ and $S = \langle \Gamma_S \rangle / (Hz)$.

For the lepton number, in addition to the decay of N_R, 2→2 scattering processes, $L + H \leftrightarrow \bar{L} + H^\dagger$ and $L + L \leftrightarrow H^\dagger + H^\dagger$, also violate the lepton number. When considering the collision term, we have to notice that the collision term of $L + H \leftrightarrow \bar{L} + H^\dagger$ includes an on-shell contribution of the right-handed neutrino propagating in the s-channel. This on-shell contribution is already taken into account in the collision term for N_R decay, thus we must subtract the on-shell N_R contribution from the amplitude of $L + H \leftrightarrow \bar{L} + H^\dagger$. After subtracting this contribution, the Boltzmann equation for the lepton number density becomes [33]

$$\frac{\mathrm{d}n_{B-L}}{\mathrm{d}t} + 3H n_{B-L} = -\varepsilon \langle \Gamma_D \rangle (n_{N_R} - n_{N_R}^{\mathrm{eq}}) - \frac{n_{B-L}}{n_l^{\mathrm{eq}}} \left(\frac{1}{2} \langle \Gamma_D \rangle n_{N_R}^{\mathrm{eq}} + \gamma_{\Delta L = 2} \right), \tag{2.2.13}$$

where n_l^{eq} represents the equilibrium density of the light neutrino and $\gamma_{\Delta L = 2}$ represents the collision term from $L + L \leftrightarrow H^\dagger + H^\dagger$ plus $L + H \leftrightarrow \bar{L} + H^\dagger$ without on-shell N_R exchange contribution. Same as before, by changing the variables, we obtain the equation for $B - L$ charge as

$$\frac{\mathrm{d}N_{B-L}}{\mathrm{d}z} = -\varepsilon D (N_{N_R} - N_{N_R}^{\mathrm{eq}}) - W N_{B-L}, \tag{2.2.14}$$

12

where W represents the washout effect induced by the scattering processes. Formally integrating the above equation, the $B - L$ charge is

$$N_{B-L}(z) = N_{B-L}^{\text{init}} \exp\left(- \int_{z_i}^{z} dz'\, W(z')\right) - \frac{3}{4} \varepsilon \kappa(z) \tag{2.2.15}$$

$$\kappa(z) = \frac{4}{3} \int_{z_i}^{z} dz'\, D(N_{N_R} - N_{N_R}^{\text{eq}}) \exp\left(- \int_{z'}^{z} dz''\, W(z'')\right). \tag{2.2.16}$$

The first term represents the washout of the initial asymmetry in $B - L$ by scattering processes and the second term represents the $B - L$ asymmetry created via right-handed neutrino decay. Notice that there is also a washout factor in the second term. We call κ as the efficiency factor and define $\kappa_f = \kappa(z \to \infty)$. To relate the predicted value from the leptogenesis with the observed baryon asymmetry, $\eta_B^{\text{obs}} \equiv n_B/n_\gamma = 2.73 \times 10^{-8} \Omega_B h^2 \sim 6 \times 10^{-10}$, we need the fraction of $B - L$ charge converted into the baryon asymmetry, $f_{\text{sph}} = 28/79$ [41, 42], and the dilution factor induced by the entropy production in the SM sector, $f_{\text{dilute}} = 2387/86$ [40]. Together with these factors, the predicted value is

$$\eta_B^{\text{pre}} = \frac{f_{\text{sph}}}{f_{\text{dilute}}} N_{B-L}^{\text{fin}} = \frac{3}{4} \frac{f_{\text{sph}}}{f_{\text{dilute}}} \varepsilon \kappa_f \simeq 0.96 \times 10^{-2} \varepsilon \kappa_f. \tag{2.2.17}$$

This value should be larger than observed asymmetry, thus the condition,

$$\varepsilon > 6 \times 10^{-8} \kappa_f^{-1} \tag{2.2.18}$$

should be satisfied. The maximum value of the CP asymmetry, ε, can be written as

$$\varepsilon \lesssim \frac{3}{16\pi} \frac{M_{R,1} m_3}{v_{\text{EW}}^2}, \tag{2.2.19}$$

where m_3 is the heaviest left-handed neutrino mass [43, 40]. Here we assumed the hierarchical mass, i.e., the mass of the first generation is negligible compared to the third generation. By using this formula, the lower limit on right-handed neutrino mass is,

$$M_{R,1} \gtrsim 6 \times 10^8\, \text{GeV} \left(\frac{0.05\, \text{eV}}{\Delta m}\right) \kappa_f^{-1}, \tag{2.2.20}$$

where we used the mass difference of neutrinos, Δm, from neutrino oscillation [44, 45, 46] for m_3. The value of the efficiency factor depends on the strength of the washout terms, but typically $\kappa_f \sim 10^{-(1\text{-}2)}$ [40], thus the lower bound is $M_{R,1} \gtrsim 10^{9\text{-}10}\, \text{GeV}$.

2.3 Motivation and Key Ingredients for ADM

So far we have seen the production mechanism for WIMP and baryons. In this section, we see how the ADM scenario is motivated and constructed [47, 48, 49].

2.3.1 Coincidence problem

As we saw in the previous sections, if the WIMP scenario is true, DM is mainly produced from the thermal freeze-out mechanism. On the other hand, in the SM baryon sector, an asymmetry is injected in the early Universe and the baryon abundance is determined by its asymmetric part. However, despite the difference in production mechanisms, the observation suggests that the ratio between DM and baryon abundances is $\mathcal{O}(1)$. The problem is that the baryon abundance predicted from freeze-out abundance is $Y_b \sim 10^{-20}$[24], which is $\mathcal{O}(10^{-10})$ times smaller than the actual value, $\eta_B \sim 6 \times 10^{-10}$, we need the baryogenesis to compensate for this discrepancy. After this compensation occurs, the $\mathcal{O}(1)$ matching between DM and baryon density seems unnatural. This matching is called "the coincidence problem" and is difficult to solve within the WIMP scenario.

To compensate for this hierarchy between DM and baryons, it seems natural to think that these two components have the same origin of the production mechanism, i.e., the baryogenesis, and the asymmetry components dominate the abundance in both sectors. This paradigm is called asymmetric dark matter (ADM), which is suggested in the literature [11]. In the ADM framework, the asymmetry is shared between baryons and DM,

$$n_{\mathrm{DM}} - n_{\mathrm{D\bar{M}}} \sim n_b - n_{\bar{b}}. \qquad (2.3.1)$$

Thus, if the DM has an $\mathcal{O}(1)\,\mathrm{GeV}$ mass and a large enough annihilation cross section to eliminate the symmetric component in DM, the energy ratio naturally ends in $\mathcal{O}(1)$. This is the motivation of ADM.

2.3.2 Key ingredients for ADM

Although the ratio of the asymmetry in both sectors and the DM-baryon mass ratio depends on the detail of models, there are key features of generic ADM models. First, we should have an asymmetry generation mechanism. This mechanism can be any type of baryogenesis; GUT baryogenesis, thermal leptogenesis, Affleck–Dine baryogenesis, etc. If we construct a dark sector which has a strong first-order phase transition, EW baryogenesis in the dark sector can be possible.

The second is the mechanism that distributes or transfers the generated asymmetry between two sectors. Whatever we choose the asymmetry generating mechanism, without the asymmetry sharing process, we cannot explain the coincidence of the number density, $n_{\mathrm{DM}} - n_{\mathrm{D\bar{M}}} \sim n_b - n_{\bar{b}}$, which is the core feature of ADM. There can be some types of scenarios for asymmetry generation and distribution:

(i) *Baryogenesis in SM*
    In this scenario, baryogenesis mainly inject asymmetry in the SM sec-

tor and then the asymmetry distribution mechanism transfer the asymmetry into the dark sector [50, 11, 51, 52]. In chapter 4, we adopt this scenario together with thermal leptogenesis.

(ii) *Baryogenesis in the dark sector*
This is the scenario with SM and dark sector interchanged in scenario (i). Although the exchange of the two sectors may not leave a big difference in the resultant asymmetry, tightly constrained baryogenesis such as EW baryogenesis can be adopted in this scenario [53, 54, 55, 56, 57, 58].

(iii) *Cogenesis*
In this scenario, baryogenesis simultaneously generates asymmetries in both sectors [59, 60, 61]. If we do not introduce an asymmetry distribution mechanism which is active below the scale baryogenesis ends, the ratio of the number density is determined by the ratio of asymmetry in two sectors generated at the era of cogenesis.

In any case of the above, the most simple construction of the asymmetry distribution mechanism which is free from constraints is to introduce a higher dimension operator. The requirement for this higher dimension operator is that it consists of SM operator charged under $U(1)_{B-L}$, $\mathcal{O}_{\mathrm{SM}}$, and dark sector operator with opposite $B - L$ charge, $\mathcal{O}_D$;

$$\mathcal{L}_{B-L\,\mathrm{portal}} = \frac{1}{M_{\mathrm{portal}}^{m-4}} \mathcal{O}_{\mathrm{SM}} \mathcal{O}_D \,, \qquad (2.3.2)$$

where m is the mass dimension of the operator $\mathcal{O}_{\mathrm{SM}} \mathcal{O}_D$ and M_{portal} is some energy scale. Hereafter, we call this higher dimensional operator as the $B - L$ portal operator. If we assume the model in which the dark sector particles are not charged under the SM gauge group, $\mathcal{O}_{\mathrm{SM}}$ should be charge neutral under the SM gauge group. The same is true for $\mathcal{O}_D$. The assumption that the dark sector (SM) particles are not charged under SM (dark sector) gauge group is quite reasonable since otherwise the interaction between SM and DM can be so strong to be constrained. Thus, there are several combinations of field operators on the SM side;

$$\mathcal{O}_{\mathrm{SM}} = \bar{U}_R \bar{D}_R \bar{D}_R, \ \bar{D}_R L Q_L, \ \bar{E}_R L L, \ L H \,, \qquad (2.3.3)$$

where Q_L is the left-handed quark doublet and $\bar{U}_R, \bar{D}_R, \bar{E}_R$ are right-handed anti-quarks and the right-handed anti-lepton. Among these operators, the lowest dimensional is LH. From the dimensional ground, the interaction rate of the portal operator is estimated as $\Gamma \sim T^{2m-7}/M_{\mathrm{portal}}^{2m-8}$. This temperature dependence suggests that the interaction rate decreases slower than the expansion rate for the renormalizable or the super-renormalizable operator with $m \leq 4$, while the reaction rate of the non-renormalizable operator

($m \geq 5$) decreases faster than the expansion rate. From this observation, we see that the higher the dimension of the operator is, the faster the reaction rate drops. Thus, in order for the portal operator to be active at the temperature below the baryogenesis end, the dimension m should be small.

Another choice for the asymmetry distribution mechanism is to utilize the sphaleron process. The simplest possibility is the model in which the DM is charged under $SU(2)_L$ of the SM and has a new global symmetry $U(1)_X$, which is an analogy of the $B-L$ charge in the dark sector. This new $SU(2)_L$-$SU(2)_L$-$U(1)_X$ anomaly implies that the DM number can be changed by the sphaleron process. However, since the scattering cross section with SM particle is large, ADM charged under weak interaction is constrained by direct detection or weak boson decay [49].

Finally, we need a large enough annihilation cross section to efficiently remove the symmetric part of the DM, otherwise the symmetric component should dominate the DM abundance and the ADM scenario loses its prediction. If we assume a higher dimension operator for the asymmetry distribution mechanism, the SM and the dark sector are thermalized, and thus there is also a thermally produced symmetric component in the dark sector despite there being no initial abundance in DM. The direct products of DM annihilation can be both SM particles or dark sector particles. However, if the dark sector products are stable, they can cause cosmological problems; they can overclose the Universe if they are massive and lead to large degrees of the neutrino types, N_{eff}. Thus, even in the case that DM and anti-DM annihilate into lighter particles in the dark sector, these products must eventually decay or annihilate into SM particles. We will see how these processes are implemented in the composite ADM with dark photon portal in chapter 4.

2.3.3   Cosmological Evolution of Asymmetric Dark Matter

As we have seen the construction of the ADM, it is worth summarizing the cosmological evolution of the ADM.

First, at high temperatures, the asymmetry is generated in the SM and/or the dark sector via baryogenesis. At this moment, the $B-L$ portal is active and distributes the asymmetry injected. Next, the portal interaction becomes inactive to maintain an equilibrium between the SM and the dark sector, and the asymmetry in each sector is fixed. Finally, after the thermal decoupling of the two sectors, each sector develops and annihilates the symmetric component independently. We show in Figure 2.1 the schematic picture of the ADM evolution process. In the figure, χ and b represent DM and baryon, respectively, and barred characters represent anti-particles. Light blue and red rectangles show the symmetric and the asymmetric components in each sector, respectively.

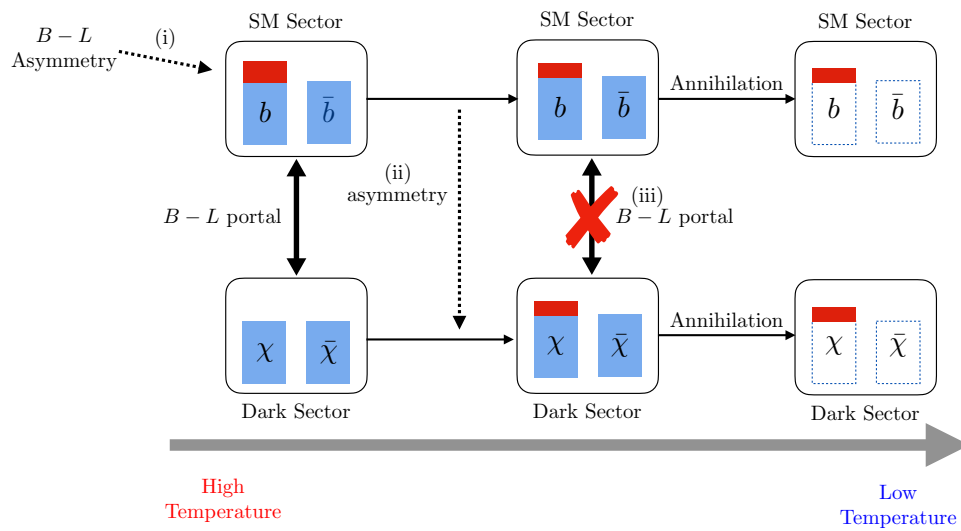Notice that through the annihilation of the symmetric component, there

Figure 2.1: A schematic picture of the evolution process of ADM with asymmetry first injected into SM. χ and b represent DM and baryon, respectively, and barred characters represent anti-particles. The dotted arrow shows the flow of asymmetry transfer and the gray arrow shows the time flow. The left of the figure corresponds to the high-temperature state and the right corresponds to the low temperature.

is no asymmetry transfer between the two sectors, thus the final abundance is determined at the freeze out of the portal interaction[3].

---

[3]If there are $B - L$ violating reactions that are active below the portal freeze-out temperature, final asymmetry is determined by the value at the freeze-out and the strength of the $B - L$ violating reactions in each sector

Chapter 3

Experimental Constraints on DM Models

In this section, we review experiments that aim to search particle DM and put constraints on general DM models. We mainly review current direct detection experiments and indirect detection experiments. The review of direct detection experiments is mainly based on Ref.[62].

3.1 Direct Detection

In most general particle DM models, we assume that the DM candidate has a feebly but non-zero interaction with SM particles. This assumption enables the DM to have a chance to scatter with nucleons. If we observe sudden recoil events in gasses or materials, the event indicates a momentum transfer caused by DM scattering.

One way to observe this event is accumulating a large number of nucleons in a cavity to compensate feebleness of DM interaction and enhance the event rate. This simple setup is a basic idea of the direct detection experiment and was first suggested in Ref. [63] (see also Refs. [9, 62, 64]).

3.1.1 Overview

To estimate the signals, we need an interaction rate for DM and nucleus-DM scattering. This rate is written as

$$\frac{\mathrm{d}R}{\mathrm{d}E_{\mathrm{nr}}} = \frac{\rho M}{m_T m_{\mathrm{DM}}} \int_{v_{\mathrm{min}}}^{v_{\mathrm{esc}}} \mathrm{d}^3 v\, v f(v) \frac{\mathrm{d}\sigma}{\mathrm{d}E_{\mathrm{nr}}}\,, \qquad (3.1.1)$$

where E_{nr} represents the nuclear recoil energy, m_{DM} is the DM mass, and $\rho = 0.3\,\mathrm{GeV/cm^3}$ represents the local DM mass density. m_T is the mass of the target nucleus and M is the targets detector mass, thus M/m_T represents the number of targets in the detector. The lower cutoff of the velocity

integration, v_{min}, is the minimum velocity of DM which gives the recoil energy E_{nr} to the target nucleus. For elastic scattering,

$$v_{\mathrm{min}} = \sqrt{\frac{m_T E_{\mathrm{nr}}}{2\mu_T^2}}, \tag{3.1.2}$$

where μ_T is the reduced mass of the DM-target system. The upper cutoff of the velocity integration is given by the escape velocity of the Milky Way galaxy, $v_{\mathrm{esc}} = 544\,\mathrm{km/s}$ [65]. To estimate the DM velocity distribution, the Standard Halo Model is commonly used. In this model, the distribution is written as,

$$f(v) = N_{\mathrm{esc}} \frac{e^{-v^2/v_c^2}}{(v_c\sqrt{\pi})^3} \Theta(v_{\mathrm{esc}} - v), \tag{3.1.3}$$

where $v_c = 220\,\mathrm{km/s}$ is the local circular velocity at the solar distance. By taking into account the truncation of the distribution function at the escape velocity, we set $N_{\mathrm{esc}}^{-1} = \mathrm{Erf}(v_{\mathrm{esc}}/v_c) - 2(v_{\mathrm{esc}}/v_c)\exp\left(-v_{\mathrm{esc}}^2/v_c^2\right)/\sqrt{\pi}$ so that $\int \mathrm{d}^3 v\, f(v) = 1$.

When we focus on the fermionic DM model, a DM-nucleus scattering cross section can be split into spin-independent and spin-dependent parts,

$$\frac{\mathrm{d}\sigma}{\mathrm{d}E_{\mathrm{nr}}} = \frac{m_T}{2v^2\mu^2}\left(\sigma_{SI} F_{SI}^2(E_{\mathrm{nr}}) + \sigma_{SD} F_{SD}^2(E_{\mathrm{nr}})\right), \tag{3.1.4}$$

where F_{SI} and F_{SD} denote the form factor for spin-independent and spin-dependent interactions, respectively. If the mass scale of the mediator particle is larger than the momentum transfer, i.e., $m_{\mathrm{med}} \gg q = \sqrt{2m_T E_{\mathrm{nr}}}$, the spin-independent interaction can be induced from scalar exchanging interaction, $\mathcal{L} = 1/m_{\mathrm{med}}^2 \bar{Q}Q\bar{\chi}\chi$, or vector exchanging interaction, $\mathcal{L} = 1/m_{\mathrm{med}}^2 \bar{Q}\gamma^\mu Q\bar{\chi}\gamma_\mu\chi$. Similarly, the spin-dependent types are induced from a pseudo-scalar exchange, $\mathcal{L} = 1/m_{\mathrm{med}}^2 \bar{Q}\gamma^5 Q\bar{\chi}\gamma^5\chi$, or axial vector exchange, $\mathcal{L} = 1/m_{\mathrm{med}}^2 \bar{Q}\gamma^\mu\gamma^5 Q\bar{\chi}\gamma_\mu\gamma^5\chi$. Here we denote the SM quarks by Q. If the mediator is light, the cross section has additional recoil energy dependence $\propto (q^2 + m_{\mathrm{med}}^2)^{-2}$ through the propagator of the mediator. This is the case for the asymmetric dark matter model described in chapter 4, in which the light dark photon plays the role of a light mediator between SM and DM.

The form factor accounts for the coherence of the nucleus depending on the momentum transfer. If q is small, we cannot resolve the structure of the nucleus, thus the DM scatters off the entire nucleus coherently. On the other hand, for high q the DM no more scatters off the entire nucleus but only a part of it. The common choice for spin-independent form factor is

$$F(q) = \frac{3j_1(qr)}{qr}\exp\left(-\frac{q^2 s^2}{2}\right), \tag{3.1.5}$$

where $j_1(x)$ is the spherical Bessel function of the first kind, r parameterizes the nucleus radius and s is the skin-thickness parameter.

If the DM couples to proton and neutron universally, the spin-independent cross section is given by,

$$\sigma_{SI} = \sigma_n \frac{\mu_T^2}{\mu_n^2} \frac{(f_p Z + f_n(A-Z))^2}{f_n^2} = \sigma_n \frac{\mu_T^2}{\mu_n^2} A^2 \,, \qquad (3.1.6)$$

where σ_n is the DM-nucleon scattering cross section and μ_n is the reduced mass of the DM-nucleon system. A is the atomic number, Z is the proton number in the nucleus, and f_p and f_n denote the coupling strength of the DM to protons and neutrons. In the case at hand, we set $f_p = f_n$. If the DM couples to protons and neutrons non-universally, i.e., in an isospin violating way, the situation is a bit changed.

For example, in the case of the dark photon mediator DM mainly couples to the proton, thus the spin-independent cross section shows the dependence of $\sigma_{SI} \propto Z^2$, not $\sigma_{SI} \propto A^2$. Thus, for the light dark photon mediator, the spin-independent cross section is written as,

$$\sigma_{SI} = \frac{16\pi Z^2 \alpha_{\mathrm{EM}} \alpha_D \mu_T \varepsilon^2}{(m_{\mathrm{med}}^2 + q^2)^2} \,, \qquad (3.1.7)$$

where α_D is the coupling strength of the dark $U(1)$ gauge and ε is a parameter characterizing the kinetic mixing between the SM photon and dark photon (see chapter 4).

For a WIMP dark matter, a spin-dependent cross section is written with the Fermi coupling constant,

$$\frac{\mathrm{d}\sigma_{SD}}{\mathrm{d}q^2} = \frac{8 G_F^2}{\pi v^2} (a_p \langle S_p \rangle + a_n \langle S_n \rangle)^2 \frac{J+1}{J} \frac{S(|\vec{q}|)}{S(0)} \,, \qquad (3.1.8)$$

where $\langle S_i \rangle$, $i = p, n$ is the expectation value of nucleons in the target nucleus, which depends on the model describing the nuclear. J is the total nuclear spin of the target and $S(|\vec{q}|)$ is the spin-structure function of the target. The spin-independent cross section shows significant dependence on the atomic number and typically the heavy nuclei are more sensitive to probe the spin-independent interaction. On the other hand, a spin-dependent one only depends on the spin structure of the nuclei and heavier nuclei do not necessarily show more sensitiveness to spin-dependent interactions. If all spins in a nucleus are paired, that nucleus is blind to the spin-dependent interactions. We should notice that in the above formula, we implicitly assume that the spin-dependent interaction is mediated by the weak interaction, and thus the cross section is proportional to the square of the Fermi coupling. If we consider a spin-dependent interaction mediated by a dark photon, the cross section receives a modification as $G_F^2 \to (m_{\mathrm{med}}^2 + q^2)^{-2}$, similar to the spin-independent cross section. However, the spin-dependent
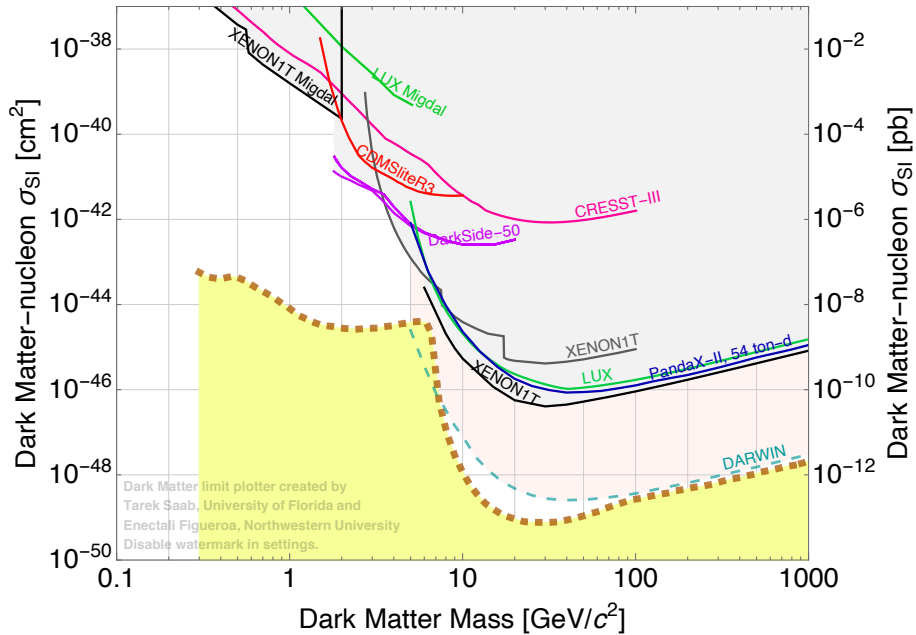
Figure 3.1: The current bounds on the WIMP cross section from direct detection experiments, for XENON1T [66, 67, 68], LUX [69, 70], PandaX-II [71], DarkSide [72], CRESST-III [73], and CDMSlite [74]. We also plot the future sensitivity of DARWIN [75] and the neutrino floor [76]. To plot this figure, we use the Dark Matter Limit Plotter distributed on the website https://supercdms.slac.stanford.edu/dark-matter-limit-plotter.

interaction is subdominant when we consider the scattering between nuclei and dark $U(1)$ charged particles because the spin-independent interaction is much larger due to the dependence on Z^2. If the DM is a dark gauge singlet, the spin-dependent cross section is relevant. Thus, in the analysis of chapter 4, we only consider spin-independent cross section because we assume that half of the DM abundance consists of the dark charged baryon, p', and the other half is the dark neutral baryon, n'.

3.1.2 Current Status

The current status of direct detection experiments is summarized in Ref. [64]. We cite the figure of the current bound on the WIMP scattering cross section in Figure 3.1. We see that the bound from XENON1T is the most stringent.

3.2 Indirect Detection

After decoupling from the SM thermal bath, DM and anti-DM rarely annihilate, and its comoving density is almost fixed. As the structure formation evolves, however, inhomogeneities grow and DM-rich regions appear. High enough DM density reignites the annihilation process and causes high energy SM particle flux such as gamma-rays or electron flux signals. If we can detect these fluxes today, this signals footprints of DM annihilation. In this section, we see how to constrain DM models with indirect detection experiments. For the review of indirect detection, we refer to Ref. [77]

3.2.1 Overview

To investigate the constraint from the indirect detection, estimation of the induced flux is important. When we consider detecting the flux from the center of the Milky Way or dwarf spheroidal galaxies (dSphs), the predicted flux for DM annihilation can be written as

$$\Phi = \int_{E_{\min}}^{E_{\max}} \mathrm{d}E\, E \int_{\Delta\Omega} \frac{\mathrm{d}\Omega}{4\pi} \langle \sigma v \rangle \frac{\mathrm{d}N}{\mathrm{d}E} \int_{\text{l.o.s.}} \mathrm{d}l\, n_X n_{\bar{X}}\,, \qquad (3.2.1)$$

where $E_{\max(\min)}$ is the maximum (minimum) energy threshold and $\Delta\Omega$ is the field of view of the detector. $\mathrm{d}N/\mathrm{d}E$ is the distribution of the produced SM particles, $n_{X,\bar{X}}$ represent the number density of the DM and anti-DM distributed within the region of interest, and l.o.s. means the integration over the line of sight. As we can see, the calculation can be split into three parts; detector-dependent part, $\mathrm{d}E\,\mathrm{d}\Omega$, particle physics model-dependent part, $\langle \sigma v \rangle$ and $\mathrm{d}N/\mathrm{d}E$, and astrophysical part, $\mathrm{d}l\, n_X n_{\bar{X}}$.

To determine the astrophysical factor, the distribution of DM is important. A commonly used mass distribution is the Navarro-Frenk-White (NFW) profile [78],

$$\rho_{\text{NFW}}(r) = \frac{\rho_0}{r/r_s(1 + r/r_s)^2}\,. \qquad (3.2.2)$$

We use this profile for estimating electron/positron flux in chapter 5, though our result is not changed significantly even if we choose a cored profile.

There is also a commonly used astrophysical parameter called the J-factor, which is defined as

$$J(\Omega) = \int_{\text{l.o.s.}} \mathrm{d}l\, \rho_{\text{DM}}^2\,, \qquad (3.2.3)$$

where Ω represents the angle dependence of the J-factor. We also use this parameter in Ref. [79] when we estimate the flux from dSphs.

The calculation of the particle model-dependent part is shown in detail in chapter 5 and appendix B.

3.2.2 Experiments

When DMs annihilate/decay into SM particles, the directly produced can be unstable particles or quarks, which immediately decay or hadronize to produce stable particles such as photons, electrons, protons, neutrinos, and their anti-particle. If the DM is massive enough, heavier nuclei can also be produced. The signals which we observe are those end products of the annihilation/decay. We briefly review experiments classified by their target particles.

Gamma-ray

First is the Fermi Large Area Telescope (LAT) [80], which is a space telescope with sensitivity to gamma-rays from $20\,\mathrm{MeV}$ to $300\,\mathrm{GeV}$ [81]. From the energy range of this telescope, it is good to constrain $\mathcal{O}(1)\,\mathrm{GeV}$ gamma-ray, and thus we use this result to constrain the ADM model in chapter 5. For higher energy gamma-rays, which have lower event rates, the Fermi-LAT loses its sensitivity because the area of the telescope is limited. The ground-based telescopes such as MAGIC [82] and CTA [83] have effective areas much larger than Fermi-LAT, thus have sensitivities to the gamma-rays with energy from $\mathcal{O}(10)\,\mathrm{GeV}$ to more than $100\,\mathrm{TeV}$. Due to the opaqueness of the atmosphere to the gamma-/cosmic-rays, these telescopes do not directly observe the gamma-/cosmic-rays, but the Cherenkov light which the particle showers eventually induce.

Electron/Positron flux

For the flux of electron/positron, we can use the data of Voyager-1 [84], which measures galactic cosmic-rays. The Voyager-1 measured electron fluxes with energy from $6\,\mathrm{MeV}$ to $100\,\mathrm{MeV}$ and other ions such as hydrogen and helium. We will use the electron flux bounds to constrain the ADM model in chapter 5.

Neutrino flux from the Galactic Center

In detecting neutrinos, we observe the Cherenkov light induced by the interaction of neutrinos and medium. Since the neutrinos only interact matters through weak interaction, we need a large volume of water or ice to accumulate large enough statistics to detect the Cherenkov light. Among water Cherenkov chamber neutrino detectors, Super-Kamiokande has a low energy threshold of $\sim 5\,\mathrm{MeV}$[85], which is low enough to detect the neutrinos from ADM decay. We will use the result [86] to constrain the portal operator in chapter 4.

Chapter 4

Composite Asymmetric Dark Matter

In this chapter, we see how to construct a realistic composite ADM model. The key point is that we utilize confinement caused by a non-Abelian strong gauge interaction. This enables us to simultaneously explain $\mathcal{O}(1)\,\mathrm{GeV}$ DM mass and a large annihilation cross section. In this model, the confinement scale controls the DM mass and DMs annihilate into lighter degrees of freedom (e.g., dark mesons) via the strong interaction.

By construction, however, the effective number of massless degrees of freedom in the composite dark sector is sizable in the early Universe. If those particles are also stable, their energy density overcloses the Universe, or contributes to the effective number of neutrino degrees of freedom, N_{eff}, too much, depending on their masses [14]. Thus, some light portal particle is needed to transfer the excessive entropy of the dark sector into the SM sector.

A simple possibility for such a portal is a light dark photon. It has a mass in the sub-GeV range and decays into the SM particles (mainly into the leptons) through kinetic mixing with the SM photon. In this chapter, we investigate the impact of decaying dark photon on N_{eff} and identify the viable parameter space.

We also construct a minimal ADM model with $B - L$ symmetry. Right-handed neutrinos are introduced to generate the $B - L$ asymmetry via thermal leptogenesis [15] (see also Refs. [33, 34, 35] for reviews). They also naturally explain the observed tiny neutrino masses via the seesaw mechanism [16, 17, 18, 19, 20]. We reach a simple model with a QCD-like SU(3) strong interaction and a QED-like U(1) gauge interaction. By taking into account the derived constraints, we show that such a model can be tested by direct detection experiments of DM through the coupling to the dark photon. The content of this chapter is based on Ref. [1].

4.1 ADM thermal history and cosmological constraints on dark photon

In this section, we discuss the thermal history of ADM where the dark photon plays a crucial role. We also derive cosmological constraints on the dark photon parameters.

4.1.1 ADM sector

Before discussing constraints on the dark photon, let us overview the models of composite ADM. For that purpose, we consider an $\mathrm{SU}(N_c)_D$ gauge dynamics, which is referred to as the QCD$'$ in the following. There are N_f-flavors of vector-like dark quarks $(Q'_i, \bar{Q}'_i)$ $(i = 1 \cdots N_f)$ with $B - L$ charges of $(q_{B-L}, -q_{B-L})$. Hereafter, fermions are taken to be the two-component Weyl fermion. We assume that the masses of the dark quarks,

$$\mathcal{L}_{\mathrm{mass}} = \sum_i m_{Q_i} Q_i \bar{Q}_i + \mathrm{h.c.}\,, \qquad (4.1.1)$$

are smaller than the dynamical scale of the QCD$'$, $\Lambda_{\mathrm{QCD}'}$.

Below the dynamical scale, we assume that the QCD$'$ exhibits a confinement where the dark quarks are confined into dark mesons and dark baryons. By assuming spontaneous chiral symmetry breaking, we expect that the lightest mesons are the pseudo-Nambu-Goldstone modes, i.e., the dark pions. The dark pions obtain masses of $m_{\pi'} = \mathcal{O}(\sqrt{m_Q \Lambda_{\mathrm{QCD}'}})$, which are smaller than the dark baryon masses of $m_{b'} = \mathcal{O}(\Lambda'_{\mathrm{QCD}})$ for $m_Q \ll \Lambda_{\mathrm{QCD}'}$. As the dark baryons carry $B - L$ charges, the lightest ones are good candidates for ADM.[1] The annihilation cross section of the dark baryons into the dark mesons is quite large due to the strong dynamics, with which the symmetric part of the DM relic is negligibly small [87, 88, 89, 90, 91]. As a result, the DM abundance is naturally dominated by the asymmetric component.

In our scenario, we assume that the $B - L$ symmetry is softly broken by right-handed neutrino masses, M_R, which carry a $B - L$ charge of -2.[2] The right-handed neutrinos couple to the SM particles via

$$\mathcal{L}_{N\text{-}\mathrm{SM}} = \frac{1}{2} M_R \bar{N}_R \bar{N}_R + y_N H L \bar{N}_R + \mathrm{h.c.}\,, \qquad (4.1.2)$$

which triggers the seesaw mechanism. Here, H and L denote the SM Higgs and the lepton doublets, respectively. The Yukawa coupling is related to the light neutrino masses via $y_N^2 \sim m_\nu M_R / v_{\mathrm{EW}}^2$ with v_{EW} being the vacuum expectation value of the Higgs. The $B - L$ (i.e., baryon) asymmetry is

---

[1]We assume that the lightest dark baryons are the ones with the lowest spin, while the detailed mass spectrum does not change the following discussion qualitatively.

[2]One can gauge the $B - L$ symmetry, which is spontaneously broken by a vacuum expectation value of a scalar whose $B - L$ charge is -2.

generated by thermal leptogenesis when the cosmic temperature is around the right-handed neutrino mass, $T \sim M_R \gtrsim 10^{9\text{-}10}$ GeV [33, 34, 35].

Once the $B - L$ asymmetry is generated, part of it is propagated into the dark sector through the portal interaction,

$$\mathcal{L}_{B-L\,\text{portal}} = \frac{1}{M_{\text{portal}}^n} \mathcal{O}_D \mathcal{O}_{\text{SM}} + \text{h.c.}, \tag{4.1.3}$$

where $\mathcal{O}_D$ ($\mathcal{O}_{\text{SM}}$) is a $B - L$ charged but gauge invariant operator consisting of the dark (SM) sector fields. Here, M_{portal} denotes a portal scale with $n+4$ ($n \in \mathbb{N}$) being the mass dimension of the operator, $\mathcal{O}_D \mathcal{O}_{\text{SM}}$. We note that this portal operator can cause DM decay. We will discuss this point later because the decay channels and the decay rate are highly model-dependent. For a while, we assume the DM lifetime is long enough that we treat DM stable.

The portal interaction eventually decouples at the cosmic temperature of

$$T_D \sim M_{\text{portal}} \left(\frac{M_{\text{portal}}}{M_{\text{PL}}} \right)^{1/(2n-1)} . \tag{4.1.4}$$

T_D is estimated as the temperature where the interaction rate, $\Gamma_{\text{portal}} \sim T^{2n+1}/M_{\text{portal}}^{2n}$ becomes equal to the Hubble rate, $H \sim T^2/M_{\text{Pl}}$. For a successful ADM scenario, T_D is required to be lower than M_R. In the following, we also assume that T_D is higher than the electroweak scale, i.e., the portal interaction decouples before the Sphaleron process decouples. After the portal interaction decouples, the $B - L$ number is conserved independently in the SM sector and in the dark sector. In the ADM models with a large annihilation cross section, the DM mass is determined by the ratio of the $B - L$ asymmetries between the DM and the SM sectors, $A_{\text{DM}}/A_{\text{SM}}$, that is,

$$m_{\text{DM}} \simeq 5\,\text{GeV} \times \frac{30 A_{\text{SM}}}{97 A_{\text{DM}}} . \tag{4.1.5}$$

Here, the numerical factor is the ratio between A_{SM} and the baryon asymmetry observed today, $A_B/A_{\text{SM}} = 30/97$ [42]. The value of $A_{\text{SM}}/A_{\text{DM}}$, which is typically of $\mathcal{O}(1)$ [as we will see later, e.g., in Eq. (4.2.9)], depends on the dark sector model. Since the DM candidate in our scenario is the dark baryons, the DM mass is controlled by $\Lambda_{\text{QCD}'}$; $m_{\text{DM}} = m_{b'} \sim \Lambda_{\text{QCD}'}$. Thus, the DM mass in the GeV range can be naturally explained by the dynamical scale of $\Lambda_{\text{QCD}'} = \mathcal{O}(1)\,\text{GeV}$. This is another advantage of the composite ADM models.

4.1.2 Dark photon portal

In the composite ADM models, we assume a strong gauge dynamics in the dark sector. Thus, the dark sector entropy is sizable in the early Universe,

27

since the dark sector is thermally connected to the SM sector via the portal interaction. Thus, if the dark pions are stable, they overclose the Universe or contribute to the effective number of neutrino degrees of freedom, N_{eff}, too much, depending on their masses [14]. To evade these problems, we introduce a dark photon of the $U(1)_D$ gauge interaction, referred to as the QED′, under which the dark quarks are charged. In the presence of the dark photon, the dark pions can annihilate or decay into the dark photons, which makes the dark pion harmless.

The mere introduction of the massless dark photon does not solve the problem, since it also contributes to N_{eff} too much. To avoid this problem, we further assume that the dark photon has kinetic mixing with the SM photon and becomes massive by a Higgs mechanism in the dark sector:

$$\mathcal{L}_{A'\text{-}A} = \frac{\epsilon}{2} F_{\mu\nu} F'^{\mu\nu} + \frac{1}{2} m_{\gamma'}^2 A'_\mu A'^\mu \,. \qquad (4.1.6)$$

Here, F and F' are the field strengths of the SM photon A and the dark photon A', respectively, and $m_{\gamma'}$ denotes the mass of the dark photon. Through the kinetic mixing parameterized by ϵ, the massive dark photon decays into SM fermions with a decay rate,

$$\Gamma_{\gamma'} = N_{\text{ch}} \frac{1}{3} \epsilon^2 \alpha m_{\gamma'} \simeq 0.3 \,\text{s}^{-1} \times N_{\text{ch}} \left(\frac{\epsilon}{10^{-10}} \right)^2 \left(\frac{m_{\gamma'}}{100 \,\text{MeV}} \right) \,. \qquad (4.1.7)$$

Here, α denotes the QED fine-structure constant. When the dark photon mass is lighter than twice the muon mass, it decays only into a pair of the electron and the positron, and hence, $N_{\text{ch}} = 1$.

Now, let us summarize the thermal history. Above the decoupling temperature of the portal interaction, T_D, the dark sector and the SM sector are in thermal equilibrium, and the $B - L$ asymmetry is distributed in the two sectors.

Below T_D, two sectors evolve independently. In the dark sector, the confinement of the strong gauge dynamics takes place at the temperature of $T_{\text{QCD}'} \sim \Lambda_{\text{QCD}'}$. DM (i.e., the lightest dark baryon) annihilates into the dark mesons with a very large cross section of $\mathcal{O}(4\pi/m_{\text{DM}}^2)$, with which the symmetric component of DM is erased and only the asymmetric component is left over. The $U(1)_D$ charged dark pions also annihilate into the dark photons with a cross section of $\mathcal{O}(4\pi\alpha_D^2/m_{\pi'}^2)$ with α_D being the QED′ fine-structure constant. This cross section is large enough to make the relic dark pions a subdominant component of DM for $\alpha_D \sim \alpha$.[3] Note that the relic density of the neutral pions is also suppressed when the neutral pions are in chemical equilibrium with the charged pions through the inelastic

---

[3]The symmetric component of the dark pions is efficiently annihilated away for $m_{\pi'}/\alpha_D < \mathcal{O}(100)\,\text{TeV}$, which is satisfied in this model. In this case, $\mathcal{O}(0.1)$ of the DM can consist of the dark pions.

scattering.[4] The dark photon eventually decays into the SM fermions via the kinetic mixing, so that the initial entropy of the dark sector is transferred to the SM sector.

To realize the above thermal history, we arrange the masses so that

$$2 \times m_e < m_{\gamma'} < m_{\pi'} < m_{\mathrm{DM}} \,, \tag{4.1.8}$$

where m_e denotes the electron mass. The first inequality is required to allow the decay of the dark photon. The second and the third inequalities are required for the annihilations of the charged dark pions and DM. As the DM mass is of $\mathcal{O}(1)\,\mathrm{GeV}$, we assume that $m_{\pi'}$ and $m_{\gamma'}$ are in the sub-GeV range.

The following analysis is almost independent of the details of the strong dynamics in the dark sector as long as the masses are arranged as in Eq. (4.1.8). In the following numerical analysis, we take the $N_f = 2$ and the $N_c = 3$ cases. $N_c = 3$ is the minimal choice as studied in Sec. 4.2.2. It should be noted that the derived constraints in the following analysis is not significantly changed for a composite ADM model with a different gauge group and/or a different number of the flavors. Furthermore, our analyses also apply to more generic dark sector (not necessarily the composite ADM) models that have a dark photon portal, with straightforward modifications.

As the dark baryon charged under $\mathrm{U}(1)_D$ interacts with SM protons via dark photon exchange, direct detection experiments provide upper bounds on ϵ for given $m_{\gamma'}$. On the other hand, the direct detection constraint highly depends on the DM mass, especially when $m_{\mathrm{DM}} = \mathcal{O}(1)\,\mathrm{GeV}$. It is also changed by the ratio between the number densities of p' and n'. Thus we will discuss the direct detection constraint later in Sec. 4.2.2.

4.1.3 Dark photon recoupling

The most stringent constraints on the dark photon property come from the constraints on $N_{\mathrm{eff}} = 3.15 \pm 0.23$ [92] by the precise measurements of the cosmic microwave background (CMB). Through the decay and the inverse decay of the dark photon, the dark sector recouples to the SM sector at the low cosmic temperature. We define the recoupling scale factor, a_{th}, by

$$3H(a_{\mathrm{th}}) = \frac{K_1(m_{\gamma'}/T_{\gamma'})}{K_2(m_{\gamma'}/T_{\gamma'})} \Gamma_{\gamma'} \,, \tag{4.1.9}$$

where H denotes the Hubble expansion rate, K_n denotes the nth order modified Bessel function of the second kind, and the dark photon decay rate at rest, $\Gamma_{\gamma'}$, is given by Eq. (4.1.7).

---

[4]If the corresponding chiral symmetry is anomalous for the QED$'$ as in the case of the SM, the lightest neutral pions decay into the dark photons with a short lifetime.

We approximate the evolution of the dark photon temperature $T_{\gamma'}$ as a function of the scale factor, a, by,

$$
T_{\gamma'} = \begin{cases}
\dfrac{a_{\text{QCD}'}}{a} T_{\text{QCD}'} & \text{for } a < a_{\text{QCD}'}\,, \\[2mm]
T_{\text{QCD}'} & \text{for } a_{\text{QCD}'} \leq a < a_{\text{F}}\,, \\[2mm]
\dfrac{a_{\text{F}}}{a} T_{\text{QCD}'} & \text{for } a_{\text{F}} \leq a\,.
\end{cases} \tag{4.1.10}
$$

Here $a_{\text{QCD}'}$ denotes the scale factor at the confinement. During the period of the dark hadron decoupling, the dark photon temperature does not scale by a^{-1} as the dark hadron energy density is transferred to the dark photon. Since the details of the QCD$'$ confinement are not tractable, we simply assume that the dark photon temperature does not change during the dark hadron decoupling. Long after the dark hadron decoupling, on the other hand, the dark photon temperature again scales by a^{-1}. The normalization of the dark photon temperature well below $T_{\text{QCD}'}$ can be reliably estimated by using the entropy conservation before and after the QCD$'$ confinement, which leads to $a_{\text{F}} = (41/3)^{1/3} a_{\text{QCD}'}$. Here, we count all the degrees of freedom including the QED$'$ breaking Higgs before the QCD$'$ confinement, while we count only the dark photon after the confinement. Thus, the degrees of freedom in the dark sector, g_*^D, before the QCD$'$ confinement is

$$
\begin{aligned}
g_*^D &= \sum_{\gamma', h', g'} g_{\text{boson}} + \frac{7}{8} \sum_{\text{dark quarks}} g_{\text{fermion}} \\
&= 2 + 2 + 8 \times 2 + \frac{7}{8} \times 2 \times 2 \times 2 \times 3 = 41\,,
\end{aligned} \tag{4.1.11}
$$

where γ', h', g' represent the dark photon, the dark Higgs, and the dark gluon respectively. After the confinement, $g_*^D = 3$. Then we obtain the numerical factor $41/3$. In the following numerical analysis, we take $T_{\text{QCD}'} = 10 \times T_{\text{QCD}}$ with the SM QCD transition temperature $T_{\text{QCD}} = 170\,\text{MeV}$, although the result does not change as long as $T_{\text{QCD}'}/T_{\text{QCD}} = \mathcal{O}(10\text{–}100)$.

We also estimate the cosmic temperature of the SM sector, T, as a function of the scale factor by the entropy conservation, following Ref. [93]. Here note that $T = T_{\gamma'}$ for $a < a_D$, where a_D denotes the scale factor when the portal operator decouples. The impact of the resultant dark photon density on N_{eff} depends on whether the reheating temperature of the SM sector by the dark photon recoupling is above or below the neutrino decoupling temperature, $T_{\nu\text{-dec}} \simeq 3\,\text{MeV}$. This is because the dark photon energy primarily heats up the electromagnetic particles only. To see the temperature at the recoupling, we define T_{cr} as

$$
\rho_{\text{SM}}(a_{\text{th}}) + \rho_{\gamma'}(a_{\text{th}}) = \rho_{\text{SM}+\gamma'}(T_{\text{cr}})\,, \tag{4.1.12}
$$

where the left-hand (right-hand) side denotes the energy densities before (after) the recoupling. Here, the energy density of the dark photon before the

recoupling, $\rho_{\gamma'}(a_{\mathrm{th}})$, is evaluated with the following distribution function:[5]

$$f_{\gamma'}(p, a, T_{\mathrm{F}}) = \frac{1}{\exp\left(\sqrt{m_{\gamma'}^2 + (a/a_{\mathrm{F}})^2 p^2}/T_{\mathrm{F}}\right) - 1}. \qquad (4.1.13)$$

The energy density after the recoupling, $\rho_{\mathrm{SM}+\gamma'}$, is simply given by the one in thermal equilibrium with a common temperature T_{cr}. For $T_{\mathrm{cr}} > T_{\nu\text{-dec}}$, we judge that the dark photon recoupling reheats the whole SM sector. Otherwise, we judge that the recoupling reheats only the electron and the photon. In the latter case, we estimate the temperature of the electron+photon system, T_{com}, by

$$\rho_{\gamma+e}(a_{\mathrm{th}}) + \rho_{\gamma'}(a_{\mathrm{th}}) = \rho_{\gamma+e+\gamma'}(T_{\mathrm{com}}), \qquad (4.1.14)$$

which differs from T_{cr}, while we assume that the neutrino temperature is not affected by the decay of the dark photon.

Before moving to the case study, let us make a comment on the neutrino decoupling temperature. The precise neutrino decoupling temperature can be slightly lower than $3\,\mathrm{MeV}$ and differs depending on what flavor of the neutrino we take into account [95]. As we will see below, the constraint gets tighter for the higher neutrino decoupling temperature. The purpose of the following estimate is to find the parameter region of the dark photon which is safely consistent with the Neff constraint. Hence, for safety and simplicity, we use $T_{\nu\text{-dec}} = 3\,\mathrm{MeV}$.

Dark photon recoupling above the neutrino decoupling temperature: $T_{\mathrm{cr}} > T_{\nu\text{-dec}}$

When the reheated temperature of the SM sector by the dark photon recoupling exceeds the neutrino decoupling temperature, i.e., $T_{\mathrm{cr}} > T_{\nu\text{-dec}}$, most energy of the dark-photon is re-distributed among the photons, the electrons, and the neutrinos. This situation corresponds to the kinetic mixing parameter of

$$\epsilon \gtrsim 10^{-10} \times \left(\frac{10\,\mathrm{MeV}}{m_{\gamma'}}\right)^{1/2}, \qquad (4.1.15)$$

where the inequality is estimated by $T_{\mathrm{cr}} \sim \epsilon\sqrt{\alpha m_{\gamma'} M_{\mathrm{Pl}}} > T_{\nu\text{-dec}} = 3\,\mathrm{MeV}$. Even in this case, a portion of the thermalized dark photons releases its

---

[5]This is valid when double Compton scattering and bremsstrahlung of the dark proton become inefficient before the dark photon becomes non-relativistic. If the dark photon is in thermal bath when it becomes non-relativistic, the entropy conservation requires $\rho_{\gamma'} \propto a^3/\ln(a)$. A similar situation can be found in the freeze-out of self-interacting DM through a $3 \to 2$ process [94]. The resultant $\rho_{\gamma'}(a_{\mathrm{th}})$ is different from our evaluation only by a small logarithmic factor.

energy at the temperature below $T_{\nu\text{-dec}}$, which reheats only the electrons and the photons. Thus, such late-time energy injection affects the neutrino-to-photon temperature ratio, T_ν/T_γ. By considering the entropy conservation in the electron+photon+dark photon plasma and that in the neutrino plasma independently, one finds

$$\frac{T_\nu}{T_\gamma} = \left(\frac{4}{11}\right)^{1/3}\left(1 + \frac{45}{11\pi^2}\frac{s_{\gamma'}(T_{\nu\text{-dec}})}{T_{\nu\text{-dec}}^3}\right)^{-1/3}. \tag{4.1.16}$$

Here, $s_{\gamma'}(T_{\nu\text{-dec}})$ is the entropy density of the dark photon at $T_{\nu\text{-dec}}$. As a result, the effective number of neutrino types is changed to

$$N_{\text{eff}} = \left(1 + \frac{45}{11\pi^2}\frac{s_{\gamma'}(T_{\nu\text{-dec}})}{T_{\nu\text{-dec}}^3}\right)^{-4/3} N_\nu^{(\text{SM})}, \tag{4.1.17}$$

where $N_\nu^{(\text{SM})} = 3.046$ [96] (3.045 in the recent analysis [97]) is the SM value. From the CMB observation, we find that the dark photon mass is bounded from below,

$$m_{\gamma'} \gtrsim 20\,\text{MeV}. \tag{4.1.18}$$

We note that the constraint does not depend on ϵ in this case since the criterion depends only on the entropy density of the dark photon at the neutrino decoupling temperature (see Fig. 4.1). As is clear from the above arguments, if we choose smaller value of the neutrino decoupling temperature, the lower mass limit gets weaker. Thus, the constraint (4.1.18) provides a rather tight constraint on the model and we can say that unconstrained region is safely consistent with the N_{eff} constraint.

Dark photon recoupling below the neutrino decoupling temperature: $T_{\text{cr}} < T_{\nu\text{-dec}}$

When the kinetic mixing parameter is smaller than Eq. (4.1.15), the dark photon recoupling reheats only the electron and the photon thermal bath, while the neutrino temperature does not get contributions from the dark photon. In this case, the entropy conservation of the neutrino plasma for $a > a_{\nu\text{-dec}}$ and that of the electron+photon+dark photon plasma leads to the neutrino-to-photon temperature ratio after the recoupling:

$$\frac{T_\nu}{T_\gamma} = \left(\frac{4}{11}\right)^{1/3}\frac{T_{\nu\text{-dec}}}{T_{\text{com}}}\frac{a_{\nu\text{-dec}}}{a_{\text{th}}}. \tag{4.1.19}$$

Accordingly, the effective number of neutrino degrees of freedom is estimated to be

$$N_{\text{eff}} = \left(\frac{T_{\nu\text{-dec}}}{T_{\text{com}}}\right)^4\left(\frac{a_{\nu\text{-dec}}}{a_{\text{th}}}\right)^4 N_\nu^{(\text{SM})}. \tag{4.1.20}$$
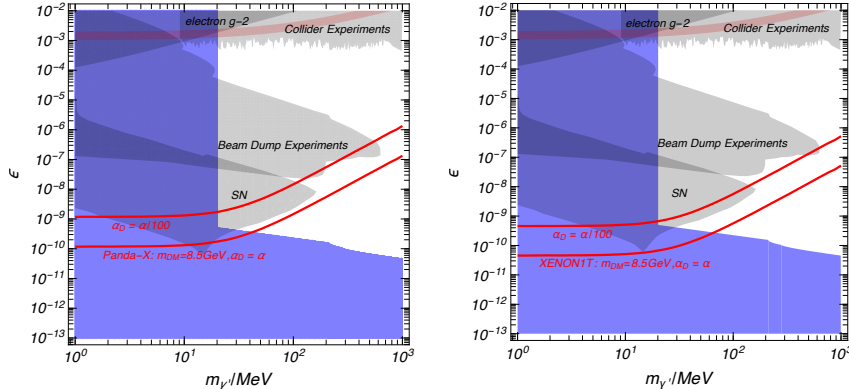
Figure 4.1:   *Constraints on the dark photon parameters. The blue shaded regions are excluded by the cosmological constraints discussed in Sec. 4.1.3. We take $T_{\mathrm{QCD}'} = 1\,\mathrm{GeV}$ and $a_{\mathrm{F}}/a_{\mathrm{QCD}'} = 3$, although the result barely depends on their values. The gray shaded regions are excluded by SN 1987A [98, 99], beam dump experiments, and collider experiments [100]. The red lines on the left panel show the upper limit on ϵ at $90\%\,\mathrm{CL}$ for $m_{\mathrm{DM}} = 8.5\,\mathrm{GeV}$ from PandaX-II experiment [71] (see Sec. 4.2.2). The red lines on the right panel shows the same limit from XENON1T experiment [66]. We set $\alpha_D = \alpha$ (lower) and $\alpha_D = \alpha/100$ (upper). In our analysis, we use the Maxwell velocity distribution with the velocity dispersion of $v_0 = 220\,\mathrm{km/s}$, which is truncated at the Galactic escape velocity, $v_{\mathrm{esc}} = 544\,\mathrm{km/s}$. The local circular velocity is also fixed to be $v_{\mathrm{circ}} = 220\,\mathrm{km/s}$ with the peculiar motions of the Earth being neglected. We use a conventional value of the local DM density, $\rho_{\mathrm{DM}} = 0.3\,\mathrm{GeV/cm}^3$, assuming that half of the total DM consists of p'. We note that the direct detection constraint is sensitive to the DM mass, while the other constraints are not.*

The lower blue shaded region of Fig. 4.1 shows the resultant constraint. Roughly speaking, the upper limit on ϵ for a given $m_{\gamma'}$ corresponds to the dark photon lifetime of $\mathcal{O}(1)\,\mathrm{s}$, and hence, to the dark photon decay at the neutrino decoupling temperature. In the figure, we take account of the muon, the charged pion, and the charged Kaon decay channels in $\Gamma_{\gamma'}$ in addition to the electron one, when those modes are kinematically allowed.

For the refined N_{eff} constraint on the dark photon, see the Ref. [101].

4.2   Bottom-up construction of a composite $B - L$ ADM model

In this section, we discuss a minimal model of a composite $B - L$ ADM, which achieves the thermal history discussed in the previous section. For $N_f = 1$, an operator $\mathcal{O}_D$ charged under the $B - L$ symmetry is also charged under $\mathrm{U}(1)_D$, and hence, no $B - L$ portal interaction is allowed. Thus we take $N_f = 2$ as a minimal model.

	SU(2)$_D$	$B-L$	U(1)$_D$
Q_1	**2**	q_{B-L}	$1/2$
$\bar{Q}_1$	**2**	$-q_{B-L}$	$-1/2$
Q_2	**2**	q_{B-L}	$-1/2$
$\bar{Q}_2$	**2**	$-q_{B-L}$	$1/2$

Table 4.1: *The charge assignment of the minimal model with $N_c = 2$ and $N_f = 2$. The QED$'$ charges of dark quarks are normalized to be $\pm 1/2$ without loss of generality.*

4.2.1 $\quad N_c = 2$ case

In this section, we discuss a model with $N_c = 2$ and $N_f = 2$. In Table 4.1, we show the charge assignment of the dark quarks. In this case, the dark pions are

$$\pi'^0 \propto Q_1 \bar{Q}_1 - Q_2 \bar{Q}_2\,, \quad \pi'^+ \propto Q_1 \bar{Q}_2\,, \quad \pi'^- \propto Q_2 \bar{Q}_1\,. \tag{4.2.1}$$

and the lightest baryons[6] are

$$b \propto Q_1 Q_2\,, \quad \bar{b} \propto \bar{Q}_1 \bar{Q}_2\,. \tag{4.2.2}$$

The lowest dimensional portal interaction is

$$\mathcal{L}_{B-L\,\text{portal}} = \frac{1}{M'^4_{\text{portal}}}(Q_1 Q_2)(LH)^2 + \text{h.c.}\,, \tag{4.2.3}$$

A drawback of this charge assignment is that it allows

$$\mathcal{L}_{B-L\,\text{mass}} = M_R(Q_1 Q_2) + M_R^\dagger(\bar{Q}_1 \bar{Q}_2) + \text{h.c.}\,, \tag{4.2.4}$$

which results in the dark quarks masses of $\mathcal{O}(M_R)$. Thus, the minimal charge assignment contradicts the assumption of the composite model.

We may take $q_{B-L} = \pm 1/2$ to avoid the unwanted mass term in Eq. (4.2.4). In this case, the lowest dimensional portal interaction is

$$\mathcal{L}_{B-L\,\text{portal}} = \frac{1}{M'^7_{\text{portal}}}(Q_1 Q_2)^2(LH)^2 + \text{h.c.} \tag{4.2.5}$$

Unlike the portal interaction in Eq. (4.2.3), this operator does not lead to decay of DM, which can be understood by the residual $\mathbb{Z}_2$ symmetry of the

---

[6]In this case the lightest baryons are also Nambu-Goldstone modes due to the enhanced symmetry breaking patter in the chiral limit, U(4)[$\supset$ SU(2)×SU(2)×U(1)] $\rightarrow$ USp(4)[$\supset$ SU(2)×U(1)]. Even if the masses of the lightest baryons are degenerate with those of the dark pions, the thermal history discussed above does not change as long as the dark baryon annihilation into the dark pions is efficient.

	SU(3)$_D$	$B - L$	U(1)$_D$
U'	**3**	q_{B-L}	$2/3$
$\bar{U}'$	**$\bar{3}$**	$-q_{B-L}$	$-2/3$
D'	**3**	q_{B-L}	$-1/3$
$\bar{D}'$	**$\bar{3}$**	$-q_{B-L}$	$1/3$

Table 4.2: *The charge assignment of the minimal model for $N_c = 3$ and $N_f = 2$. The QED$'$ charges are assigned so that one of the dark baryons becomes neutral.*

$B-L$ subgroup. As a result, this choice leads to a viable model of ADM. This portal operator is a valid choice for the purpose of the ADM scenario. As we will see shortly, however, we have a model with a simpler portal interaction for $N_c = 3$. Hence, we do not pursue this possibility further, although it is phenomenologically consistent. We also stress that the constraints on the dark photon parameter space in the previous section are not significantly changed for the model with $N_c = 2$ and $N_f = 2$, although they are derived for $N_c = 3$ and $N_f = 2$.

4.2.2 $N_c = 3$ case

Now, let us consider the case with $N_c = 3$ and $N_f = 2$. In Table 4.2, we show the charge assignment of the dark quarks. In analogy with SM QCD, we call Q_1 as U' and Q_2 as D'. As the charge assignment is parallel to the QCD charge, it is apparently free from quantum anomalies.[7] In this case, the dark pions are

$$\pi'^0 \propto U'\bar{U}' - D'\bar{D}', \quad \pi'^+ \propto U'\bar{D}', \quad \pi'^- \propto D'\bar{U}', \tag{4.2.6}$$

and the dark baryons are

$$p' \propto U'U'D', \quad \bar{p}' \propto \bar{U}'\bar{U}'\bar{D}', \quad n' \propto U'D'D', \quad \bar{n}' \propto \bar{U}'\bar{D}'\bar{D}'. \tag{4.2.7}$$

We summarize hadron mass formulas in the appendix A.1. We emphasize that the QED$'$ charge assignment in Table 4.2 is the unique choice (up to trivial normalization) that makes one of the dark baryon neutral and allows the following portal interaction.

The lowest dimensional portal interaction is

$$\mathcal{L}_{B-L\,\text{portal}} = \frac{1}{M_{\text{portal}}^3}(U'D'D')LH + \text{h.c.}, \tag{4.2.8}$$

---

[7]This model has a similarity to models based on the idea of the mirror matter [102, 103, 104, 105]. In such scenarios, mirror baryons are DM candidates, although the mirror photon is massless.

which requires $q_{B-L} = 1/3$. For now, we assume that the operator (4.2.8) exists and is efficient enough to distribute the $B - L$ asymmetry between the SM and the dark sector.

As we mentioned earlier, we assume that T_D is below the right-handed neutrino mass scale and is above the decoupling temperature of the sphaleron process. In this case, the ratio of the $B - L$ asymmetries between the dark and the SM sectors is [106]

$$\frac{A_{\mathrm{DM}}}{A_{\mathrm{SM}}} = \frac{44}{237} \, . \tag{4.2.9}$$

As a result, we find that the mass of DM is $m_{\mathrm{DM}} = 8.5 \, \mathrm{GeV}$ [see Eq. (4.1.5)], for which we take $\Lambda_{\mathrm{QCD}'} \sim 10 \times \Lambda_{\mathrm{QCD}}$ with $\Lambda_{\mathrm{QCD}} \sim 200 \, \mathrm{MeV}$ denoting the QCD dynamical scale. We consider a dark pion mass of $\mathcal{O}(10\text{–}100) \, \mathrm{MeV}$ or larger, which corresponds to a quark mass of $\mathcal{O}(1) \, \mathrm{MeV}$ or larger. The dark neutron can be heavier or lighter than the dark proton depending on the quark mass parameters m_1 and m_2 [see Eq. (A.1.4)].

An interesting feature of the portal interaction [see Eq. (4.2.8)] is that it leads to a decay of the dark nucleon into a pair of the dark pion and the SM neutrino. Although the predicted lifetime of the dark nucleon is much longer than the age of the Universe, the dark nucleon decay is constrained by the measurements of the neutrino flux by the Super-Kamiokande (SK) experiment [107, 108]. Following the analysis of Ref. [106], the decay rate caused by the portal operator is estimated to be

$$\Gamma_{n' \to \pi^{0\prime} \bar{\nu}} = \frac{3v^2 m_{n'}}{64\pi M_{\mathrm{portal}}^6} |W_0(0)|^2 \left(1 - \frac{m_{\pi'}^2}{m_{n'}^2} \right)^2 , \tag{4.2.10}$$

where the form factor is estimated as $W_0(0) \sim 0.1 \, \mathrm{GeV}^2 (m_{n'}/1 \, \mathrm{GeV})^2$. From the experimental result of Ref. [107, 108], we obtain the lower limit on the portal scale from below as $M_{\mathrm{portal}} \gtrsim 10^9 \, \mathrm{GeV}$ (see also Ref. [109]). The dark proton does not mix with the dark neutron when the dark Higgs boson has a $\mathrm{U}(1)_D$ charge of -2, since the $\mathbb{Z}_2$ subgroup of $\mathrm{U}(1)_D$ remains unbroken. When the dark Higgs boson charge is -1, on the other hand, the dark proton slightly mixes with the dark neutron. In the following, we consider the model with the dark Higgs charge of -2, although the case with the dark Higgs charge of -1 is also a viable option as discussed in appendix A.2.

As another interesting feature of the model, the dark proton has a coupling to the SM fermions through the dark photon, with which DM can be searched. As the dark neutron does not couple to the dark photon, the expected event rate of the DM direct detection depends on the dark proton fraction in DM. The dark proton fraction is determined by the dark nucleon inelastic scattering with the dark pion, which freezes out when the dark pions annihilate into the dark photons, $T_{\gamma'} \sim m_{\pi'}/20\text{–}30$. Resultantly, the

dark proton fraction is given by

$$\frac{n_{p'}}{n_{n'} + n_{p'}} = \frac{1}{\exp\left[-(m_{n'} - m_{p'})/T_{\gamma'}\right] + 1}.\qquad(4.2.11)$$

Since the n'–p' mass difference, $m_{n'} - m_{p'} = \mathcal{O}(m_{1,2})$, is basically smaller than the dark pion mass, $m_{\pi'} = \mathcal{O}(\sqrt{m_{1,2}\Lambda_{\mathrm{QCD'}}})$ (see appendix A.1), we consider that p' accounts for half of DM. [8]

Following the analysis in Ref. [117], we place the upper bound on ϵ on the dark photon parameter from the 54 ton×day exposure of PandaX-II [71] on the left panel in Fig. 4.1 (red lines). With this exposure, no signal candidates were observed while the expected background in the signal region was 1.8 ± 0.5. This leads to an upper limit of 0.63 signal events in the signal region at 90% CL. We also show a similar limit from XENON1T experiment [66] on the right panel in Figure 4.1. We see that the constraint from XENON1T is slightly tighter, though this limit is easily changed by tuning the dark gauge coupling, α_D. Similar constraints are expected from the results of LUX [69]. The direct detection experiment constraint is severer than that from SN 1987A for the QED$'$ fine-structure constant $\alpha_D = \alpha$. For $\alpha_D = \alpha$ and $m_{\gamma'} \lesssim 100\,\mathrm{MeV}$, a large portion of the parameter region can be tested by future experiments such as XENONnT [118], LZ [119], and Darwin [120]. With a light mediator, $m_{\gamma'} \lesssim 100\,\mathrm{MeV}$, the nuclear recoil energy spectrum of DM scattering is distinguishable from that of the neutrino background [121].

Finally, let us comment on the constraint of the DM scattering. The dark photon exchange can cause the velocity independent self-interaction cross section $\sigma_0/m_{\mathrm{DM}} \sim 4\pi\alpha_D^2 m_{\mathrm{DM}}/m_{\gamma'}^4$, which is of $\mathcal{O}(0.01\text{–}0.1)\,\mathrm{cm}^2/\mathrm{g}$. This cross section is consistent with the constraints, $\sigma_0/m_{\mathrm{DM}} \lesssim 0.1\text{–}1\mathrm{cm}^2/\mathrm{g}$, obtained from the galaxy clusters [122, 123, 124, 125, 126, 127, 128, 129, 130], and, $\sigma_0/m_{\mathrm{DM}} \lesssim 0.01\text{–}0.1\mathrm{cm}^2/\mathrm{g}$, obtained from the ultra-faint dwarf galaxies [131, 132]. Even if we consider self scattering induced by the QCD$'$, the geometric cross section, $\sigma_0/m_{\mathrm{DM}} = 4\pi/m_{\mathrm{DM}}^3 \sim 10^{-5}\mathrm{cm}^2/\mathrm{g}$, satisfies these constraints. This is true for the models which we will consider in the following chapters.

---

[8]If the dark photon mass is smaller than the dark deuterium binding energy, the dark nucleosynthesis could proceed [110, 111, 112, 113, 114, 115, 116] and significantly change direct detection signals. If one estimates the dark deuterium binding energy as $B_{d'} \sim B_d \times \Lambda_{\mathrm{QCD'}}/\Lambda_{\mathrm{QCD}}$ with the SM value, $B_d \simeq 2.2\,\mathrm{MeV}$, the direct detection constraint would differ from our analysis for $m_{\gamma'} \lesssim 20\,\mathrm{MeV}$.

Chapter 5

Effect of Majorana Mass on ADM

In the last chapter, we constructed the concrete model of composite ADM and consider the constraints from direct detection experiments and CMB observations. In general ADM models, because the anti-DM rarely remains in the late Universe, we expect indirect detection signals are so rare to observe and usually we do not consider the constraint from indirect detections. However, with a tiny Majorana mass, the DM can be converted into anti-DM through late time oscillation and induce a pair-annihilation of ADM at late times [133, 134, 135, 136, 137, 138, 139]. A pair of DM particles and the antiparticle annihilates into multiple dark pions, and the (neutral) dark pion subsequently decays into a pair of dark photons. The dark photon eventually decays into an electron-positron pair. Thus, the late time annihilation of ADM results in multiple soft electrons/positrons. In addition, soft photons are also emitted as final state radiation. This annihilation signal may constrain the ADM model discussed in the previous chapter.

A higher dimensional operator which induces a Majorana mass in the dark baryons can washout the $B - L$ asymmetry generated via the leptogenesis. For the leptogenesis to be successful, the $B - L$ breaking higher dimensional operator is required to be sufficiently suppressed by a large mass scale.

In this chapter, we consider the constraints on the $B - L$ breaking higher dimensional operator from cosmological requirements and indirect detection experiments such as the searches for the γ-ray from the dwarf spheroidal galaxies (dSphs) by the Fermi-LAT and the interstellar electron/positron flux detection by the Voyager-1.

The organization of this chapter is as follows. In section 5.1, we briefly review the composite ADM model constructed in chapter 4 and introduce the higher dimensional operator which induces a Majorana mass term in the dark neutron and consider a requirement from successful leptogenesis. In

section 5.2, we derive the expected γ-ray flux from the dSphs and discuss the constraints on the model by comparing the flux with the Fermi-LAT results. We also estimate the interstellar electron/positron flux in cosmic rays from the late time annihilation and compare it with the Voyager-1 result. The final section is devoted to the conclusions. The content of this chapter is based on Ref. [2].

5.1 DM anti-DM oscillation in the composite ADM model

5.1.1 Simplified Model with Majorana Mass

As we saw, for successful ADM models, we need a $B - L$ breaking effect such as a large Majorana mass of the right-handed neutrino to invoke an asymmetry in the dark sector. Thus, when we consider higher dimensional operators, there can be other $B - L$ breaking terms and they might induce a small Majorana mass in the lightest dark baryon. Because we consider the baryogenesis, there should be a $B - L$ violation term. Thus, we cannot deny that there is a Majorana mass term in the dark hadron sector. From now on, we consider a simplified model wherein the DM has a tiny Majorana mass term induced by a higher dimensional operator.

We assume the $B - L$ portal interaction,

$$\mathcal{L}_{B-L\,\text{portal}} = \frac{1}{M_{\text{portal}}^3}(U'D'D')(LH)\,, \tag{5.1.1}$$

and dimension 9 operator,

$$\mathcal{L}_{\text{Majorana}} = \frac{1}{\Lambda_{\text{Majorana}}^5}(U'D'D')^2\,, \tag{5.1.2}$$

which induce the Majorana mass term of dark neutrons at the energy scale below $\Lambda_{\text{QCD}'}$,

$$\frac{1}{\Lambda_{\text{Majorana}}^5}(U'D'D')^2 \to \frac{\Lambda_{\text{QCD}'}^6}{\Lambda_{\text{Majorana}}^5}n'n'\,. \tag{5.1.3}$$

Here, the factor $\Lambda_{\text{QCD}'}^6$ comes from a dimensional ground. The late time oscillation of n' into $\bar{n}'$ induced by the Majorana mass leads to pair annihilation signals. Obviously, this term violates $B - L$ symmetry and thus it can wash out the $B - L$ asymmetry produced by baryogenesis or leptogenesis.

5.1.2 Leptogenesis and Washout by Majorana mass

The Majorana mass term (5.1.2) violates the $B - L$ conservation, thus if the processes induced by this term are active enough to maintain thermal

equilibrium, it leads to asymmetry washout. We roughly estimate the temperature at which these interactions are inactive as,

$$\frac{T_{\text{Majo}}^{11}}{\Lambda_{\text{Majorana}}^{10}} = H(T_{\text{Majo}}) \sim \frac{T_{\text{Majo}}^2}{M_{\text{Pl}}} . \tag{5.1.4}$$

Thus, if we denote the temperature at which the leptogenesis efficiently produces $B-L$ asymmetry as T_{lepto} these two temperatures must satisfy $T_{\text{Majo}} > T_{\text{lepto}}$ not to harm the leptogenesis scenario. At the same time, the portal operator must be kept efficient until the temperature drops below T_{lepto}. This condition is given by $T_{\text{portal}} < T_{\text{lepto}}$, where the portal decoupling temperature T_{portal} is determined by

$$\frac{T_{\text{portal}}^7}{M_{\text{portal}}^6} \sim \frac{T_{\text{portal}}^2}{M_{\text{Pl}}} . \tag{5.1.5}$$

These conditions combined, the energy scales must satisfy

$$M_{\text{portal}} \left(\frac{M_{\text{portal}}}{M_{\text{Pl}}} \right)^{1/5} < T_{\text{lepto}} < \Lambda_{\text{Majorana}} \left(\frac{\Lambda_{\text{Majorana}}}{M_{\text{Pl}}} \right)^{1/9} . \tag{5.1.6}$$

First, we consider the case that we adopt the thermal leptogenesis scenario. As we saw in the last chapter, the portal scale is bounded from below, $M_{\text{portal}} > 10^9 \, \text{GeV}$. This bound satisfies the above condition for $T_{\text{lepto}} \sim M_R \gtrsim 10^9 \, \text{GeV}$. From the inequality of the left-hand side, $\Lambda_{\text{Majorana}} \gtrsim 10^{10} \, \text{GeV}$.

Moreover, we have to care about the effect of the dark neutron decay induced by the portal interaction. As we saw in chapter 4, the decay process $n' \to \pi^{0\prime} + \bar{\nu}$ is possible due to the $B-L$ portal operator. The decay rate can be estimated as in Eq.(4.2.10). The produced $\pi^{0\prime}$ eventually decays into two dark photons and these dark photons finally decay into two pairs of electrons and positrons. This cascade process can affect the CMB polarization spectrum due to the CMB ionization. We estimate this effect via the analysis depicted in Ref. [140]. For 95% confidence level, the lifetime of the dark scalar is limited as

$$\tau \gtrsim f_X g_{\text{eff}} \times 2.6 \times 10^{25} \, \text{sec} , \tag{5.1.7}$$

where f_X is the energy fraction of the DM which participates in the decay and g_{eff} is the function provided in Ref. [140], which depends on the energy injected into the SM plasma, the lifetime of the DM, τ, and the decay channel. This analysis results in a lower bound on the lifetime of n', $\tau_{n'} \gtrsim 10^{24.4} \, \text{sec}$ for $m_{n'} = 8.5 \, \text{GeV}, m_{\pi'} = 1 \, \text{GeV}, m_{\gamma'} = 40 \, \text{MeV}$, which corresponds to the lower limit on $M_{\text{portal}} \gtrsim 10^9 \, \text{GeV}$ and comparable to the limit from Super-Kamiokande experiment.

However, these bounds can be evaded by modifying the portal interaction and the baryogenesis scenario in the following way. By imposing a $\mathbb{Z}_2$ matter parity under which only the dark quarks flip their sign, $U', D' \to -U', -D'$, we find that the lowest dimensional portal operator,

$$\mathcal{L}_{\text{portal}}^{\text{new}} = \frac{1}{M_{\text{portal}}^{10}}(U'D'D')^2(LH)^2 \,. \tag{5.1.8}$$

This operator does not cause dark neutron decay but pair annihilation, $n' + n' \to \nu + \nu$. The bound on M_{portal} comes from the neutrino signal in Super-Kamiokande, which places an upper bound on the annihilation cross section as $\langle \sigma v \rangle \lesssim 10^{-24}\,\text{cm}^3\text{s}^{-1}$ [141]. From a dimensional analysis, we can estimate that the annihilation cross section induced by the new portal operator is

$$\sigma \sim \frac{v^4}{M_{\text{portal}}^{20}}m_{n'}^{14} \,, \tag{5.1.9}$$

thus even if we take the portal scale as law as the electroweak scale, $M_{\text{portal}} = \mathcal{O}(100)\,\text{GeV}$, this bound can be easily avoided. This means that we can combine non-thermal leptogenesis via inflaton decay [142], in which we can take the leptogenesis temperature as law as $T_{\text{lepto}} \gtrsim 10^6\,\text{GeV}$ [143]. Under this construction, the portal decoupling temperature must satisfy

$$T_{\text{portal}} = M_{\text{portal}}(M_{\text{portal}}/M_{\text{Pl}})^{1/19} \lesssim 10^6\,\text{GeV} \,, \tag{5.1.10}$$

which means $M_{\text{portal}} \lesssim 10^6\,\text{GeV}$.

Since the bound on T_{lepto} is loosened, we can take the Majorana mass scale as $\Lambda_{\text{Majorana}} \gtrsim 10^7\,\text{GeV}$. Although we take $\Lambda_{\text{Majorana}} = 10^{10}\,\text{GeV}$ as a benchmark point, we continue our analysis for the annihilation signal keeping the above modification as an option for the portal operator.

5.2 Gamma-ray and Electron/Positron Fluxes

As we have seen in the previous section, the dark neutron obtains a Majorana mass when the portal operator is generated in association with the seesaw mechanism. Due to the Majorana mass of the dark neutron, the dark neutron can oscillate into the anti-dark neutron. The typical time scale of the oscillation, $t_{\text{osc}} = m_M^{-1}$, is estimated as

$$t_{\text{osc}} \simeq 1 \times 10^{24}\,\text{sec} \left(\frac{\Lambda_{\text{QCD}'}}{2\,\text{GeV}}\right)^{-6} \left(\frac{\Lambda_{\text{Majorana}}}{10^{10}\,\text{GeV}}\right)^5 \,. \tag{5.2.1}$$

We now see that some fraction of n' can convert into $\bar{n}'$ at a late time, and then n'/p' and $\bar{n}'$ annihilate into the dark pions. The neutral dark pions

decay into the dark photons, and the dark photons finally decay into e^+e^- pairs. γ can be also emitted by the final state radiation (FSR) process as depicted in figure 5.1. In this section, we discuss the constraints on the late-time annihilation from the observations of the γ-ray from the dSphs and the interstellar $e^+ + e^-$ flux.

5.2.1 Gamma-ray flux from the Dwarf Spheroidal Galaxies

The γ-ray signal is one of the most promising channels to search for dark matter annihilation (e.g., [144, 145] for review). In particular, dSphs in our galaxy are the ideal targets to search for the γ-ray signal, since they have high dynamical mass-to-light ratios, $(M/L \sim 10 - 1000)$, while they lack contaminating astrophysical γ-ray sources [146, 147]. In this subsection, we estimate the γ-ray fluxes from the dSphs and compare them with the upper limits on the fluxes put by the Fermi-LAT.

First, we calculate the γ-ray spectrum at production by the $n'\bar{n}'$ annihilation processes:

$$n'\bar{n}' \to m\pi'^0 + l\pi'^+ + l\pi'^- , \quad (m, l = 0, 1, 2, \cdots) . \tag{5.2.2}$$

The cascade spectrum can be calculated by using the technique developed in [148, 149, 150].

We start to calculate the γ-ray spectrum at the rest frame of γ'. For $m_{\gamma'} \gg m_e$, the spectrum is given by the Altarelli-Parisi approximation formula [148],[1]

$$\frac{d\tilde{N}_\gamma}{dx_0} = \frac{\alpha}{\pi} \frac{1 + (1 - x_0)^2}{x_0} \left[-1 + \ln \left(\frac{4(1 - x_0)}{\epsilon_0^2} \right) \right] , \tag{5.2.3}$$

where $\epsilon_0 = 2m_e/m_{\gamma'}$ and $x_0 = 2E_0/m_{\gamma'}$ with E_0 being the energy of γ at the rest frame of γ'. α denotes the fine structure constant of SM QED.

The next step is to translate the spectrum in the rest frame of γ' to that in the rest frame of π'^0. For the case where $m_{\pi'} \gg m_{\gamma'}$, the spectrum is calculated as

$$\frac{d\tilde{N}_\gamma}{dx_1} = 2 \int_{x_1}^1 \frac{dx_0}{x_0} \frac{d\tilde{N}_\gamma}{dx_0} f \left(\frac{2x_1}{x_0} - 1 \right) + \mathcal{O} \left(\frac{m_{\gamma'}^2}{m_{\pi'}^2} \right) , \tag{5.2.4}$$

where $x_1 = 2E_1/m_{\pi'}$ with E_1 being the energy of γ at the rest frame of π'. The function f represents the effect of the anisotropy of the γ' decay. According to [151, 149], we take

$$f(\cos\theta) = \frac{3}{8}(1 + \cos^2\theta) , \tag{5.2.5}$$

---

[1]In the appendix B.1, we compare the direct calculation of the FSR with the Altarelli-Parisi approximation formula, and confirm the validity of the approximation in the parameter region we are interested in.
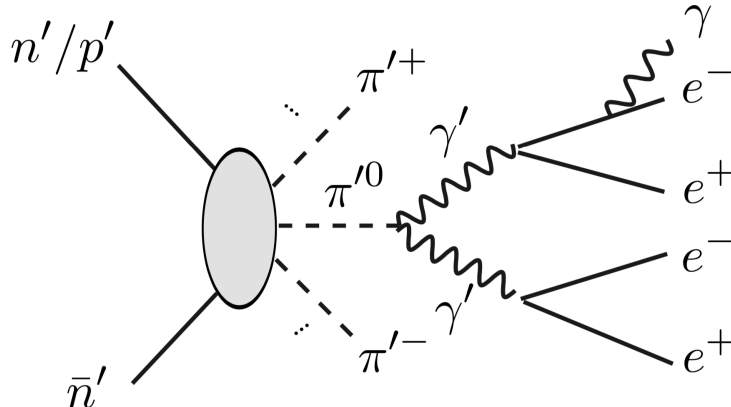
Figure 5.1: ADM annihilation which happens at late time: $\bar{n}'$ can be generated from the ADM oscillation. Once the $\bar{n}'$ is generated, dark nucleons (n'/p') and $\bar{n}'$ annihilate into dark pions ($\pi'^{\pm}$ and π'^0). π'^0 subsequently decays into a pair of dark photons (γ'). γ' eventually decays into $e^+ + e^-$, and emits γ through the FSR process.

with θ being the angle between the γ emission line and the boost axis of γ'. Note that the angle θ is kinematically constrained as

$$\cos\theta = \frac{2x_1}{x_0} - 1 + \mathcal{O}\left(\frac{m_{\gamma'}^2}{m_{\pi'}^2}\right) \; . \tag{5.2.6}$$

This is the reason why we put $f(2x_1/x_0 - 1)$ in Eq. (5.2.4).

We next translate the spectrum Eq. (5.2.4) to that in the center of mass (CM) frame for the ADM annihilation. In order to do that, we need to know how much π'^0 is boosted. If the total number of the dark pions is two ($m + 2l = 2$), we can exactly know the energy/boost of the dark pions since they should be emitted back to back in the CM frame. In this case, the γ spectrum is calculated as

$$\frac{d\tilde{N}_\gamma^{(m,l)}}{dx_2} = 2 \int_{x_2}^{1} \frac{dx_1}{x_1} \frac{d\tilde{N}_\gamma}{dx_1} + \mathcal{O}\left(\frac{m_{\pi'}^2}{m_{\text{DM}}^2}\right) \; , \quad \text{for} \; m + 2l = 2 \; , \tag{5.2.7}$$

where $x_2 = E_2/m_{\text{DM}}$ with E_2 being the energy of γ at the CM frame.

On the other hand, in the case of $m + 2l \geq 3$, it becomes highly non-trivial to know how much the π'^0 can be boosted even when we assume that the matrix element of the annihilation is constant as a function of the final state momenta. This is because, in this case, the energy spectrum of the dark pion is given as

$$\frac{dN_{\pi'}}{d\xi} = \frac{1}{R_n} \frac{dR_n}{d\xi} \; , \tag{5.2.8}$$

44

where $\xi = E_{\pi'}/m_{\rm DM}$ and R_n is the $n = m + 2l$ body phase space integration [152]. $E_{\pi'}$ denotes the energy of the dark pion in the CM frame. In general, it is difficult to perform the phase space integration for $n \geq 3$. However, as discussed in [152, 150], under the assumption that $m_{\pi'^0} = m_{\pi'^+} \equiv m_{\pi'} \ll m_{\rm DM}$, we can perform the phase space integrations analytically as

$$\frac{dN_{\pi'}}{d\xi} = (n-1)(n-2)(1-\xi)^{n-3}\xi + \mathcal{O}\left(\frac{m_{\pi'}^2}{m_{\rm DM}^2}\right), \qquad (5.2.9)$$

for $n = m + 2l \geq 3$. Using the results, we finally obtain

$$\frac{d\tilde{N}_\gamma^{(m,l)}}{dx_2} = 2(n-1)(n-2)\int_{x_2}^1 d\xi (1-\xi)^{n-3} \int_{x_2/\xi}^1 \frac{dx_1}{x_1}\frac{d\tilde{N}_\gamma}{dx_1} + \mathcal{O}\left(\frac{m_{\pi'}^2}{m_{\rm DM}^2}\right),$$
$$(5.2.10)$$

for $n = m + 2l \geq 3$ where we assume $m_{\pi'^0} = m_{\pi'^+} \equiv m_{\pi'}$.

Finally, we sum over the possible intermediate states and take into account the number of the final states. It turns out that the total γ spectrum from the $n'\bar{n}'$ annihilation is expressed as

$$\frac{dN_\gamma^{(n'\bar{n}')}}{dx_2} = \sum_{m,l} 2m\left(\mathrm{Br}^{(n'\bar{n}')}(m,l)\frac{d\tilde{N}_\gamma^{(m,l)}}{dx_2}\right), \qquad (5.2.11)$$

where $\mathrm{Br}^{(n'\bar{n}')}(m,l)$ denotes the branching ratio for the $n'\bar{n}' \to m\pi'^0 + l\pi'^+ + l\pi'^-$ annihilation process. The factor $2m$ corresponds to the number of e^+e^- pairs in the annihilation process.

In the same way, we can estimate the γ spectrum from the $p'\bar{n}'$ annihilation processes:

$$p'\bar{n}' \to m\pi'^0 + l\pi'^+ + (l-1)\pi'^- , \quad (m = 0, 1, 2, \cdots, l = 1, 2, \cdots). $$
$$(5.2.12)$$

The γ spectrum is calculated as

$$\frac{dN_\gamma^{(p'\bar{n}')}}{dx_2} = \sum_{m,l} 2m\left(\mathrm{Br}^{(p'\bar{n}')}(m,l)\frac{d\tilde{N}_\gamma^{(m,l)}}{dx_2}\right), \qquad (5.2.13)$$

with replacing $n = m+2l$ by $n = m+2l-1$ in the calculation of $d\tilde{N}_\gamma^{(m,l)}/dx_2$.

In the following analysis, we simply assume that the branching ratio of the dark nucleon annihilation can be estimated as that of nucleon-antinucleon annihilation. According to [153], we approximate the branching ratios by

45

the fireball model,[2]

$$\mathrm{Br}^{(n'\bar{n}')}(m,l) = \frac{2\alpha^{2l}}{(1+\alpha)^n + (1-\alpha)^n} \, {}_nC_{2l} \, P_n \, , \quad \text{with} \ \ n = m + 2l \, ,$$

(5.2.14)

$$\mathrm{Br}^{(p'\bar{n}')}(m,l) = \frac{2\alpha^{2l-1}}{(1+\alpha)^n + (1-\alpha)^n} \, {}_nC_{2l-1} \, P_n \, , \quad \text{with} \ \ n = m + 2l - 1 \, ,$$

(5.2.15)

where

$$P_n = \frac{1}{\sqrt{2\pi}\sigma} \exp\left(-\frac{(n - \langle n \rangle)^2}{2\sigma^2}\right) \, ,$$

(5.2.16)

with $a = 1/4$, $\langle n \rangle = 5.05$, $\sigma^2 = a\langle n \rangle$ and

$$\alpha = \begin{cases} \sqrt{2} & \text{for} \ \ n = 2 \, , \\ 1.5 & \text{for} \ \ n \neq 2 \, . \end{cases}$$

(5.2.17)

We are now ready to estimate the γ-ray spectrum emitted from the ADM annihilation. Figure 5.2 shows the value of the γ-ray spectrum. Here, we take $m_{\mathrm{DM}} = 10\,\mathrm{GeV}$, $m_{\pi'} = 1\,\mathrm{GeV}$ and $m_{\gamma'} = 40\,\mathrm{MeV}$. The black solid and the dashed lines correspond to the spectra predicted from the $n'\bar{n}'$ and $p'\bar{n}'$ annihilation, respectively. In the analysis, we ignore the contributions from the annihilation with large (m,l) since the branching ratios of them are much suppressed. We stop taking the sum over (m,l) if the size of the contribution is less than 1% of the total amount.

The figure shows that the ADM annihilation predicts the continuous γ-ray spectrum peaked at the energy of $\mathcal{O}(m_{\mathrm{DM}}/10)$. This is expected as the typical number of the dark pions for annihilation is five, and the neutral dark pion decays into two pairs of e^+e^-.

It should be reminded that the γ-ray emission from the ADM annihilation can happen at the present universe since the ADM oscillation effectively happens at the late time scale. The ADM signals can therefore be tested by γ-ray telescope experiments from nearby sources while evading the constraints from the observations of the cosmic microwave observations (see e.g. [150]).

The γ-ray flux from the dSphs for an energy bin from $E_{\min}$ to $E_{\max}$ is calculated as

$$\Phi = \int_{E_{\min}}^{E_{\max}} dE E \int_{\Delta\Omega} \frac{d\Omega}{4\pi} \int_{\mathrm{l.o.s.}} dl \left(n_{n'}n_{\bar{n}'} \langle\sigma v\rangle_{n'\bar{n}'} \frac{dN_\gamma^{(n'\bar{n}')}}{dE} + n_{p'}n_{\bar{n}'} \langle\sigma v\rangle_{p'\bar{n}'} \frac{dN_\gamma^{(p'\bar{n}')}}{dE} \right) \, ,$$

(5.2.18)

---

[2]In this approximation, the Parity violating mode, $(m,l) = (2,0)$, is allowed, although it is not significant numerically.
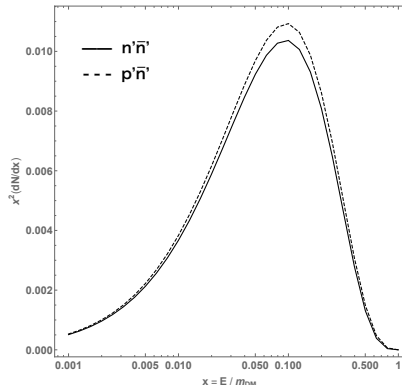
Figure 5.2: The γ-ray spectrum at production from the $n'\bar{n}'$ (Solid line) and $p'\bar{n}'$ (Dashed line) annihilation. We take $m_{\pi'} = 1\,\mathrm{GeV}$ and $m_{\gamma'} = 40\,\mathrm{MeV}$.

where we perform the integrations over a solid angle, $\Delta\Omega$, and the line-of-sight (l.o.s.). Here n_i and $\langle\sigma v\rangle_{ij}$ denote the number density of a particle i at the dSphs and the kinematically averaged cross section for ij annihilation, respectively. $N_\gamma^{(n'\bar{n}')}$ and $N_\gamma^{(p'\bar{n}')}$ are the photon spectra from $n'\bar{n}'$ and $p'\bar{n}'$ annihilation which can be calculated from Eqs. (5.2.11) and (5.2.13), respectively.

It should be noted that the total amount of the γ-ray flux can be large enough to be tested by the γ-ray searches on the dSphs although the flux is suppressed by the factor,

$$\frac{n_{\bar{n}'}}{n_{n'}} \simeq \left(\frac{t_0}{t_{\mathrm{osc}}}\right)^2$$

$$\simeq 1.7 \times 10^{-13} \left(\frac{\Lambda_{\mathrm{QCD}'}}{2\,\mathrm{GeV}}\right)^{12} \left(\frac{\Lambda_{\mathrm{Majorana}}}{10^{10}\,\mathrm{GeV}}\right)^{-10} . \tag{5.2.19}$$

where $t_0 \simeq 4.3 \times 10^{17}\,\mathrm{sec}$ is the age of the universe. This is because the thermally-averaged cross section can be large due to the strong interaction. In the following analysis, we take the annihilation cross sections to be

$$\langle\sigma v\rangle_{n'\bar{n}'} = \langle\sigma v\rangle_{p'\bar{n}'} = \frac{4\pi}{m_{\mathrm{DM}}^2} , \tag{5.2.20}$$

to give a rough estimation. Such a large annihilation cross section multiplied by the relative velocity is supported by the cross section measurements of the non-relativistic nucleon and anti-nucleon annihilation [154, 155] (see also [156, 157]).[3]

_____

[3]The cross section multiplied by the relative velocity in Eq. (5.2.20) is much smaller
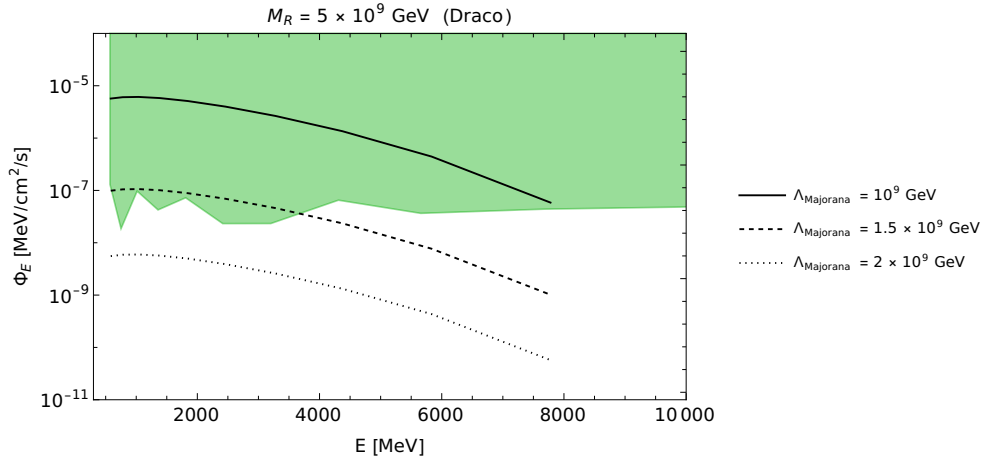
Figure 5.3: The predicted γ-ray flux from the Draco dSph and the 95% C.L. upper bound obtained by the Fermi-LAT (green shaded region). The black solid, dashed, and dotted lines correspond to the γ-ray flux when we take $\Lambda_{\text{Majorana}} = 10^9\,\text{GeV}$, $1.5 \times 10^9\,\text{GeV}$, and $2 \times 10^9\,\text{GeV}$, respectively. Here, we assume $m_{n'} = m_{p'} = m_{\text{DM}} = 10\,\text{GeV}$ and fix $m_{\pi'} = 1\,\text{GeV}$, $M_R = 5 \times 10^9\,\text{GeV}$ and $m_{\gamma'} = 40\,\text{MeV}$. For the the detail of the calculation, see equations from (5.2.2) to (5.2.18).

In Figure 5.3, we show the predicted γ-ray flux from the Draco dSph. The black solid, dashed, and dotted lines correspond to the γ-ray flux when we take $\Lambda_{\text{Majorana}} = 10^9\,\text{GeV}$, $1.5 \times 10^9\,\text{GeV}$, and $2 \times 10^9\,\text{GeV}$, respectively. Here, we assume $m_{n'} = m_{p'} = m_{\text{DM}} = 10\,\text{GeV}$ and fix $m_{\pi'} = 1\,\text{GeV}$ and $m_{\gamma'} = 40\,\text{MeV}$. To obtain the predicted γ-ray spectrum, we use the J-factors estimated in [79] which takes into account the effects of the non-sphericity of the dSphs.[4] The green line corresponds to the upper bound (95% C.L.) on the γ-ray flux based on the 6 years of Pass 8 data by the Fermi-LAT collaboration [159]. The figure shows that the γ-ray flux from the late-time annihilation becomes comparable to the upper limit on the observed flux for $\Lambda_{\text{Majorana}} = \mathcal{O}(10^9)\,\text{GeV}$, which corresponds to the oscillation time scale of $t_{\text{osc}} = \mathcal{O}(10^{21})\,\text{sec}$. We discuss the constraints on the model parameters by the Fermi-LAT in subsection 5.2.3.

---

than the unitarity limit.

In Appendix B.2, we discuss the Sommerfeld enhancement effects by the exchange of the dark pions. There, we find that the enhancement effects are not significant in the present setup.

[4] As for the J-factor of the Ursa Minor classical dSphs, we use the value given in [158] as it is not analyzed in [79].
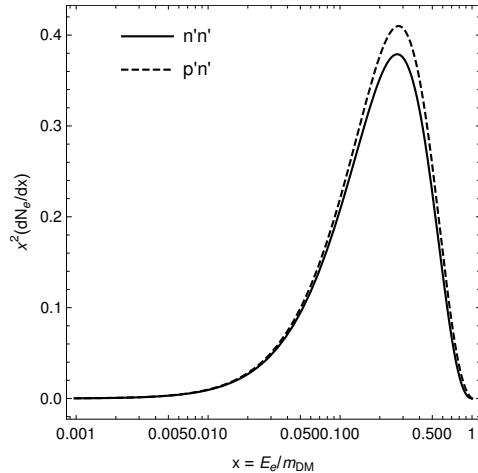
Figure 5.4: The e^-/e^+ spectrum predicted from the $n'\bar{n}'$ (Solid line) and $p'\bar{n}'$ (Dashed line) annihilation for $m_e \ll m_{\gamma'} \ll m_{\pi'} \ll m_{\mathrm{DM}}$.

5.2.2 Interstellar Electron/Positron Flux

The Fermi-LAT observation does not constrain the late-time annihilation for $m_{\mathrm{DM}} \lesssim 3\,\mathrm{GeV}$, since the Fermi-LAT is sensitive to the γ-ray with energy higher than $500\,\mathrm{MeV}$[5]. For such a rather light ADM, the most stringent constraint is put by the observation of the interstellar $e^+ + e^-$ flux by the Voyager-1 [160, 84] (see also [161]). In this subsection, we estimate the $e^+ + e^-$ flux from the late-time annihilation in the Milky Way.

The energy spectrum of $e^+ + e^-$ at production by the late-time ADM annihilation is obtained by replacing $d\tilde{N}_\gamma/dx_0$ in Eq. (5.2.3) with the e^+/e^- spectrum in the dark photon rest frame,

$$\frac{d\tilde{N}_e}{dx_0} = \delta(x_0 - 1) \ . \tag{5.2.21}$$

Here, $x_0 = 2E_0/m_{\gamma'}$ with E_0 being the energy of either e^- or e^+. By repeating the same analysis in the previous section, we can convert this spectrum to the one in the rest frame of the ADM annihilation. In Figure 5.4, we show the e^+/e^- spectrum at production for $m_e \ll m_{\gamma'} \ll m_{\pi'} \ll m_{\mathrm{DM}}$.

For a given e^+/e^- spectra at production, the interstellar $e^+ + e^-$ flux

---

[5]More precisely, the point-source function broadens below $500\,\mathrm{MeV}$, thus the event data between $500\,\mathrm{MeV}$ to $500\,\mathrm{GeV}$ are selected [159].
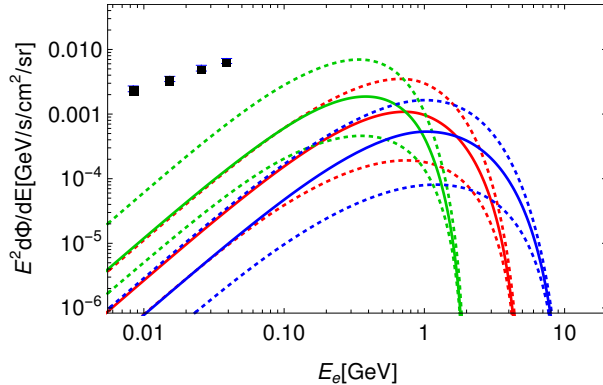
Figure 5.5: The interstellar $e^+ + e^-$ flux in cosmic ray at around the location of the Earth from the late-time ADM annihilation. The annihilation cross section and the oscillation time scale is taken to be $(t_0/t_{\rm osc})^2 \times \langle \sigma v \rangle = 1\,{\rm pb}$ ($t_{\rm osc} \gg t_0$). The green, red, and blue lines show the spectrum for $m_{\rm DM} = 3\,{\rm MeV}$, $5\,{\rm MeV}$, and $10\,{\rm MeV}$, respectively. The solid lines assume the MED propagation model, while the upper and the lower dotted lines assume the MAX and the MIN propagation models, respectively. The NFW halo profile is used.

around the location of the Earth is given by [162, 163],[6]

$$\frac{d\Phi}{dE_e} = \frac{1}{4\pi b(E)} \left(\frac{\rho_{\rm DM}}{m_{\rm DM}} \right)^2 \left(\frac{t_0}{t_{\rm osc}} \right)^2 \sum_{i=n'\bar{n}',p'\bar{n}'} \langle \sigma v \rangle_i \int_E^{E_{\rm DM}} dE_s \, I(E, E_s) \frac{dN_{e\,i}}{dE}(E_s) \ .$$

(5.2.22)

Here, $\rho_{\rm DM}$ denotes a local dark matter density at around the location of the Earth, $I(E, E_s)$ is a Green function which encodes the propagation of $e^{\pm}$ from a source with a given energy E_s to any energy E, and $b(E)$ is the $e^{\pm}$ energy loss function.[7]

In Figure 5.5, we show the interstellar $e^+ + e^-$ flux at around the location of the Earth from the late-time ADM annihilation. Here, the annihilation cross section and the oscillation time scale are set to be $(t_0/t_{\rm osc})^2 \times \langle \sigma v \rangle = 1\,{\rm pb}$. The Green function, $I(E, E_s)$, and the energy loss rate, $b(E)$, are those provided by [162, 163]. In the figure, the solid lines assume the MED propagation model, while the upper and the lower dotted lines assume the MAX and the MIN propagation models, respectively (see [164]). The dark matter profile is assumed to be the NFW profile [78],[8] with the local dark

---

[6]A typical propagation time of the cosmic ray to travel of $\mathcal{O}(1)\,{\rm kpc}$ is much shorter than the age of the universe.

[7]The Green function is dimensionless while $b(E)$ has a unit of GeV/sec which is typically $b(E) \simeq 10^{-(16-15)}\,{\rm GeV/sec}$ for $E = \mathcal{O}(10)\,{\rm MeV}$ to $\mathcal{O}(1)\,{\rm GeV}$ [162, 163].

[8]We numerically checked that the spectra are not significantly changed even for a cored Burkert profile [165], though they are slightly suppressed.
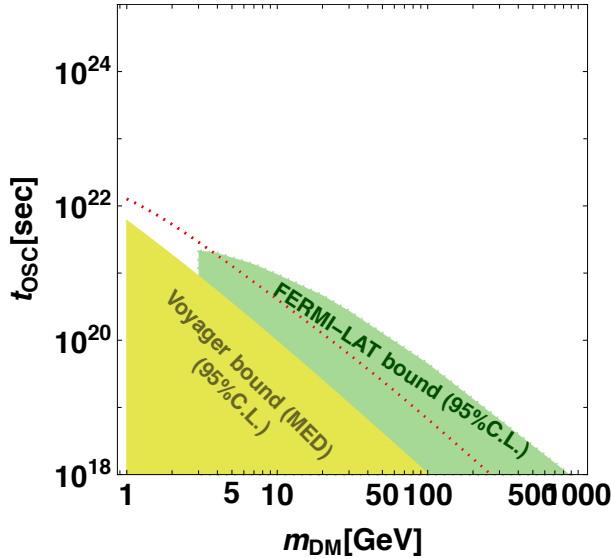
Figure 5.6: Constraints on the oscillation time scale. The green and the yellow shaded regions are excluded by the γ-ray constraint (Fermi-LAT), and by the constraint on the $e^+ + e^-$ flux (Voyager-1), respectively. We here assume $m_{n'} = m_{p'} = m_{DM}$ and take $n_{n'} = n_{p'}$. We also assume $m_{\pi'} \ll m_{DM}$ while fixing $m_{\gamma'} = 40\,\text{MeV}$. The red dotted line is a prospected lower limit by the γ-ray search from the dSphs by e-ASTROGAM in one year of effective exposure.

matter density at around the Earth to be $\rho_{DM} = 0.3\,\text{GeV/cm}^3$.

In the figure, we also show the interstellar $e^+ + e^-$ spectrum observed by the Voyager-1 [160, 84], where the data is taken from [166]. The figure shows that the $e^+ + e^-$ flux from the late-time ADM annihilation is much smaller than the observed flux for $(t_0/t_{osc})^2 \times \langle \sigma v \rangle = \mathcal{O}(1)\,\text{pb}$. We will summarize the constraints from the Voyager-1 in the next subsection.

5.2.3 Constraints on Parameter Space

As we have seen in the previous subsections, we can probe the time scale of the matter-antimatter oscillation by the γ-ray observation up to $t_{osc} = \mathcal{O}(10^{21})\,\text{sec}$ for $m_{DM} \simeq 10\,\text{GeV}$. This oscillation time scale corresponds to the effective annihilation cross section,[9]

$$\left(\frac{t_0}{t_{osc}}\right)^2 \langle \sigma v \rangle \sim 10\,\text{pb} \left(\frac{10\,\text{GeV}}{m_{DM}}\right)^2 \left(\frac{10^{21}\text{sec}}{t_{osc}}\right)^2 . \tag{5.2.23}$$

A lighter ADM can be also tested by the observation of the interstellar $e^+ + e^-$ flux.

---

[9]The effective cross section into the γ-ray is further suppressed by Eq. (5.2.3).

In Figure 5.6, we show the constraints on the oscillation time scale from the observations by the Fermi-LAT and the Voyager-1. Here, we assume $m_e \ll m_{\gamma'} \ll m_{\pi'} \ll m_{\mathrm{DM}}$ while we fix $m_{\gamma'} = 40\,\mathrm{MeV}$.[10] Although the typical mass range of the ADM is $m_{\mathrm{DM}} < \mathcal{O}(10)\,\mathrm{GeV}$, we show a wider mass range so that the result can be used for general models. The green region corresponds to the 95% C.L. excluded region from the Fermi-LAT observations (see also [167, 150]), where we take into account the γ-ray fluxes from the 8-classical dSphs. The yellow shaded region corresponds to the 95% C.L. excluded region from the Voyager-1 observation for the MED propagation model with the NFW dark halo profile. We see that for $m_{\mathrm{DM}} \simeq 5\text{--}10\,\mathrm{GeV}$, the more stringent constraints are put by the Fermi-LAT observation, where the oscillation time scale shorter than $t_{\mathrm{osc}} \sim 10^{21}\,\mathrm{sec}$ is excluded. For a lighter mass region, the Voyager-1 observation excludes the oscillation time scale shorter than $t_{\mathrm{osc}} \sim 10^{21-22}\,\mathrm{sec}$.

In Figure 5.7, we translate the constraints on the oscillation time scale to those on the parameters of the present model. In the figure, we consider $m_{\mathrm{DM}} = 2, 5, 10\,\mathrm{GeV}$. We also take $\Lambda_{\mathrm{QCD'}} = 2\,\mathrm{GeV} \times (m_{\mathrm{DM}}/10\,\mathrm{GeV})$ to mimic QCD for each choice of the dark matter mass. We also assume $m_e \ll m_{\gamma'} \ll m_{\pi'} \ll m_{\mathrm{DM}}$. The green and yellow shaded regions correspond the 95% C.L. excluded regions by the Fermi-LAT and the Voyager-1, respectively. The solid line corresponds to the lower limit on $\Lambda_{\mathrm{Majorana}}$, which comes from the requirement that the Majorana mass term does not wash out the $B - L$ asymmetry generated via the leptogenesis. Although the figure seems to suggest that the requirement from the leptogenesis constrains mass parameters is more stringent, we note that this bound can be avoided with the modification of the portal operator in Eq. (5.1.8). Thus, we should notice that the solid line is model-dependent.

Several comments are in order. In our discussion, we consider only the γ-ray emitted by the FSR. This should be justified as the γ-rays made by the Synchrotron radiation and the inverse Compton scattering from the sub-GeV e^+/e^- are very soft and below the Fermi-LAT sensitivity [162]. It should be also noted that the γ-ray signal from the galactic center does not lead to more stringent constraints, despite the signal strength being higher than that from the dSphs. This is because the γ-ray background is much higher for the galactic center, and hence, it is difficult to distinguish the continuous signal spectrum from the background spectrum.

Future γ-ray searches such as e-ASTROGAM [168, 169], SMILE [170], GRAINE [171], and GRAMS [172] projects will be important to test the model further. It should be emphasized that those experiments are sensitive to the MeV γ-rays, and hence, they are also able to constrain the ADM with a few GeV mass to which the Fermi-LAT loses sensitivity. In Figure 5.6,

---

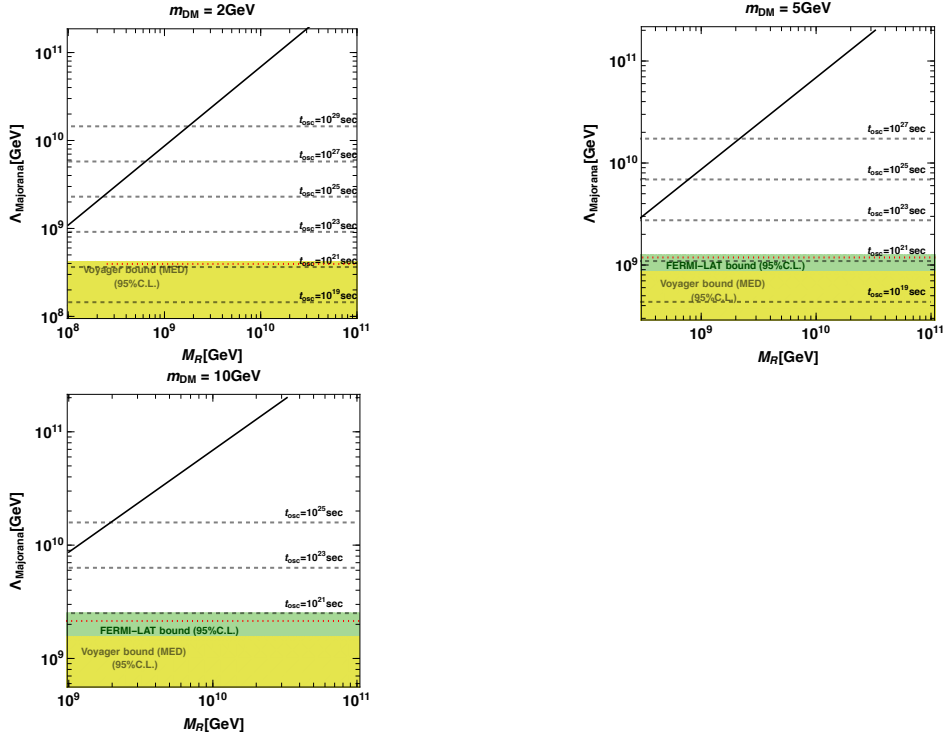[10]The constraints do not depend on $m_{\gamma'}$ significantly, as long as $m_e \ll m_{\gamma'} \ll m_{\pi'} \ll m_{\mathrm{DM}}$.

Figure 5.7: Constraint on our ADM scenario for $m_{\rm DM} = 2, 5, 10\,{\rm GeV}$. The green and yellow shaded regions correspond to the 95% C.L. excluded regions by the Fermi-LAT and the Voyager-1, respectively. The solid line corresponds to the lower bound of $\Lambda_{\rm Majorana}$ from Eq.(5.1.6). We also show the prospected limits by e-ASTROGAM translated from Figure 5.6 as red dotted lines.

we show the prospected lower limit on $t_{\rm osc}$ at 95%CL by the γ-ray search from the dSphs by e-ASTROGAM in one year of effective exposure. In our analysis, we used the effective area and the prospected sensitivities for a γ-ray flux from a point-like source at a high latitude (in Galactic coordinates) in [168]. The testable parameter region can be wider when the J-factors of the ultra-faint dSphs are determined more precisely by future spectroscopic observations such as the Prime Focus Spectrograph [173]. For example, if the J-factor of Triangulum II converges to the central value in [79], i.e. $\log_{10} J \simeq 20$, the prospected lower limit on $t_{\rm osc}$ becomes higher for about a factor of $2^{1/2}$.

Constraints on the DM scattering are the same as we discussed in the last paragraph in chapter 4 since we take similar values for the particle masses and the kinetic mixing parameter. Thus, we can say that the model is consistent with the astrophysical constraints [122, 123, 124, 125, 126, 127, 128, 129, 130, 131, 132] (see chapter 4).

Chapter 6

Chiral ADM Model

In this chapter, we construct a chiral composite ADM model where the $U(1)_D$ gauge symmetry is embedded into the chiral flavor symmetry. Due to the dynamical breaking of the chiral flavor symmetry, the model naturally provides the masses of the dark photon and the dark pions in the sub-GeV range, both of which play crucial roles for a successful ADM model.

As we saw in the previous chapters, the composite ADM models contain numerous particles since the models are based on the strong dynamics of a non-Abelian gauge theory. As repeatedly emphasized in this thesis, if the dark sector decouples from the visible sector, the lightest particles in the dark sector overclose the Universe or result in a too large contribution to the effective number of neutrinos, N_{eff} [14] (see also Ref. [101]). Therefore, we need a light portal particle that transfers the entropy of the dark sector into the visible sector to avoid the problems, and we have added a dark photon which has a kinetic mixing with QED photon.[1] We also have seen that the dark photon with a mass in the sub-GeV range successfully transfers the excessive energy density of the dark sector into the visible sector.

However, in the previous model, we assume that the dark photon mass is generated via the dark Higgs mechanism while the dark baryons obtain their mass by the dark QCD phase transition, thus there is no guarantee that the dark photon mass satisfies the inequality, $m_{\gamma'} < m_{\pi'} < m_{n',p'}$.

In this chapter, we construct a model that naturally provides the dark photon mass in the sub-GeV range while the mass of the composite ADM is in the GeV range. For this purpose, we rely on the dynamical generation of the dark photon mass proposed in Refs. [21, 22]. There, the $U(1)_D$ gauge symmetry is embedded into the chiral flavor symmetry. Due to the dynamical breaking of the chiral flavor symmetry, the model naturally provides the masses of the dark photon and the dark pions in the sub-GeV range.

---

[1]We assume that the two sectors are in thermal equilibrium at the temperature around the baryogenesis. It is also possible to avoid the problems without a portal particle if the dark sector temperature is lower than that of the visible sector when the lightest dark sector particle is massless.

The organization of the chapter is as follows. In Sec. 6.1, we first review the composite ADM model in chapter 4 and the mechanism in Refs. [21, 22] which gives the dark photon mass dynamically. Next, we apply this dynamical mechanism to a simple composite ADM model. Finally, we discuss a concrete example where the asymmetries in the dark sector and the visible sector are thermally distributed through higher-dimensional operators. In Sec. 6.2, we discuss the phenomenology of the models. The final section is devoted to our conclusions. The content of this chapter is based on Ref. [3].

6.1 MODEL

In this section, we first review the mechanism by which the dark photon obtains the mass dynamically. After that, we construct a chiral composite ADM model with two flavors of the dark quarks as a simple example. Finally, we construct a three-flavor model compatible with $B - L$ portal interactions which distribute a $B - L$ asymmetry between the visible sector and the dark sector. Hereafter, N_f represents the number of the flavors of dark quarks.

6.1.1 Dynamical Generation of Dark Photon Mass

In the model of chapter 4, We assumed that we introduce a Higgs boson or the Stückelberg mechanism [174] to produce the dark photon mass. In these models, however, we require parameter tuning so that the dark photon mass is of $\mathcal{O}(10\text{–}100)\,\mathrm{MeV}$ while the DM mass is of $\mathcal{O}(1)\,\mathrm{GeV}$. To avoid such parameter tuning, we apply a mechanism which generates a dark photon mass due to strong dynamics [21, 22]. In this subsection, we review the dynamical generation of the dark photon mass.

Let us continue to consider a model with $N_f = 2$ which has $\mathrm{SU}(3)_D \times \mathrm{U}(1)_D$ gauge symmetry as in the previous chapter. The charge assignment of $\mathrm{U}(1)_D$ is, on the other hand, changed to the one in Tab. 6.1. For $0 < a < 1$, the $\mathrm{U}(1)_D$ gauge symmetry is no more vector-like symmetry, and hence, the mass terms of U' and D' quarks are now forbidden. The $\mathrm{U}(1)_D$ gauge symmetry is free from gauge anomalies. The global $\mathrm{U}(1)_{B-L}$ symmetry, on the other hand, has the global anomaly of $\mathrm{U}(1)_{B-L} \times \mathrm{U}(1)_D^2$, although this does not affect the ADM scenario unless there is a dark helical magnetic field in the Universe (see, e.g., Ref. [175]).

The assumption of the chiral $\mathrm{U}(1)_D$ is crucial for the dynamical breaking of $\mathrm{U}(1)_D$, since the vector-like symmetry cannot be broken spontaneously by strong dynamics [176]. Note also that the $\mathrm{U}(1)_D$ gauge symmetry explicitly breaks the $\mathrm{SU}(2)'_L \times \mathrm{SU}(2)'_R$ flavor symmetry of the dark quarks into the third component of the dark isospin symmetry, $\mathrm{U}(1)'_3$. Hereafter, I'_3 refers to the charge under $\mathrm{U}(1)'_3$. The $\mathrm{SU}(2)'_L \times \mathrm{SU}(2)'_R$ flavor symmetry remains an approximate symmetry as long as the $\mathrm{U}(1)_D$ gauge interaction is perturbative.

	$SU(3)_D$	$U(1)_D$	$U(1)_{B-L}$	$U(1)'_3$
U'	**3**	1	1/3	1
D'	**3**	−1	1/3	−1
$\bar{U}'$	$\bar{\mathbf{3}}$	−a	−1/3	−1
$\bar{D}'$	$\bar{\mathbf{3}}$	a	−1/3	1

Table 6.1: *The charge assignment of the chiral composite ADM model. We take $0 < a < 1$, and hence, the $U(1)_D$ gauge symmetry is not vector-like. The $U(1)'_3$ symmetry is the third component of the dark isospin symmetry, $SU(2)'_V$.*

Below Λ'_D, the dark quark bilinears condense as follows,

$$\left\langle U'\bar{U}' + U'^\dagger \bar{U}'^\dagger \right\rangle = \left\langle D'\bar{D}' + D'^\dagger \bar{D}'^\dagger \right\rangle = \mathcal{O}\big(\Lambda'^3_D\big) \ . \qquad (6.1.1)$$

The condensate in this channel is expected to be favored than other channels such as $\langle U'\bar{D}' \rangle$ since this channel has the smallest $U(1)_D$ charge, that is $|1 - a| < |1+a|$, for $0 < a < 1$ [21]. These condensations spontaneously break the $U(1)_D$ gauge symmetry. Besides, they also break the approximate $SU(2)'_L \times SU(2)'_R$ flavor symmetry into the diagonal subgroup, $SU(2)'_V$. On the other hand, $U(1)_{B-L}$ is not broken by the condensations, and hence, $U(1)_{B-L}$ and $U(1)'_3$ are exact (accidental) symmetries up to $U(1)_D$ anomaly.[2]

Associated with spontaneous breaking of $SU(2)'_L \times SU(2)'_R$ into $SU(2)'_V$, there are three pseudo-Nambu-Goldstone (NG) bosons. The low energy effective theory of the NG bosons is well described by the matrix-valued SU(2) field,

$$U(x) = \exp\left[\frac{i}{f'_\pi} \sum_{i=1}^3 \pi'_i(x)\sigma_i\right] \ , \qquad (6.1.2)$$

where f'_π denotes the dark pion decay constant, $\pi'_i(x)$ $(i = 1, 2, 3)$ are three Nambu-Goldstone (NG) bosons and σ_i $(i = 1, 2, 3)$ are the Pauli matrices.[3] Of these three NG bosons, π'_3 becomes the longitudinal component of the dark photon, since the $U(1)_D$ symmetry is realized by the shift of π'_3 at around $\vec{\pi}' = 0$. Hereafter, we call the two remaining NG bosons, $\pi' \equiv (\pi'_1 + i\pi'_2)/\sqrt{2}$ (and its complex conjugate $\pi'^\dagger$), the dark pions.

The kinetic term and the $U(1)_D$ gauge interaction of the dark pion is described by

$$\mathcal{L} = \frac{f'^2_\pi}{4} \text{tr}[(D_\mu U)(D^\mu U)^\dagger] \ , \qquad (6.1.3)$$

---

[2]The appearance of the accidental symmetries is a generic advantage of the composite dark matter models [177, 178].

[3]We take the normalization of Eqs. (6.1.2) and (6.1.3) so that the corresponding f_π in the QCD is $f_\pi \simeq 93\,\text{MeV}$.

where the covariant derivative of $U(x)$ is given by,

$$D_\mu U = \partial_\mu U(x) - i e_D A'_\mu \sigma_3 U(x) + i a e_D A'_\mu U(x) \sigma_3 . \qquad (6.1.4)$$

Here, e_D is the gauge coupling constant of U(1)$_D$. In the "unitary gauge", $\pi'_3 = 0$, we obtain interactions between the dark pion and the dark photon,

$$\mathcal{L} = (D_\mu \pi')^\dagger (D^\mu \pi') - e_D^2 (1-a)^2 A'_\mu A'^\mu \pi'^\dagger \pi' + \frac{1}{2} e_D^2 (1-a)^2 f_\pi'^2 A'^2_\mu + \cdots , \qquad (6.1.5)$$

where the ellipses denote the higher dimensional terms suppressed by $f_{\pi'}$. We introduced the "covariant" derivative of π',

$$D_\mu \pi' = \partial_\mu \pi' + i e_D (1+a) A'_\mu \pi' . \qquad (6.1.6)$$

The U(1)$_D$ invariance of Eq. (6.1.5) is not manifest due to the non-linear realization of U(1)$_D$, although the effective theory in Eq. (6.1.3) is manifestly U(1)$_D$ invariant.

The third term of Eq. (6.1.5) gives the dark photon mass,

$$m_{\gamma'} = e_D (1-a) f'_\pi \simeq \frac{\sqrt{3}}{4\pi} e_D (1-a) m_{\rho'} , \qquad (6.1.7)$$

In the final expression, we have used the naive dimensional analysis between the (dark) pion decay constant and the (dark) rho meson mass [179],

$$f'_\pi \simeq \frac{\sqrt{N_c}}{4\pi} m_{\rho'} , \qquad (6.1.8)$$

with $N_c = 3$. Here, $m_{\rho'}$ is the mass of the dark rho meson. The dark photon becomes massless for $a = 1$, which corresponds to the vector-like U(1)$_D$.

Since the U(1)$_D$ gauge symmetry forbids the mass term of the U' and D' dark quarks, the mass of the dark pion is generated by the U(1)$_D$ gauge interaction which breaks the SU(2)$'_L \times$ SU(2)$'_R$ symmetry explicitly. At the leading order of the U(1)$_D$ gauge coupling, the masses of the dark pions are given by [180, 181],

$$m_a^2 \delta^{ab} = \frac{e_D^2}{2 f_{\pi'}^2} \int d^4 x D_{\mu\nu}(x) \langle [Q_A^a [Q_A^b, T(j_D^\mu(x) j_D^\nu(0))]] \rangle . \qquad (6.1.9)$$

Here, $D_{\mu\nu}$ is the dark photon propagator, and $Q_A^a (a = 1, 2, 3)$ is the axial charges of SU(2)$'_L \times$ SU(2)$'_R$ symmetry. Since the dark pion is defined by $\pi' = (\pi'_1 + i\pi'_2)/\sqrt{2}$, we take $a = b = 1$ in the following. The decay constant $f_{\pi'}$ is defined so that it corresponds to $f_\pi \simeq 93 \, \text{MeV}$ in the visible sector.

The U(1)$_D$ current is given by,

$$j_D^\mu = \alpha j_V^{3\mu} + \beta j_A^{3\mu} \ , \tag{6.1.10}$$

$$j_V^{3\mu} = \frac{1}{2}U'^\dagger \bar{\sigma}^\mu U' - \frac{1}{2}D'^\dagger \bar{\sigma}^\mu D' - \frac{1}{2}\bar{U}'^\dagger \bar{\sigma}^\mu \bar{U}' + \frac{1}{2}\bar{D}'^\dagger \bar{\sigma}^\mu \bar{D}' \ , \tag{6.1.11}$$

$$j_A^{3\mu} = \frac{1}{2}U'^\dagger \bar{\sigma}^\mu U' - \frac{1}{2}D'^\dagger \bar{\sigma}^\mu D' + \frac{1}{2}\bar{U}'^\dagger \bar{\sigma}^\mu \bar{U}' - \frac{1}{2}\bar{D}'^\dagger \bar{\sigma}^\mu \bar{D}' \ , \tag{6.1.12}$$

$$\alpha = 1 + a \ , \quad \beta = 1 - a \ . \tag{6.1.13}$$

By using the commutation relations between Q_A^1 and $j_{A,V}^{3\mu}$, we obtain,

$$m_{\pi'}^2 = \frac{4ae_D^2}{f_{\pi'}^2}\int d^4x D_{\mu\nu}(x)(V^{\mu\nu}(x) - A^{\mu\nu}(x)) \ , \tag{6.1.14}$$

$$V^{\mu\nu}(x) = \langle Tj_V^{3\mu}(x)j_V^{3\nu}(0)\rangle \ , \tag{6.1.15}$$

$$A^{\mu\nu}(x) = \langle Tj_A^{3\mu}(x)j_A^{3\nu}(0)\rangle \ . \tag{6.1.16}$$

Then, we obtain,

$$m_{\pi'}^2 \simeq \frac{3a\log 2}{2\pi^2}e_D^2 m_{\rho'}^2 \ , \tag{6.1.17}$$

where we have neglected the dark photon mass in the propagator, whose effects are suppressed by $\mathcal{O}\left(m_{\gamma'}^2/m_{\rho'}^2\right)$. The dark pion becomes massless for $a = 0$, where the U(1)$_D$ gauge symmetry does not break SU(2)$'_R$ explicitly. By comparing Eqs. (6.1.7) and (6.1.17), we find that the condition $a \gtrsim 0.2$ is required for the dark pion mass to be larger than the dark photon mass.

Some constraints on the dark photon/pion masses put bounds on a and e_D. In Fig. 6.1, we show the viable parameter region. The figure shows that the requirement $m_{\pi'} > m_{\gamma'}$ is achieved for $a \gtrsim 0.13$ (outside the green shaded region). We also show the lower limits on $m_{\gamma'}$ from the effective number of neutrino degrees of freedom, N_{eff} [101] as blue/orange shaded regions. The blue shaded region, which corresponds to $m_{\gamma'} \lesssim 8.5\,\text{MeV}$, is excluded by the N_{eff} constraint from the Planck observation of the cosmic microwave background (CMB) [10] for $\epsilon \gtrsim 10^{-9}$. The orange one corresponding to $m_{\gamma'} \lesssim 17\,\text{MeV}$ shows the future sensitivity of the stage-IV CMB experiment [182].

6.1.2   Chiral Composite ADM for $N_f = 2$

By combining the ideas in chapter 4 and Sec. 6.1.1, we construct the chiral composite ADM model in which the dark photon mass is generated dynamically. In the model with $N_f = 2$ so far considered, the lightest dark baryons are

$$p' \propto U'U'D' \ , \ \ \bar{p}' \propto \bar{U}'\bar{U}'\bar{D}' \ , \ \ n' \propto U'D'D' \ , \ \ \bar{n}' \propto \bar{U}'\bar{D}'\bar{D}' \ , \tag{6.1.18}$$
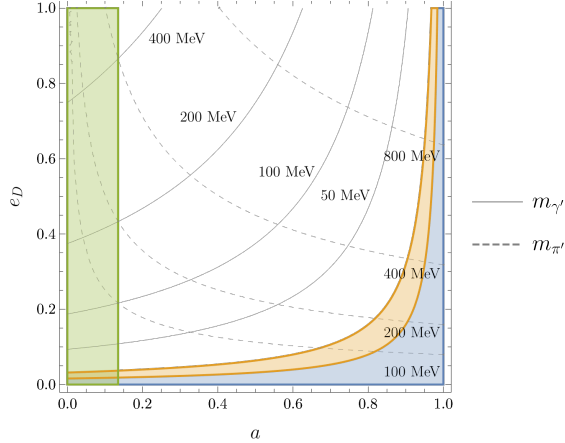
Figure 6.1: The contours of the dark photon/pion masses on a (a, e_D) plane. Here, we take $m_{\rho'} = m_\rho \times 5$ ($m_\rho \simeq 775\,\text{MeV}$), which corresponds to the dark baryon mass, $m_{p',n'} \simeq 5$–$6\,\text{GeV}$. The green shaded region corresponding to $m_{\pi'} < m_{\gamma'}$ is disfavored. The blue and the orange shaded regions correspond to the N_{eff} constraints from the current and the future CMB observations for $\epsilon \gtrsim 10^{-9}$ [101].

as in QCD. Due to the non-trivial baryon charges, they are stable and eventually become DM. The mass partner of p' is $\bar{p}'$, and that of n' is $\bar{n}'$. This combination results from the $U(1)'_3$ and the $\text{U}(1)_{B-L}$ symmetries. Besides, the masses of the dark proton and the dark neutron are identical due to the charge conjugation symmetry which interchanges U' and D'. Therefore, both the dark proton and the dark neutron become dark matter.

In summary, we obtain the chiral composite ADM model based on the charge assignment in Tab. 6.1, which naturally provides the desirable spectrum,

$$m_{\gamma'} < m_{\pi'} < m_{\text{DM}} \; . \tag{6.1.19}$$

In this model,

- The dark baryons are stable due to $B - L$ symmetry.

- The dark baryon density is dominated by the asymmetric components due to the large annihilation cross section of the dark baryons into the dark pions.

- The chiral $\text{U}(1)_D$ gauge symmetry is broken dynamically, whose mass is suppressed compared with the dark baryons.

- The dark pion mass is generated by the radiative correction of the $\text{U}(1)_D$ interaction. The mass can be larger than the dark photon

mass, and hence, the dark pion annihilates into the dark photon pairs efficiently.[4]

For $A_{\mathrm{DM}}/A_{\mathrm{SM}} = \mathcal{O}(1)$, the dark matter density is reproduced by $m_{\mathrm{DM}} = \mathcal{O}(1)\,\mathrm{GeV}$, with which the masses of the dark photon and the dark pion are predicted in the sub-GeV due to the dynamical symmetry breaking.

6.1.3   Chiral Composite ADM for $N_f = 3$

For successful ADM models, we need a portal interaction with which the $B - L$ asymmetry is thermally distributed between the visible and the dark sectors. One of such portal interactions can be given by higher-dimensional operators [183, 106],

$$\mathcal{L}_{B-L\,\mathrm{portal}} = \frac{1}{M_{\mathrm{portal}}^n}\mathcal{O}_D LH \; + \mathrm{h.c.} \tag{6.1.20}$$

Here, L and H denote the lepton and the Higgs doublets in the visible sector. $\mathcal{O}_D$ is a $B - L$ charged but $\mathrm{U}(1)_D$ neutral operator in the dark sector with the mass dimension $d_D = n + 3/2$. M_{portal} encapsulates the energy scale of the portal interactions. With this portal interaction, the visible and the dark sectors are in the thermal equilibrium at the high temperature. The $B - L$ asymmetry is also thermally distributed through the same operators. The portal interaction eventually decouples at the temperature,

$$T_D \sim M_{\mathrm{portal}} \left(\frac{M_{\mathrm{portal}}}{M_{\mathrm{Pl}}} \right)^{1/(2n-1)}. \tag{6.1.21}$$

Below the decoupling temperature, the $B - L$ asymmetries in the two sector are conserved separately.

In the model in the previous subsection, however, there is no good candidate for $\mathcal{O}_D$ which is $B - L$ charged but neutral under the $\mathrm{SU}(3)_D \times \mathrm{U}(1)_D$ gauge symmetry. To allow the $B - L$ portal interaction in Eq. (6.1.20), we extend the composite ADM model with an additional generation of dark quarks so that $N_f = 3$.[5] The charge assignment of the dark quarks under the gauge and the global symmetries are given in Tab. 6.2. In this model, the third flavor, $(S', \bar{S}')$, is vector-like, and hence, it has a mass $m_{S'}$, where we assume $m_{S'} < \Lambda'_D$. In the presence of the third flavor dark quark, the $B - L$ portal interaction can be given by,

$$\mathcal{L}_{B-L\,\mathrm{portal}} = \frac{1}{M_*^3}(U'D'S')LH + \frac{1}{M_*^3}(\bar{U}'^\dagger \bar{D}'^\dagger S')LH + \mathrm{h.c.} \tag{6.1.22}$$

---

[4]In the present model, there is no "dark neutral pion" as it is absorbed by the dark photon. Thus, there is no need to assume that the dark pion mass is twice larger than the dark photon mass.

[5]We may instead extend the non-Abelian gauge group to $\mathrm{SU}(2)_D$ while keeping $N_f = 2$.

	$SU(3)_D$	$U(1)_D$	$U(1)_{B-L}$	$U(1)'_3$	$U(1)'_8$
U'	**3**	1	1/3	1	1
D'	**3**	-1	1/3	-1	1
S'	**3**	0	1/3	0	-2
$\bar{U}'$	$\bar{\bf 3}$	$-a$	$-1/3$	-1	-1
$\bar{D}'$	$\bar{\bf 3}$	a	$-1/3$	1	-1
$\bar{S}'$	$\bar{\bf 3}$	0	$-1/3$	0	2

Table 6.2: *The charge assignment of the dark quarks for $N_f = 3$. The $U(1)'_3$ and $U(1)'_8$ symmetries are the two components of the Cartan subgroup of the vector-like $SU(3)'_V$ symmetry.*

For the $B - L$ asymmetry generation mechanism, we assume, for example, the thermal leptogenesis [15]. In the thermal leptogenesis, the reheating temperature, T_R, after inflation is required to be higher than, $T_R \gtrsim 10^{9\text{-}10}\,\mathrm{GeV}$ [33, 34]. Thus, for the scenario to be successful, we require $T_D \lesssim T_R$, which reads,

$$M_{\mathrm{portal}} \lesssim T_R \left(\frac{M_{\mathrm{Pl}}}{T_R}\right)^{1/2n} \simeq 10^{11}\,\mathrm{GeV} \times \left(\frac{T_R}{10^{9.5}\,\mathrm{GeV}}\right)^{5/6} , \qquad (6.1.23)$$

where we have used $n = 3$ in the last inequality. In this case, we assume that the portal interaction is generated by a new sector at $M_{\mathrm{portal}} \simeq 10^{11}\,\mathrm{GeV}$ as in chapter 4.

Our portal mechanism works with other types of baryogenesis in the visible sector. Again, T_D should be lower than the temperature of the completion of the baryogenesis. In addition, when the baryogenesis does not generate the lepton asymmetry directly, T_D is required to be lower than the temperature $T_{\mathrm{sph}} \sim 10^{12}\,\mathrm{GeV}$, below which the sphaleron process is in equilibrium (see e.g. Ref. [184]). Other leptogenesis in the visible sector which completes above T_D also works. However, the numerical value of the dark sector asymmetry will be altered from the one used in the present paper if $T_{\mathrm{sph}} < T_D$.

For $m'_S \lesssim \Lambda'_D$, we assume that the dark quark bilinears condense as,

$$\left\langle U'\bar{U}' + U'^\dagger \bar{U}'^\dagger \right\rangle = \left\langle D'\bar{D}' + D'^\dagger \bar{D}'^\dagger \right\rangle = \left\langle S'\bar{S}' + S'^\dagger \bar{S}'^\dagger \right\rangle = \mathcal{O}\left(\Lambda'^3_D\right) .$$
$$(6.1.24)$$

The condensates spontaneously break the $U(1)_D$ gauge symmetry and the approximate $SU(3)'_L \times SU(3)'_R$ symmetry to the diagonal subgroup $SU(3)'_V$. Note that the two components of the Cartan subgroup of $SU(3)'_V$, $U(1)'_3$ and $U(1)'_8$, are exact (accidental) symmetry up to $U(1)_D$ anomaly and remain unbroken by the condensates in Eq. (6.1.24). As in the model with $N_f = 2$,

the NG boson corresponding to π'_3 becomes the longitudinal component of the U(1)$_D$ gauge boson.

As in QCD, the dark quarks are confined into hadrons, and the lightest baryons and the NG bosons form the octet representations of $SU(3)'_V$,

$$
B'_\alpha = \begin{pmatrix} \Sigma'^3_\alpha + \Lambda'_\alpha/\sqrt{3} & \sqrt{2}\Sigma'^1_\alpha & \sqrt{2}p'_\alpha \\ \sqrt{2}\Sigma'^2_\alpha & -\Sigma'^3_\alpha + \Lambda'_\alpha/\sqrt{3} & \sqrt{2}n'_\alpha \\ \sqrt{2}\Xi'^2_\alpha & \sqrt{2}\Xi'^1_\alpha & -2\Lambda'_\alpha/\sqrt{3} \end{pmatrix} ,
$$

$$
M' = \begin{pmatrix} \eta'/\sqrt{3} & \sqrt{2}\pi' & \sqrt{2}K'^1 \\ \sqrt{2}\pi'^\dagger & \eta'/\sqrt{3} & \sqrt{2}K'^2 \\ \sqrt{2}K'^{1\dagger} & \sqrt{2}K'^{2\dagger} & -2\eta'/\sqrt{3} \end{pmatrix} , \tag{6.1.25}
$$

where we have taken the unitary gauge, i.e., $\pi'_3 = 0$. The index α denotes the Weyl spinor components. The names of the dark baryons and the dark mesons are after the corresponding baryons and the mesons in the visible sector.[6] The U(1)$_D$ charges of them are not parallel with the U(1)$_{\rm QED}$ charges in the visible sector. The dark baryons are also associated with their antiparticles, $\bar{B}_\alpha$. The mesons π' and $K'^{1,2}$ are complex scalars, while η' is a pseudo scalar.

As in the model with $N_f = 2$, all the physical NG bosons become massive. The π' mass is from the U(1)$_D$ interaction as in Eq. (6.1.17). The NG bosons which have the S components obtain masses of $\mathcal{O}\big(\sqrt{m_{S'}\Lambda'_D}\big)$ due to the explicit mass term of $(S', \bar{S}')$.[7] In the following, we assume that they are slightly heavier than the dark pion, so that they annihilate into the dark pions very efficiently. Note that all the NG bosons other than η' are stable when no NG bosons are twice heavier than the other NG bosons.[8]

The leading mass term of the baryons is from

$$
\mathcal{L}_{\rm mass} \simeq \frac{1}{2}m_B \,{\rm tr}\Big[BU\bar{B}U^\dagger\Big] + {\rm h.c.} \,, \tag{6.1.26}
$$

$$
\simeq m_B(p'\bar{p}' + n'\bar{n}' + \Lambda'\bar{\Lambda}' + \sum_{i=1}^{3}\Sigma'^i\bar{\Sigma}'^i + \sum_{i=1}^{2}\Xi'^i\bar{\Xi}'^i) + {\rm h.c.} \,, \tag{6.1.27}
$$

where

$$
U(x) = \exp\left[\frac{i}{f'_\pi}M(x)\right] . \tag{6.1.28}
$$

The term in Eq. (6.1.26) is invariant under U(1)$_D\times$ SU(3)$'_L\times$ SU(3)$'_R$. Note that the dark baryon masses are not identical due to the U(1)$_D$ gauge interaction and the mass of $(S', \bar{S}')$.

---

[6]The dark η' corresponds to η in the visible sector.

[7]Due to the charge conjugation symmetry which exchanges U' and D', the masses of $K'^{1,2}$ are identical.

[8]When η' is twice heavier than γ', it decays into a pair of the dark photons. For a lighter η', it decays into $\gamma' + e^+ + e^-$ through the kinetic mixing.

6.2 Phenomenology and Cosmology of $N_f = 3$ Model

When the mass difference between the dark baryons larger than the dark NG boson masses, the heavier baryons decay into the lighter baryons by emitting a dark NG boson. Besides, Σ'^3 decays into a pair of Λ' and the dark photon when their mass difference is larger than the mass of the dark photon. Even if the mass difference is smaller than the dark photon mass, Σ'^3 eventually decays into $\Lambda' + e^+ + e^-$ through the kinetic mixing of the dark photon. As the total dark baryon number is conserved, however, the details of the decay properties of the dark baryons do not affect the number density of the dark baryons. Since all the dark baryon masses are around m_B, the dark baryon mass density is also insensitive to the details of the decay properties.

Here, let us comment on the dark baryon density. As shown in Ref. [106], the ratio $A_{\mathrm{DM}}/A_{\mathrm{SM}}$ is given by

$$\frac{A_{\mathrm{DM}}}{A_{\mathrm{SM}}} = \frac{22}{237} N_f \ , \tag{6.2.1}$$

when T_D in Eq. (6.1.21) is lower than the temperature T_e at which the electron Yukawa coupling becomes effective in the thermal bath. When T_D is higher than T_e but lower than the temperature T_{ud} at which the up and down Yukawa couplings become effective, the ratio is slightly changed to

$$\frac{A_{\mathrm{DM}}}{A_{\mathrm{SM}}} = \frac{20}{213} N_f \ , \tag{6.2.2}$$

(see the Appendix C.1). When T_D is higher than T_{ud}, the ratio is given by,

$$\frac{A_{\mathrm{DM}}}{A_{\mathrm{SM}}} = \frac{17}{149} N_f \ . \tag{6.2.3}$$

From these ratios and Eq. (4.1.5), we find that the DM mass is predicted to be $m_{\mathrm{DM}} \simeq 5\text{--}6\,\mathrm{GeV}$ for $N_f = 3$ for wide range of T_D. In order to achieve this m_{DM}, we take $\Lambda'_D = \mathcal{O}(1)\,\mathrm{GeV}$.

Note that each dark baryon decays into a pair of a dark meson and an anti-neutrino in the visible sector through the portal interaction of Eq.(6.1.22). Thus, the dark baryons are not absolutely stable, although their lifetime is longer than the age of the Universe for $M_{\mathrm{portal}} \gtrsim 10^{7.7}\,\mathrm{GeV} \times (m_{\mathrm{DM}}/5\,\mathrm{GeV})^{1/2}$ [106]. From the the upper limit on the anti-neutrino flux over the predicted atmospheric flux measured by the Super-Kamiokande experiment [185], we require $M_{\mathrm{portal}} \gtrsim 10^{8.2}\,\mathrm{GeV}$ [109, 106, 107, 108] for $m_{\mathrm{DM}} = 5\text{--}6\,\mathrm{GeV}$, which corresponds to the lifetime, $\tau_{\mathrm{DM}} \gtrsim 10^{21}\,\mathrm{sec}$.

When the mass difference between the dark baryons are smaller than the dark NG boson masses, multiple dark baryons with different masses and different $\mathrm{U}(1)_D$ charges become dark matter. The dark baryons with

non-vanishing $U(1)_D$ charges can be tested by the direct detection signal by exchanging the dark photon with the proton in the visible sector. When the dark $U(1)_D$ gauge coupling constant is equal to QED coupling constant, a large portion of the parameter space can be tested by the future XENONnT [186], LZ [119] and DARWIN [75] experiments for $m_{\gamma'} \lesssim 100\,\mathrm{MeV}$ as we saw in chapter 4.

Finally, we discuss the constraints on the dark NG boson density. As we mentioned earlier, most of the dark NG bosons are stable. When the NG bosons containing S' are slightly heavier than the dark pions, the heavier NG bosons annihilate into the dark pions, while the dark pions annihilate into a pair of dark photons.[9] Accordingly, the dark pion has the largest number density, and hence, we concentrate on the constraint on the dark pion density.

The thermally averaged annihilation cross-section of the dark pion is given by

$$\langle \sigma v \rangle = \frac{\pi \alpha_D^2}{m_{\pi'}^2} \mathcal{F}\left(\frac{m_{\gamma'}}{m_{\pi'}}\right) , \qquad (6.2.4)$$

where $\alpha_D = e_D^2/4\pi$ and

$$\mathcal{F}(x) = 16\frac{\sqrt{1-x^2}}{x^4(2-x^2)^2}[(a^4+1)(x^2-1)^2 + 2a(a^2+1)(x^6-3x^4+4x^2-2)$$
$$+ 3a^2(x^8-4x^6+6x^4-4x^2+2)] . \qquad (6.2.5)$$

At first glance, this formula looks divergent if $m_{\gamma'} = 0$. However, this limit corresponds to $a \to 1$, then the formula becomes finite and reproduces the massless $U(1)$ gauge theory. With this annihilation cross-section, the mass density of the dark pion is given by,

$$\Omega_{\pi'} \sim \frac{3 \times 10^{-26}\,\mathrm{cm}^3\,\mathrm{sec}^{-1}}{\langle \sigma v \rangle} \times \Omega_{\mathrm{DM}} , \qquad (6.2.6)$$

where we have used the WIMP cross-section, $\sigma v \sim 3 \times 10^{-26}\,\mathrm{cm}^3\,\mathrm{sec}^{-1}$, with which the observed dark matter abundance is achieved by the freeze-out mechanism.[10]

If the relic abundance of the dark pion is sizable, the late time annihilation injects extra energy into the galactic medium after the recombination time. The anisotropies of the cosmic microwave background (CMB) are sensitive to such energy injection, which put severe constraint on the energy injection rate [10]. The effective parameter constrained by the CMB

---

[9]The dark photon decays before the neutrino decoupling temperature (see Ref. [101]).

[10]Here, we assume that there is no asymmetry between the dark pion and the dark anti-pion, which is justified in the Appendix C.1.

anisotropies is given by

$$p_{\text{ann}} = f_{\text{eff}} \frac{\langle \sigma v \rangle}{m_{\pi'}} \times \left(\frac{\Omega_{\pi'}}{\Omega_{\text{DM}}} \right)^2 \simeq f_{\text{eff}} \frac{\langle \sigma v \rangle}{m_{\pi'}} \times \left(\frac{3 \times 10^{-26} \,\text{cm}^3 \,\text{sec}^{-1}}{\langle \sigma v \rangle} \right)^2 .$$
(6.2.7)

Here, the scaling factor $(\Omega_{\pi'}/\Omega_{\text{DM}})^2$ comes from the fact that the energy injection rate is proportional to $m_{\pi'} n_{\pi'}^2 = \rho_{\pi'}^2/m_{\pi'}$ where $n_{\pi'}$ and $\rho_{\pi'}$ are the number and the energy densities of the dark pion, respectively. f_{eff} is an energy fraction released into the intergalactic medium around the red-shift $z \simeq 600$ [187]. The dark photons produced by the dark pion annihilation eventually decays into a pair of the electron and the positron, and hence, $f_{\text{eff}} = \mathcal{O}(1)$ [188]. By substituting (6.2.4), we obtain

$$p_{\text{ann}} \simeq \frac{(m_{\pi'}/\text{GeV})}{\pi \alpha_D^2 \mathcal{F}(m_{\gamma'}/m_{\pi'})} \times 10^{-34} \,\text{cm}^3 \,\text{s}^{-1} \,\text{GeV}^{-1} .$$
(6.2.8)

For $m_{\pi'} > m_{\gamma'}$, $\mathcal{F}(m_{\gamma'}/m_{\pi'})$ is $\mathcal{O}(1)$ or larger, and hence, the dark pion density satisfies the current CMB constraint [10],

$$p_{\text{ann}} < 3.5 \times 10^{-28} \,\text{cm}^3 \,\text{s}^{-1} \,\text{GeV}^{-1} .$$
(6.2.9)

Therefore, we find that the stable NG bosons do not cause observational problems.

Though the model is different from the one that we discussed in chapter 4, constraints on the DM scattering are the same, since we take similar value for the particle masses and kinetic mixing parameter. Thus, we can say that the model is consistent with the astrophysical constraints [122, 123, 124, 125, 126, 127, 128, 129, 130, 131, 132] (see chapter 4).

Chapter 7

Conclusions

In this thesis, we constructed the concrete model for composite ADM with the dark photon portal, studied the effect of Majorana mass term on this ADM model, and finally constructed the chiral composite ADM model that dynamically generates $\mathcal{O}(100)\,\mathrm{MeV}$ dark photon mass.

In chapter 4, motivated by the composite ADM scenario, we have investigated the viable parameter space of the dark photon portal, through which the energy of the dark sector is transferred to the SM sector. As we have seen, the stringent bound comes from the observational constraint on N_{eff}, where the bound depends on whether the reheating temperature of the SM sector by the dark photon recoupling is above or below the neutrino decoupling temperature. If the neutrinos are in the thermal bath at the dark photon recoupling, the recoupling itself does not affect N_{eff}. Still, the thermalized dark photons affect N_{eff} by heating only electron and photon plasma after the neutrino decoupling. The observational constraint on N_{eff} places an upper bound on the dark photon mass in this case. f the neutrinos already decoupled from the thermal bath at the dark photon recoupling, the recoupling directly heats the electrons and the photons and thus changes N_{eff}. We have obtained a lower bound on the kinetic mixing parameter for a given dark photon mass.

In addition, we have constructed a minimal model of composite ADM, which is compatible with the seesaw mechanism and thermal leptogenesis. It has a QCD-like SU(3) gauge theory and a QED-like U(1) gauge interaction. As the dark proton is charged under $\mathrm{U}(1)_D$, our ADM can be tested by direct detection experiments. We have found that the current direct detection constraint is severer than that from SN 1987A. A large portion of the parameter space can be tested by future experiments such as XENONnT, LZ, and Darwin.

In chapter 5, we discussed the impact of the small Majorana mass term in the dark baryon by considering the indirect detection bound of the composite ADM and requirement from a successful leptogenesis.

As we have discussed, the late time annihilation of ADM results in multiple soft electrons/positrons and soft photons emitted as the FSR. As a result, some parameter region of the composite ADM is constrained by the Fermi-LAT and the Voyager-1 observations. At first sight, the obtained constraint is looser than one from the requirement that the Majorana mass term does not washout the $B - L$ asymmetry generated via the leptogenesis. As we discussed before, however, the bound can be avoided by changing the portal operator and combining it with non-thermal leptogenesis scenarios. Thus, we should notice that the bound from the thermal leptogenesis is model-dependent. To investigate the wider region of the parameter space via indirect detection, we have to track other channels of the signal induced by DM annihilation or decay. We expect that combining the new channels, the future experiments which are sensitive to sub-GeV γ-rays such as e-ASTROGAM [168, 169], SMILE [170], GRAINE [171], and GRAMS [172] projects will be important to test the oscillating ADM model further.

In chapter 6, we constructed a chiral composite ADM model where the $U(1)_D$ gauge symmetry is embedded into the chiral flavor symmetry. Due to the dynamical breaking of the chiral flavor symmetry, the model naturally provides the masses of the dark photon and the dark pions in the sub-GeV range, both of which play crucial roles for successful ADM models. Let us emphasize that the dark photon mass is determined by the dynamical scale, which is an attractive feature of the present model compared with models with an additional Higgs boson to break $U(1)_D$ spontaneously.

The model with $N_f = 3$ fits well with the scenario where the $B - L$ asymmetry in the visible sector is thermally distributed to the dark sector through higher-dimensional $B - L$ portal operators, as in chapter 4 (see also Refs. [183, 1]). This type of scenario can be tested by multiple channels such as the direct detection (see the chapter 4 and Ref. [1]), the anti-neutrino flux from the decay of the dark baryons [106], and the electron/positron flux from the annihilation of the dark baryons and the dark anti-baryons through the late-time oscillation [2].

Let us also comment on the possibility of the first-order phase transition of the dark QCD. In the present model, the chiral $U(1)_D$ gauge symmetry forbids the dark quark masses of U' and D'. The QCD with the vanishing up and down quark masses can exhibit the first-order phase transition depending on the strange quark mass (see, e.g., [189, 190]). Thus, the dark QCD in the present model may also have the first-order phase transition, although the dark pion mass induced by the $U(1)_D$ gauge interaction could also affect the order of the phase transition. Once the dark QCD undergoes the first-order transition at the GeV range, the gravitational waves generated at the transition could be observed by the pulsar timing array experiments (see, e.g., [191, 192]) as well as the gravitational wave detection experiments [193].

Finally, note that the baryon-DM coincidence problem is not fully solved

by the ADM scenario without specifying the origin of the dark matter mass. In fact, the puzzle is divided into two subproblems, which are the coincidence of masses and that of the number densities between baryons and DM. The ADM scenario naturally explains the coincidence of the number density while it does not answer the mass coincidence. The composite ADM ameliorate the mass coincidence problem as it provides the dark matter mass via the dynamical transmutation in the dark QCD. However, it does not answer the coincidence problem unless the gauge coupling of the dark QCD is related to that of QCD. In Ref. [194], we introduced a mirror symmetry under which the dark sector and the visible sector are exchanged so that the gauge coupling constants in the two sectors are related to each other. In the present model, however, introducing the exchanging symmetry is difficult because the $U(1)_D$ gauge symmetry is chiral. One possibility is to embed the dark QCD and dark QED into a chiral non-Abelian gauge theory, although we have not succeeded in constructing a concrete example. We leave this issue for a future work.

Acknowledgement

First of all, I would like to express my sincere gratitude for my supervisor, Masahiro Ibe. In our collaborations, he always gave me crucial ideas and advice. I enjoyed enthusiastic discussions of physics with him throughout my student life. Additionally, I gratefully thank my collaborators, Ayuki Kamada, Ryo Nagai, Wakutaka Nakano and Keiichi Watanabe, who made my research life wonderful. I also thank Satoshi Shirai, my collaborators in other works, and colleagues of the theory group at Institute for Cosmic Ray Research for reviewing my thesis and presentation.

This thesis is thankfully judged by Koichi Hamaguchi, Masahiro Kawasaki, Takeo Moroi, Tadayuki Takahashi, and Jun'ichi Yokoyama. I would express my appreciation to them.

Appendix A

Mass Spectrum and Charge Assignment of ADM

In this appendix, we show the mass spectrum of the dark sector for the model discussed in section 4.2. In A.1, we show the parameter dependence of the dark nucleon mass difference. In A.2, we show how to stabilize (or destabilize) the heavy dark baryon.

A.1 Hadron mass spectrum in the $\text{QCD}' + \text{QED}'$ model

By analogy to the QCD, the masses of the dark pions are estimated as

$$m_{\pi'^0}^2 \simeq m_{\pi^0}^2 \times \frac{\Lambda_{\text{QCD}'}}{\Lambda_{\text{QCD}}} \frac{m_1 + m_2}{m_u + m_d} \,, \tag{A.1.1}$$

where $m_{u\,(d)}$ is the SM up-type (down-type) quark mass and $m_{u'\,(d')}$ is the dark up-type (down-type) quark mass. The squared mass difference of the dark pions is given by

$$m_{\pi'^\pm}^2 \simeq m_{\pi'^0}^2 + \alpha_D \Lambda_{\text{QCD}'}^2 \,. \tag{A.1.2}$$

The average dark (SM) nucleon mass $m_{N'\,(N)}$ is given by

$$m_{N'} \simeq m_N \times \frac{\Lambda_{\text{QCD}'}}{\Lambda_{\text{QCD}}} \,, \tag{A.1.3}$$

while the nucleon mass difference is given by

$$m_{n'} - m_{p'} \simeq \delta m_{n\text{-}p}^{\text{QED}} \times \frac{\Lambda_{\text{QCD}'}}{\Lambda_{\text{QCD}}} \times \alpha_D + \kappa_N (m_1 - m_2) \,. \tag{A.1.4}$$

Here, $\delta m_{n\text{-}p}^{\text{QED}} = -0.178^{+0.004}_{-0.064} \, \text{GeV}$ and $\kappa_N = 0.95^{+0.08}_{-0.06}$ parameterize the electromagnetic and the isospin-violating contributions, respectively [195].

A.2   U(1)$_D$ Higgs with a charge of -1

For the U(1)$_D$ Higgs charge of -1, Yukawa couplings,

$$\mathcal{L}_{\mathrm{U(1)}_D\,\mathrm{mass}} = yH_D Q_1 \bar{Q}_2 + \bar{y}H_D^\dagger \bar{Q}_1 Q_2 + \mathrm{h.c.}\,, \qquad (\mathrm{A.2.1})$$

induce mixing between the QED$'$ breaking Higgs and the charged pion. The charged pion also develops a vacuum expectation value. It induces dark proton mixing with the dark neutron once the U(1)$_D$ symmetry is spontaneously broken. In this case, the heavier nucleon can decay into the lighter one and the dark photon or the charged leptons, depending on the mass difference $m_{n'} - m_{p'}$ [see Eq. (A.1.4)]. If the dark photon channel is kinematically forbidden, the lifetime of the heavier nucleon is of $\mathcal{O}(10^{10})\,\mathrm{s}$ for $\epsilon = \mathcal{O}(10^{-10})$, and its fraction in the whole DM is severely constrained to be smaller than $\mathcal{O}(10^{-4})$ by the light element abundance [196]. The fraction is determined by the dark nucleon inelastic scattering with the dark photon, which is induced by the vacuum expectation value of the charged pion. This interaction decouples when $T_{\gamma'} \sim |m_{n'} - m_{p'}|/20\text{–}30$ if the dark photon decays below this dark photon temperature. The resultant fraction is of $\mathcal{O}(10^{-9})$ [see Eq. (4.2.11)], which evades the above cosmological constraint. If the dark photon decays before $T_{\gamma'} \sim |m_{n'} - m_{p'}|/20\text{–}30$, the freeze-out temperature is given by $T_{\gamma'} \sim m_{\gamma'}/20\text{–}30$.[1] In this case, the resultant fraction tends to exceed the upper bound from the cosmological constraint.

The charged pion also mixes with the SM Higgs boson through the vacuum expectation value of the charged pion and the Higgs portal coupling, $|H|^2|H_D|^2$. Resultantly the charged pion decays into the SM fermions. Such decay modes provide an alternative route (to kinetic mixing) to transfer the entropy in the dark sector to the SM sector (see, e.g., Ref. [197]). A detailed discussion will be given elsewhere.

---

[1]If the SM reheating temperature [see Eqs. (4.1.12) and (4.1.14)] is lower than this dark photon temperature, the freeze-out temperature is the dark photon temperature at recoupling. If double Compton scattering and bremsstrahlung of the dark proton are efficient, the freeze-out of the dark photon becomes non-trivial. This is because the dark photon temperature drops only slowly as $T_{\gamma'} \propto 1/\ln a$ after dark photon becomes non-relativistic.

Appendix B

Calculation Detail for Annihilation Signal

This appendix corresponds to section 5.2, where we calculate the signals in the indirect detection experiments. In B.1, we show the detailed calculation of the final state radiation spectrum. In B.2, we estimate the effect of the Sommerfeld enhancement in the DM annihilation and show that the effect does not change the result of chapter 5.
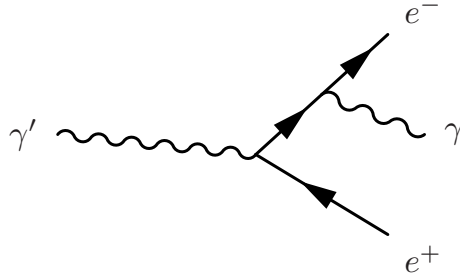
B.1 Final State Radiation In the Dark Photon Decay

Figure B.1: One of the Feynman diagrams of the final state radiation.

This appendix is devoted to the photon energy spectrum of the final state radiation in the dark photon decay, $\gamma' \to e^+ e^- \gamma$. One of the diagrams is shown in figure B.1.

The invariant amplitude for this process is

$$\mathcal{M} = -4\pi\epsilon\alpha_{\text{EM}}\bar{u}(p_1)\left[\not{\epsilon}^*(p_3)\frac{\not{p}_1 + \not{p}_3 + m_e}{(p_1 + p_3)^2 - m_e^2}\not{\epsilon}(p_0) + \not{\epsilon}(p_0)\frac{-\not{p}_2 - \not{p}_3 + m_e}{(p_2 + p_3)^2 - m_e^2}\not{\epsilon}^*(p_3)\right]v(p_2),$$
$$(\text{B.1.1})$$

75

where ϵ represents the strength of kinetic mixing, α_{EM} the fine structure constant of QED, ε the polarization vector, m_e the electron mass, u and v spinors, and p momentum vector. Here the subscripts $(0, 1, 2, 3)$ denote the $(\gamma', e^-, e^+, \gamma)$.

Summing over the spins of the final state e^-, e^+ and averaging over the helicity of initial state γ', we obtain

$$
\begin{aligned}
\frac{1}{3}\sum_{\mathrm{spin}}|\mathcal{M}|^2 = & \frac{8(4\pi\epsilon\alpha_{\mathrm{EM}})^2}{3}\frac{1}{(m_{13}^2 - m_e^2)^2(m_{23}^2 - m_e^2)^2} \\
& \big[m_{13}^2 m_{23}^2 \{ 2m_{12}^4 + 2m_{12}^2(m_{13}^2 + m_{23}^2) + m_{13}^4 + m_{23}^4 \} \\
& - m_e^2(m_{13}^2 + m_{23}^2)\{ 2m_{12}^4 + 4m_{12}^2(m_{13}^2 + m_{23}^2) + 3(m_{13}^2 + m_{23}^2)^2 \} \\
& + m_e^4 \{ 2m_{12}^4 + 10m_{12}^2(m_{13}^2 + m_{23}^2) + 11(m_{13}^2 + m_{23}^2)^2 \} \\
& - 4m_e^6 \{ 2m_{12}^2 + 3(m_{13}^2 + m_{23}^2) \} + 2m_e^8 \big] \ ,
\end{aligned}
\tag{B.1.2}
$$

by using the Mandelstam invariants, $m_{ij}^2 = (p_i - p_j)^2$, with the subscripts defined above. There is a relation between the invariants, $m_{\gamma'}^2 + 2m_e^2 = m_{12}^2 + m_{13}^2 + m_{23}^2$, with $m_{\gamma'}$ being the dark photon mass. This expression is symmetric under the exchange between m_{13}^2 and m_{23}^2 as expected.

Now, let us calculate the decay rate with the final state radiation. In the following calculation, we use the center of mass frame in which three outgoing particles lie in the same plane. Thus, we can transform the three-body phase space integral into integration over the energy of two particles and three angles. By taking into account the energy-momentum conservation, the three-body phase space has $9 - 4 = 5$ d.o.f. After fixing the energy of e^-, three d.o.f. remain. Two of them are angles (α, β) that specify the direction of $\vec{p}_3$. The last one is an angle δ which determines the plane of decay around $\vec{p}_3$. Thus, $\Gamma_{\gamma' \to e^+ e^- \gamma}$ can be written as

$$
\Gamma_{\gamma' \to e^+ e^- \gamma} = \int \frac{1}{16m_{\gamma'}} \frac{1}{3}\sum_{\mathrm{spin}}|\mathcal{M}|^2 \frac{dE_3 dE_1 d\alpha d(\cos\beta) d\delta}{(2\pi)^5} \ ,
\tag{B.1.3}
$$

$$
= \frac{m_{\gamma'}}{32(2\pi)^3}\int \frac{1}{3}\sum_{\mathrm{spin}}|\mathcal{M}|^2 dx\,dy \ ,
\tag{B.1.4}
$$

$$
= \frac{m_{\gamma'}}{32(2\pi)^3}\int dx \sum_{n=0}^{2} \epsilon_0^{2n} \left[f_n(x, y_{\max}(x, \epsilon_0)) - f_n(x, y_{\min}(x, \epsilon_0)) \right] \ .
\tag{B.1.5}
$$

Here we define $x = 2E_3/m_{\gamma'}$, $y = 2E_1/m_{\gamma'}$ and $\epsilon_0 = 2m_e/m_{\gamma'}$. Each $f_n(x, y)$ is defined as the integration of the invariant scattering amplitude over E_1,
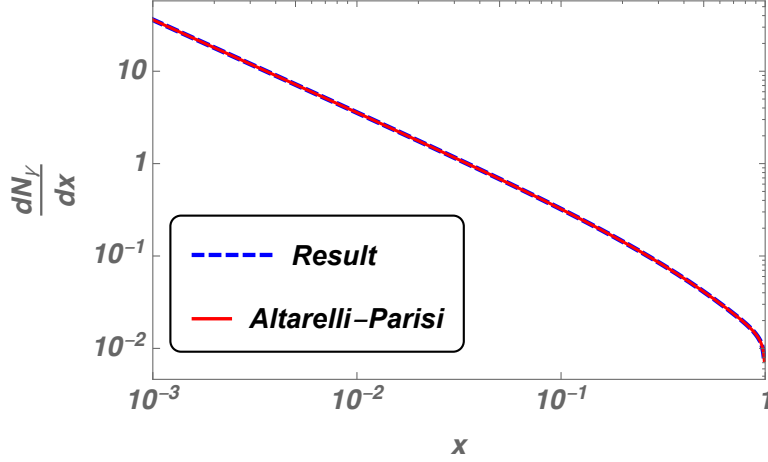
Figure B.2: The plot of the analytic formula and the approximation. Here we take $m_{\gamma'} = 40\,\mathrm{MeV}$. Two expressions are in good agreement.

i.e., y. The analytical formula for each $f_n(x,y)$ is as follows:

$$f_0(x,y) = \frac{8}{3}(4\pi\epsilon\alpha_{\mathrm{EM}})^2 \left[2(1-y) - \frac{1+(1-x)^2}{x} \ln\left(\frac{1-y}{1-x-y}\right) \right] , \quad \text{(B.1.6)}$$

$$f_1(x,y) = \frac{4}{3}(4\pi\epsilon\alpha_{\mathrm{EM}})^2 \left[\frac{x+2y-2}{(1-y)(1-x-y)} + 2\ln\left(\frac{1-y}{1-x-y}\right) \right] , \quad \text{(B.1.7)}$$

$$f_2(x,y) = \frac{2}{3}(4\pi\epsilon\alpha_{\mathrm{EM}})^2 \left[\frac{x+2y-2}{(1-y)(1-x-y)} + \frac{2}{x}\ln\left(\frac{1-y}{1-x-y}\right) \right] . \quad \text{(B.1.8)}$$

Here $y_{\min}$ and $y_{\max}$ are the lower and the upper bounds of the integration region of y corresponding to the Dalitz region. The explicit forms of $y_{\min}$ and $y_{\max}$ are

$$y_{\min} = \max\left[1 - \frac{x}{2} - \frac{x}{2}\sqrt{1 - \frac{\epsilon_0^2}{1-x}}, \epsilon_0 \right] , \quad \text{(B.1.9)}$$

$$y_{\max} = \min\left[1 - \frac{x}{2} + \frac{x}{2}\sqrt{1 - \frac{\epsilon_0^2}{1-x}}, 1 \right] . \quad \text{(B.1.10)}$$

From above, we obtain the energy spectrum of the final state radiation photon. The energy spectrum is expressed as [149]

$$\frac{1}{N_\gamma}\frac{\mathrm{d}N_\gamma}{\mathrm{d}x} = \frac{1}{\Gamma_{\gamma'\to e^+e^-}}\frac{d\Gamma_{\gamma'\to e^+e^-\gamma}}{dx} . \quad \text{(B.1.11)}$$

Here, $\Gamma_{\gamma'\to e^+e^-} = \frac{1}{3}\epsilon^2\alpha_{\mathrm{EM}}m_{\gamma'}$ is the decay rate of the process $\gamma' \to e^+e^-$. We compare the result with twice the Altarelli-Parisi approximation formula

77

[148]

$$\frac{1}{\Gamma_{\gamma'\to e^+e^-}}\frac{d\Gamma_{\gamma'\to e^+e^-\gamma}}{dx} = \frac{\alpha_{\text{EM}}}{\pi}\frac{1+(1-x)^2}{x}\ln\left(\frac{4(1-x)}{\epsilon_0^2}\right), \qquad \text{(B.1.12)}$$

in figure B.2. We take $m_{\gamma'} = 40\,\text{MeV}$. We see that two formulae are in good agreement in a wide range of the photon momentum.

B.2 Sommerfeld enhancement

The dark pion exchange between the dark nucleons generates attractive/repulsive forces between them depending on their spins and the isospins.[1] For example, one dark pion exchange results in a static potential,

$$V(\mathbf{r}) = \frac{g_A'^2}{16\pi f_{\pi'}^2}(\tau_1\cdot\tau_2)(\sigma_1\cdot\partial)(\sigma_2\cdot\partial)\frac{1}{r}e^{-m_{\pi'}r}, \qquad \text{(B.2.1)}$$

which goes like $1/r^3$ in the region of $r \ll m_{\pi'}^{-1}$. This potential is obtained from the axial-current interaction,

$$\mathcal{L} = \frac{g_A'}{f_{\pi'}}\,\partial^a\pi'\bar{N}'\gamma_\mu\gamma_5\left(\frac{\tau^a}{2}\right)N', \qquad \text{(B.2.2)}$$

where $f_{\pi'}$ is the decay constant of the dark pion and g_A' is the form factor of the dark nucleon axial current.[2] The spin and the isospin indices are implicit, where σ and τ denote the Pauli matrices applying to the spin and the isospin of each nucleon, respectively. The way of the isospin transition can be read off by noting $\tau_{1\,ij}\cdot\tau_{2,k\ell} = 2(\delta_{i\ell}\delta_{jk} - \delta_{ij}\delta_{k\ell}/2)$.

As discussed in [198, 199, 200], the attractive potential forces mediated by the pseudo-scalar field cause the Sommerfeld enhancement of the dark matter annihilation [201, 202, 203, 204]. In this appendix, we discuss the Sommerfeld enhancement caused by the dark pion exchange. In our analysis, we rely on the formalism of the Sommerfeld enhancement in [205], in which the lower cut-off on the relative velocity is taken into account in a self-consistent way.

Following [200], we approximate the potential by a spherical one,

$$V(\mathbf{r}) \simeq -\frac{g_A'^2}{16\pi f_{\pi'}^2}\frac{1}{r^3}e^{-m_{\pi'}}, \qquad \text{(B.2.3)}$$

---

[1]Since the dark quark masses are assumed to be much smaller than the dark dynamical scale, the dark sector possesses the isospin symmetry as in the case of the QCD in the SM sector.

[2]We take the normalization such that $f_\pi \simeq 93\,\text{MeV}$ and $g_A \simeq 1.26$ in the case of the SM.

and estimate the enhancement of the s-wave annihilation.[3] Under this approximation, the Sommerfeld enhancement factor can be obtained by solving the effective Schrödinger equation,

$$\left[-\frac{\nabla^2}{2m_{\text{RED}}} + V(\mathbf{r}) + u\delta^{(3)}(\mathbf{r})\right]\psi(\mathbf{r}) = \frac{p^2}{2m_{\text{RED}}}\psi(\mathbf{r}) .$$ (B.2.4)

Here, $m_{\text{RED}} = m_{\text{DM}}/2$ is the reduced mass and p denotes the relative momentum of the incident dark matter. The boundary condition of the wave function $\psi(\mathbf{r})$ is taken to be an incident plane wave with an outgoing spherical wave, i.e. $\psi(\mathbf{r}) \to e^{ipz} + fe^{ipr}/r$ at $r \to \infty$. The complex parameter u encodes the annihilation cross section at a short distance without the Sommerfeld enhancement factor, i.e. $u = -i\sigma v_0/2$.[4]

Since the potential goes to infinity faster than r^{-2} at the origin, it must be regularized at short distances. In our analysis, we introduce a short distance cutoff r_0 satisfying $V(r_0) = m_{\text{DM}}$ and regulate the scalar potential by replacing $V(r) \to V_{\text{reg}}(r) = V(r + r_0)$ [199, 200].[5] With the regulated potential, the Sommerfeld enhancement factor is given by [205],

$$S_{\text{ENF}}(v) = \frac{\sigma v}{\sigma v_0} \simeq \frac{S(v)}{\left|1 - i\frac{m_{\text{RED}}^2}{4\pi}\sigma v_0(T(v) + iS(v))v\right|^2} .$$ (B.2.5)

Here, $T(v)$ and $S(v)$ are given by,

$$T(v) = \frac{1}{p}\left(\text{Re}\left.\frac{dg_p}{dr}\right|_{r=0} - \text{Re}\left.\frac{dg_{p_0}}{dr}\right|_{r=0}\right) ,$$ (B.2.6)

$$S(v) = \frac{1}{p}\text{Im}\left.\frac{dg_p}{dr}\right|_{r=0} ,$$ (B.2.7)

with the function $g_p(r)$ being a solution of

$$\left[-\frac{d^2}{dr^2} + 2m_{\text{RED}}V_{\text{reg}}(r) - p^2\right]g_p(r) = 0 ,$$ (B.2.8)

$$g_p(0) = 1 ,$$ (B.2.9)

$$\lim_{r\to\infty} g_p(r) \propto e^{ipr} .$$ (B.2.10)

The short distance cross section σv_0 is fixed at a high momentum p_0.

---

[3]Strictly speaking, we need to solve a coupled equation between the states with angular momenta, since the potential force in Eq. (B.2.1) changes the nucleon angular momentum by $\Delta\ell = \pm 2$.

[4]The dark-nucleon self-scattering due to short-range forces can be also encoded in the real part of u. In our analysis, we assume the self-scattering by short-range forces is subdominant and take $\text{Re}\, u \simeq 0$.

[5]Our conclusions do not depend on the choice of the regularization significantly.
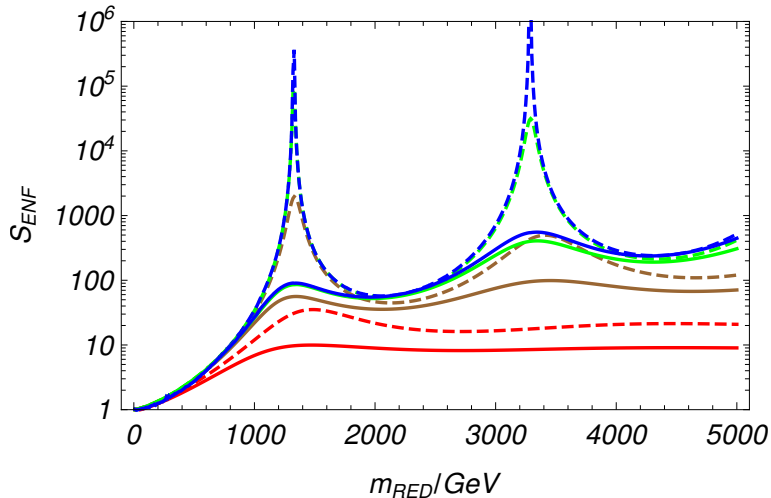
Figure B.3: The self-consistent Sommerfeld enhancement factor for an s-wave annihilation by the $1/r^3$ potential for $v = 10^{-1}$(red), 10^{-2}(brown), 10^{-3}(green), and 10^{-5}(blue). We take the same parameters with [200] (Figure 3 in the reference) for comparison. The short-range annihilation cross section is assumed to be $\sigma v_0 = 4\pi/m_{\mathrm{DM}}^2$. The solid lines are the enhancement factor in Eq. (B.2.5), and the dashed ones are the naive enhancement factor $S(v)$.

In Eq. (B.2.5), the factor $S(v)$ corresponds to the naive Sommerfeld enhancement factor. The denominator, on the other hand, provides an IR cutoff in the limit of $v \to 0$ with which the unitarity violation by the naive Sommerfeld enhancement factor is regulated self-consistently. The regularization effect is particularly important when the short-distance cross section is large as in the case of the ADM scenario. In Figure B.3, we compare the naive enhancement factor shown in [200] and the one in Eq. (B.2.5) by assuming $\sigma v_0 = 4\pi/m_{\mathrm{DM}}^2$.[6] The figure shows that the enhancement factors at the resonances are significantly suppressed when the short-distance annihilation cross section is large.

Now, let us apply Eq. (B.2.5) to the dark nucleon annihilation. In Figure B.4, we show the Sommerfeld enhancement factor as a function of m_{DM} for $g_A = 1$, $f_{\pi'} = 1\,\mathrm{GeV}$, and $m_{\pi'} = 1\,\mathrm{GeV}$. The figure shows that the regularization effects are important at around the resonance, $m_{\mathrm{DM}} \simeq 21\,\mathrm{GeV}$. The figure also shows that the Sommerfeld enhancement factor for the mass region of the ADM, $m_{\mathrm{DM}} \lesssim 10\,\mathrm{GeV}$, is less significant.

As we fix the short-range cross section of the ADM, $\sigma v_0 \simeq 4\pi/m_{\mathrm{DM}}^2$, to mimic the measured nucleon annihilation cross section at $v = \mathcal{O}(10^{-1})$ [154,

---

[6]Due to a slightly different choice of $V_{\mathrm{reg}}(r)$, the positions of the resonances appearing in $S(v)$ are shifted from those in [206].
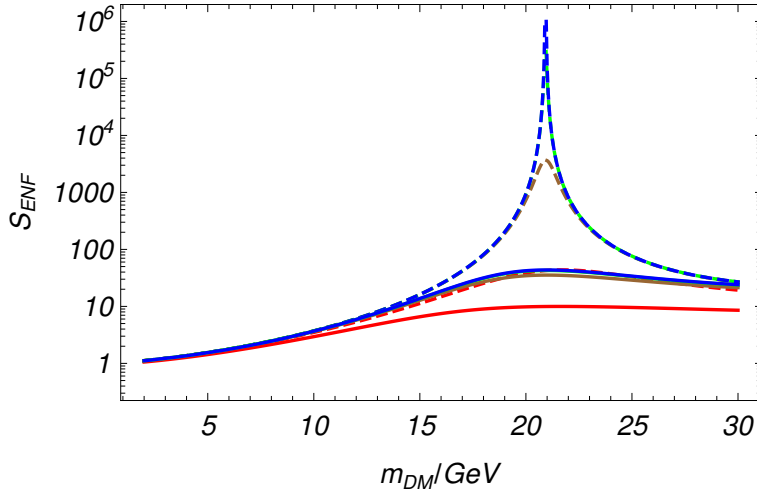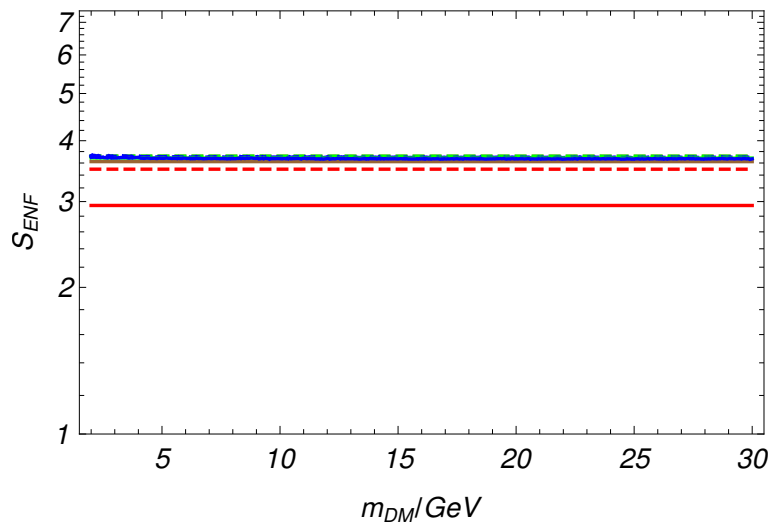
Figure B.4: The self-consistent Sommerfeld enhancement factor for an s-wave dark nucleon annihilation by the $1/r^3$ potential for $v = 10^{-1}$(red), 10^{-2}(brown), 10^{-3}(green) and 10^{-4}(blue). The parameters are fixed to be $g_A = 1$, $f_{\pi'} = 1\,\mathrm{GeV}$, and $m_{\pi'} = 1\,\mathrm{GeV}$. The solid lines are the enhancement factor in Eq. (B.2.5), and the dashed ones are the naive enhancement factor $S(v)$.

155], the effective Sommerfeld enhancement factor corresponds to $S_{\mathrm{ENF}}(v)/S_{\mathrm{ENF}}(10^{-1})$. The figure shows that the effective enhancement factor is close to unity for $m_{\mathrm{DM}} \lesssim 10\,\mathrm{GeV}$.

In Figure B.5, we also show the Sommerfeld enhancement factor for more realistic relations between the parameters,

$$f_{\pi'} = 0.1 \times m_{\mathrm{DM}} \ , \quad m_{\pi'} = 0.1 \times m_{\mathrm{DM}} \ , \tag{B.2.11}$$

which mimic QCD. The figure shows that no resonance appears when the parameters satisfy these relations. As a result, we find that the effective enhancement factor, $S_{\mathrm{ENF}}(v)/S_{\mathrm{ENF}}(10^{-1})$, is $\mathcal{O}(1)$.[7] We also numerically confirmed that the results do not depend on the dark pion mass as long as it is much lighter than the dark nucleon. Therefore, we conclude that the Sommerfeld enhancement is not significant in the present setup.

---

[7]The Sommerfeld enhancement for coupled channels between different angular momenta requires more careful analysis. However, as the centrifugal barriers of the higher angular momenta make the attractive potential wells shallower and smaller in spatial size, the resonances are expected to appear at a higher dark nucleon mass than those for $\ell = 0$. Thus, the coupled equations do not lead to resonances in the mass range $m_{\mathrm{DM}} \lesssim 10\,\mathrm{GeV}$.

Figure B.5: The self-consistent Sommerfeld enhancement factor for an *s*-wave dark nucleon annihilation by the $1/r^3$ potential for $v = 10^{-1}$ (red), 10^{-2} (brown), 10^{-3} (green) and 10^{-4} (blue). The parameters are chosen to be $g_A = 1$, $f_{\pi'} = 0.1 \times m_{\mathrm{DM}}$, and $m_{\pi'} = 0.1 \times m_{\mathrm{DM}}$. The solid lines are the enhancement factor in Eq. (B.2.5), and the dashed ones are the naive enhancement factor $S(v)$.

Appendix C

Asymmetry in Chiral ADM

In this appendix, we show the detailed calculation of the asymmetry, which appears in section 6.2.

C.1   Calculation of Asymmetry

In this appendix, we calculate the ratio of the $B-L$ asymmetries in the dark and the visible sectors, $A_{\mathrm{DM}}/A_{\mathrm{SM}}$, following Ref. [207]. We also calculate the asymmetry between the dark pion and the dark anti-pion.

Let q_{ia} be a charge of a massless particle species i in thermal equilibrium, where a denotes a conserved quantum number such as $B-L$ or the weak hypercharge, Y. The chemical potential of the particle i, μ_i, can be written as

$$\mu_i = \sum_a q_{ia}\mu_a, \qquad (\mathrm{C.1.1})$$

where μ_a is a chemical potential associated with the conserved quantity. The difference between the number density of i and its antiparticle at temperature T is given by,

$$n_i - \bar{n}_i = \frac{T^2}{6}\tilde{g}_i\mu_i\,. \qquad (\mathrm{C.1.2})$$

Here, $\tilde{g}_i$ is (twice of) a spin degree of freedom for a fermion (boson). From these equations, the following equation holds,

$$n_i - \bar{n}_i = \sum_{a,b} \tilde{g}_i q_{ia} M_{ab}^{-1} A_b\,, \qquad (\mathrm{C.1.3})$$

where $M_{ab} = \sum_i \tilde{g}_i q_{ia} q_{ib}$ and $A_a = \sum_i A_{ia} = \sum_i q_{ia}(n_i - \bar{n}_i)$. Thus, by giving the asymmetries of the conserved quantum number, A_a, we obtain the particle-antiparticle asymmetries of each particle.

83

Asymmetry Ratio For $T_e > T_D$

When the decoupling temperature of the $B-L$ portal interaction in Eq. (6.1.21), T_D, is lower than the temperature T_e at which the electron Yukawa coupling becomes effective, the ratio of the $B-L$ asymmetries are given by [106],

$$\frac{A_{\rm DM}}{A_{\rm SM}} = \frac{22}{237} N_f \ . \tag{C.1.4}$$

Note that $U(1)_D$ gauge symmetry is conserved at $T \gg \Lambda'_D$ in the present model while there is no $U(1)_D$ gauge symmetry in the model in Ref. [106]. With the additional conserved quantity, $A_{\rm DM}/A_{\rm SM}$ can be different in general. In the present model, however, $M^{-1}_{B-L,U(1)_D} = 0$, and hence, the ratio $A_{\rm DM}/A_{\rm SM}$ coincides with the model in Ref. [106]. For the model in chapter 4, on the other hand, $M^{-1}_{B-L,U(1)_D} \neq 0$, and hence, the asymmetry ratio is slightly changed to $A_{\rm DM}/A_{\rm SM} = 66 N_f/395$.

Asymmetry Ratio For $T_{ud} > T_D > T_{\rm e}$

When T_D is higher than T_e, we have an additional conserved quantum number, i.e., the number of the right-handed electron number in the visible sector. The presence of the additional conserved quantum number alters the $B-L$ ratio. By assuming the initial condition, $\mu_{e_R} = 0$, we obtain,

$$\frac{A_{\rm DM}}{A_{\rm SM}} = \frac{20}{213} N_f \ . \tag{C.1.5}$$

After the decoupling of the $B-L$ portal, this value does not change, since the $B-L$ charge is conserved separately in the dark and the visible sectors.

Asymmetry Ratio For $T_D > T_{ud}$

When the up and down Yukawa couplings are ineffective, we also have an additional conserved quantum number in the visible sector corresponding to the charge under the $U(1)_{T_{3R}}$ symmetry, which is the third component of the $SU(2)_R$ in the visible sector. In this case, the asymmetry ratio becomes

$$\frac{A_{\rm DM}}{A_{\rm SM}} = \frac{17}{149} N_f \ . \tag{C.1.6}$$

As in the case of $T_{ud} > T_D > T_e$, this value does not change after the decoupling of the $B-L$ portal.

Asymmetry of the Dark Pions

Since we assume that only the $B-L$ asymmetry is generated, the asymmetry between the dark pion and dark anti-pion is given by,

$$n_{\pi'} - n_{\bar{\pi}'} = 2 q_{\pi',I'_3} M^{-1}_{I'_3 B-L} A_{B-L} \ , \tag{C.1.7}$$

since $q_{\pi',B-L} = 0$. In the chiral ADM in Tab. 6.1 and in Tab. 6.2, we find that $M^{-1}_{I'_3 B-L} = 0$, and hence, the dark pion does not have asymmetry.

Bibliography

[1] M. Ibe, A. Kamada, S. Kobayashi, and W. Nakano, "Composite Asymmetric Dark Matter with a Dark Photon Portal," *JHEP* **11** (2018) 203, `arXiv:1805.06876 [hep-ph]`.

[2] M. Ibe, S. Kobayashi, R. Nagai, and W. Nakano, "Oscillating Composite Asymmetric Dark Matter," *JHEP* **01** (2020) 027, `arXiv:1907.11464 [hep-ph]`.

[3] M. Ibe, S. Kobayashi, and K. Watanabe, "Chiral Composite Asymmetric Dark Matter," `arXiv:2105.07642 [hep-ph]`.

[4] F. Zwicky, "Die Rotverschiebung von extragalaktischen Nebeln," *Helv. Phys. Acta* **6** (1933) 110–127.

[5] G. D'Amico, M. Kamionkowski, and K. Sigurdson, "Dark Matter Astrophysics," `arXiv:0907.1912 [astro-ph.CO]`.

[6] G. Bertone and D. Hooper, "History of dark matter," *Rev. Mod. Phys.* **90** no. 4, (2018) 045002, `arXiv:1605.04909 [astro-ph.CO]`.

[7] G. B. Gelmini, M. Gleiser, and E. W. Kolb, "Cosmology of Biased Discrete Symmetry Breaking," *Phys. Rev.* **D39** (1989) 1558.

[8] G. Arcadi, M. Dutra, P. Ghosh, M. Lindner, Y. Mambrini, M. Pierre, S. Profumo, and F. S. Queiroz, "The waning of the WIMP? A review of models, searches, and constraints," *Eur. Phys. J. C* **78** no. 3, (2018) 203, `arXiv:1703.07364 [hep-ph]`.

[9] L. Roszkowski, E. M. Sessolo, and S. Trojanowski, "WIMP dark matter candidates and searches—current status and future prospects," *Rept. Prog. Phys.* **81** no. 6, (2018) 066201, `arXiv:1707.06277 [hep-ph]`.

[10] **Planck** Collaboration, N. Aghanim *et al.*, "Planck 2018 results. VI. Cosmological parameters," `arXiv:1807.06209 [astro-ph.CO]`.

[11] D. E. Kaplan, M. A. Luty, and K. M. Zurek, "Asymmetric Dark Matter," *Phys. Rev.* **D79** (2009) 115016, `arXiv:0901.4117 [hep-ph]`.

[12] D. S. M. Alves, S. R. Behbahani, P. Schuster, and J. G. Wacker, "Composite Inelastic Dark Matter," *Phys. Lett.* **B692** (2010) 323–326, `arXiv:0903.3945 [hep-ph]`.

[13] D. S. M. Alves, S. R. Behbahani, P. Schuster, and J. G. Wacker, "The Cosmology of Composite Inelastic Dark Matter," *JHEP* **06** (2010) 113, `arXiv:1003.4729 [hep-ph]`.

[14] M. Blennow, E. Fernandez-Martinez, O. Mena, J. Redondo, and P. Serra, "Asymmetric Dark Matter and Dark Radiation," *JCAP* **1207** (2012) 022, `arXiv:1203.5803 [hep-ph]`.

[15] M. Fukugita and T. Yanagida, "Baryogenesis Without Grand Unification," *Phys. Lett.* **B174** (1986) 45–47.

[16] P. Minkowski, "$\mu \to e\gamma$ at a Rate of One Out of 10^9 Muon Decays?," *Phys. Lett.* **67B** (1977) 421–428.

[17] T. Yanagida, "HORIZONTAL SYMMETRY AND MASSES OF NEUTRINOS," *Conf. Proc.* **C7902131** (1979) 95–99.

[18] M. Gell-Mann, P. Ramond, and R. Slansky, "Complex Spinors and Unified Theories," *Conf. Proc.* **C790927** (1979) 315–321, `arXiv:1306.4669 [hep-th]`.

[19] S. L. Glashow, "The Future of Elementary Particle Physics," *NATO Sci. Ser. B* **61** (1980) 687.

[20] R. N. Mohapatra and G. Senjanovic, "Neutrino Mass and Spontaneous Parity Nonconservation," *Phys. Rev. Lett.* **44** (1980) 912. [,231(1979)].

[21] K. Harigaya and Y. Nomura, "Light Chiral Dark Sector," *Phys. Rev.* **D94** no. 3, (2016) 035013, `arXiv:1603.03430 [hep-ph]`.

[22] R. T. Co, K. Harigaya, and Y. Nomura, "Chiral Dark Sector," *Phys. Rev. Lett.* **118** no. 10, (2017) 101801, `arXiv:1610.03848 [hep-ph]`.

[23] P. Gondolo and G. Gelmini, "Cosmic abundances of stable particles: Improved analysis," *Nucl. Phys.* **B360** (1991) 145–179.

[24] E. W. Kolb and M. S. Turner, *The Early Universe*, vol. 69. 1990.

[25] **Planck** Collaboration, N. Aghanim *et al.*, "Planck 2018 results. VI. Cosmological parameters," *Astron. Astrophys.* **641** (2020) A6, `arXiv:1807.06209 [astro-ph.CO]`.

[26] **Planck** Collaboration, Y. Akrami *et al.*, "Planck 2018 results. VII. Isotropy and Statistics of the CMB," *Astron. Astrophys.* **641** (2020) A7, `arXiv:1906.02552 [astro-ph.CO]`.

[27] S. Dodelson, *Modern Cosmology.* Academic Press, Amsterdam, 2003.

[28] A. D. Sakharov, "Violation of CP Invariance, C asymmetry, and baryon asymmetry of the universe," *Pisma Zh. Eksp. Teor. Fiz.* **5** (1967) 32–35.

[29] N. S. Manton, "Topology in the Weinberg-Salam Theory," *Phys. Rev. D* **28** (1983) 2019.

[30] F. R. Klinkhamer and N. S. Manton, "A Saddle Point Solution in the Weinberg-Salam Theory," *Phys. Rev. D* **30** (1984) 2212.

[31] K. Kajantie, M. Laine, K. Rummukainen, and M. E. Shaposhnikov, "Is there a hot electroweak phase transition at $m_H \gtrsim m_W$?," *Phys. Rev. Lett.* **77** (1996) 2887–2890, `arXiv:hep-ph/9605288`.

[32] Y. Aoki, F. Csikor, Z. Fodor, and A. Ukawa, "The Endpoint of the first order phase transition of the SU(2) gauge Higgs model on a four-dimensional isotropic lattice," *Phys. Rev. D* **60** (1999) 013001, `arXiv:hep-lat/9901021`.

[33] G. F. Giudice, A. Notari, M. Raidal, A. Riotto, and A. Strumia, "Towards a complete theory of thermal leptogenesis in the SM and MSSM," *Nucl. Phys.* **B685** (2004) 89–149, `arXiv:hep-ph/0310123 [hep-ph]`.

[34] W. Buchmuller, R. D. Peccei, and T. Yanagida, "Leptogenesis as the origin of matter," *Ann. Rev. Nucl. Part. Sci.* **55** (2005) 311–355, `arXiv:hep-ph/0502169 [hep-ph]`.

[35] S. Davidson, E. Nardi, and Y. Nir, "Leptogenesis," *Phys. Rept.* **466** (2008) 105–177, `arXiv:0802.2962 [hep-ph]`.

[36] A. G. Cohen and D. B. Kaplan, "Thermodynamic Generation of the Baryon Asymmetry," *Phys. Lett. B* **199** (1987) 251–258.

[37] I. Affleck and M. Dine, "A New Mechanism for Baryogenesis," *Nucl. Phys.* **B249** (1985) 361–380.

[38] M. A. Luty, "Baryogenesis via leptogenesis," *Phys. Rev. D* **45** (1992) 455–465.

[39] W. Buchmuller, P. Di Bari, and M. Plumacher, "Cosmic microwave background, matter - antimatter asymmetry and neutrino masses,"

Nucl. Phys. B **643** (2002) 367–390, `arXiv:hep-ph/0205349`.
[Erratum: Nucl.Phys.B 793, 362 (2008)].

[40] W. Buchmuller, P. Di Bari, and M. Plumacher, "Leptogenesis for pedestrians," *Annals Phys.* **315** (2005) 305–351, `arXiv:hep-ph/0401240`.

[41] S. Y. Khlebnikov and M. E. Shaposhnikov, "The Statistical Theory of Anomalous Fermion Number Nonconservation," *Nucl. Phys. B* **308** (1988) 885–912.

[42] J. A. Harvey and M. S. Turner, "Cosmological baryon and lepton number in the presence of electroweak fermion-number violation," *Phys. Rev.* **D42** (1990) 3344–3349.

[43] S. Davidson and A. Ibarra, "A Lower bound on the right-handed neutrino mass from leptogenesis," *Phys. Lett. B* **535** (2002) 25–32, `arXiv:hep-ph/0202239`.

[44] G. L. Fogli, E. Lisi, A. Marrone, D. Montanino, A. Palazzo, and A. M. Rotunno, "Neutrino oscillations: A Global analysis," *eConf* **C030626** (2003) THAT05, `arXiv:hep-ph/0310012`.

[45] **K2K** Collaboration, M. H. Ahn *et al.*, "Indications of neutrino oscillation in a 250 km long baseline experiment," *Phys. Rev. Lett.* **90** (2003) 041801, `arXiv:hep-ex/0212007`.

[46] **T2K** Collaboration, L. Haegel, "The latest T2K neutrino oscillation results," *PoS* **EPS-HEP2017** (2017) 112, `arXiv:1709.04180 [hep-ex]`.

[47] H. Davoudiasl and R. N. Mohapatra, "On Relating the Genesis of Cosmic Baryons and Dark Matter," *New J. Phys.* **14** (2012) 095011, `arXiv:1203.1247 [hep-ph]`.

[48] K. Petraki and R. R. Volkas, "Review of asymmetric dark matter," *Int. J. Mod. Phys.* **A28** (2013) 1330028, `arXiv:1305.4939 [hep-ph]`.

[49] K. M. Zurek, "Asymmetric Dark Matter: Theories, Signatures, and Constraints," *Phys. Rept.* **537** (2014) 91–121, `arXiv:1308.0338 [hep-ph]`.

[50] D. Hooper, J. March-Russell, and S. M. West, "Asymmetric sneutrino dark matter and the Omega(b) / Omega(DM) puzzle," *Phys. Lett. B* **605** (2005) 228–236, `arXiv:hep-ph/0410114`.

[51] T. Cohen and K. M. Zurek, "Leptophilic Dark Matter from the Lepton Asymmetry," *Phys. Rev. Lett.* **104** (2010) 101301, `arXiv:0909.2035 [hep-ph]`.

[52] E. Hall, R. McGehee, H. Murayama, and B. Suter, "Asymmetric Dark Matter May Not Be Light," `arXiv:2107.03398 [hep-ph]`.

[53] B. Dutta and J. Kumar, "Asymmetric Dark Matter from Hidden Sector Baryogenesis," *Phys. Lett. B* **699** (2011) 364–367, `arXiv:1012.1341 [hep-ph]`.

[54] J. Shelton and K. M. Zurek, "Darkogenesis: A baryon asymmetry from the dark matter sector," *Phys. Rev. D* **82** (2010) 123512, `arXiv:1008.1997 [hep-ph]`.

[55] K. Petraki, M. Trodden, and R. R. Volkas, "Visible and dark matter from a first-order phase transition in a baryon-symmetric universe," *JCAP* **02** (2012) 044, `arXiv:1111.4786 [hep-ph]`.

[56] D. G. E. Walker, "Dark Baryogenesis," `arXiv:1202.2348 [hep-ph]`.

[57] G. Servant and S. Tulin, "Baryogenesis and Dark Matter through a Higgs Asymmetry," *Phys. Rev. Lett.* **111** no. 15, (2013) 151601, `arXiv:1304.3464 [hep-ph]`.

[58] E. Hall, T. Konstandin, R. McGehee, and H. Murayama, "Asymmetric Matters from a Dark First-Order Phase Transition," `arXiv:1911.12342 [hep-ph]`.

[59] A. Falkowski, J. T. Ruderman, and T. Volansky, "Asymmetric Dark Matter from Leptogenesis," *JHEP* **05** (2011) 106, `arXiv:1101.4936 [hep-ph]`.

[60] C. Cheung and K. M. Zurek, "Affleck-Dine Cogenesis," *Phys. Rev. D* **84** (2011) 035007, `arXiv:1105.4612 [hep-ph]`.

[61] C. Cheung and Y. Zhang, "Electroweak Cogenesis," *JHEP* **09** (2013) 002, `arXiv:1306.4321 [hep-ph]`.

[62] M. Schumann, "Direct Detection of WIMP Dark Matter: Concepts and Status," *J. Phys. G* **46** no. 10, (2019) 103003, `arXiv:1903.03026 [astro-ph.CO]`.

[63] M. W. Goodman and E. Witten, "Detectability of Certain Dark Matter Candidates," *Phys. Rev.* **D31** (1985) 3059.

[64] J. Billard *et al.*, "Direct Detection of Dark Matter – APPEC Committee Report," `arXiv:2104.07634 [hep-ex]`.

[65] M. C. Smith *et al.*, "The RAVE Survey: Constraining the Local Galactic Escape Speed," *Mon. Not. Roy. Astron. Soc.* **379** (2007) 755–772, `arXiv:astro-ph/0611671`.

[66] **XENON** Collaboration, E. Aprile *et al.*, "Dark Matter Search Results from a One Ton-Year Exposure of XENON1T," *Phys. Rev. Lett.* **121** no. 11, (2018) 111302, `arXiv:1805.12562 [astro-ph.CO]`.

[67] **XENON** Collaboration, E. Aprile *et al.*, "Light Dark Matter Search with Ionization Signals in XENON1T," *Phys. Rev. Lett.* **123** no. 25, (2019) 251801, `arXiv:1907.11485 [hep-ex]`.

[68] **XENON** Collaboration, E. Aprile *et al.*, "Search for Light Dark Matter Interactions Enhanced by the Migdal Effect or Bremsstrahlung in XENON1T," *Phys. Rev. Lett.* **123** no. 24, (2019) 241803, `arXiv:1907.12771 [hep-ex]`.

[69] **LUX** Collaboration, D. S. Akerib *et al.*, "Results from a search for dark matter in the complete LUX exposure," *Phys. Rev. Lett.* **118** no. 2, (2017) 021303, `arXiv:1608.07648 [astro-ph.CO]`.

[70] **LUX** Collaboration, D. S. Akerib *et al.*, "Results of a Search for Sub-GeV Dark Matter Using 2013 LUX Data," *Phys. Rev. Lett.* **122** no. 13, (2019) 131301, `arXiv:1811.11241 [astro-ph.CO]`.

[71] **PandaX-II** Collaboration, X. Cui *et al.*, "Dark Matter Results From 54-Ton-Day Exposure of PandaX-II Experiment," *Phys. Rev. Lett.* **119** no. 18, (2017) 181302, `arXiv:1708.06917 [astro-ph.CO]`.

[72] **DarkSide** Collaboration, P. Agnes *et al.*, "Low-Mass Dark Matter Search with the DarkSide-50 Experiment," *Phys. Rev. Lett.* **121** no. 8, (2018) 081307, `arXiv:1802.06994 [astro-ph.HE]`.

[73] **CRESST** Collaboration, A. H. Abdelhameed *et al.*, "First results from the CRESST-III low-mass dark matter program," *Phys. Rev. D* **100** no. 10, (2019) 102002, `arXiv:1904.00498 [astro-ph.CO]`.

[74] **SuperCDMS** Collaboration, R. Agnese *et al.*, "Search for Low-Mass Dark Matter with CDMSlite Using a Profile Likelihood Fit," *Phys. Rev. D* **99** no. 6, (2019) 062001, `arXiv:1808.09098 [astro-ph.CO]`.

[75] **DARWIN** Collaboration, J. Aalbers *et al.*, "DARWIN: towards the ultimate dark matter detector," *JCAP* **11** (2016) 017, `arXiv:1606.07001 [astro-ph.IM]`.

[76] F. Ruppin, J. Billard, E. Figueroa-Feliciano, and L. Strigari, "Complementarity of dark matter detectors in light of the neutrino background," *Phys. Rev. D* **90** no. 8, (2014) 083510, `arXiv:1408.3581 [hep-ph]`.

[77] J. M. Gaskins, "A review of indirect searches for particle dark matter," *Contemp. Phys.* **57** no. 4, (2016) 496–525, `arXiv:1604.00014 [astro-ph.HE]`.

[78] J. F. Navarro, C. S. Frenk, and S. D. M. White, "A Universal density profile from hierarchical clustering," *Astrophys. J.* **490** (1997) 493–508, `arXiv:astro-ph/9611107 [astro-ph]`.

[79] K. Hayashi, K. Ichikawa, S. Matsumoto, M. Ibe, M. N. Ishigaki, and H. Sugai, "Dark matter annihilation and decay from non-spherical dark halos in galactic dwarf satellites," *Mon. Not. Roy. Astron. Soc.* **461** no. 3, (2016) 2914–2928, `arXiv:1603.08046 [astro-ph.GA]`.

[80] **Fermi-LAT** Collaboration, W. B. Atwood *et al.*, "The Large Area Telescope on the Fermi Gamma-ray Space Telescope Mission," *Astrophys. J.* **697** (2009) 1071–1102, `arXiv:0902.1089 [astro-ph.IM]`.

[81] **Fermi-LAT** Collaboration, M. Ackermann *et al.*, "The Fermi Large Area Telescope On Orbit: Event Classification, Instrument Response Functions, and Calibration," *Astrophys. J. Suppl.* **203** (2012) 4, `arXiv:1206.1896 [astro-ph.IM]`.

[82] **MAGIC** Collaboration, V. Fonseca, "The MAGIC telescope project," *Acta Phys. Polon. B* **30** (1999) 2331–2349.

[83] **CTA Consortium** Collaboration, B. S. Acharya *et al.*, "Introducing the CTA concept," *Astropart. Phys.* **43** (2013) 3–18.

[84] E. C. Stone, A. C. Cummings, F. B. McDonald, B. C. Heikkila, N. Lal, and W. R. Webber, "Voyager 1 observes low-energy galactic cosmic rays in a region depleted of heliospheric ions," *Science* **341** no. 6142, (June, 2013) 150–153. `https://doi.org/10.1126/science.1236408`.

[85] **Super-Kamiokande** Collaboration, Y. Fukuda *et al.*, "The Super-Kamiokande detector," *Nucl. Instrum. Meth. A* **501** (2003) 418–462.

[86] **Super-Kamiokande** Collaboration, K. Abe *et al.*, "Indirect search for dark matter from the Galactic Center and halo with the Super-Kamiokande detector," *Phys. Rev. D* **102** no. 7, (2020) 072002, `arXiv:2005.05109 [hep-ex]`.

[87] M. L. Graesser, I. M. Shoemaker, and L. Vecchi, "Asymmetric WIMP dark matter," *JHEP* **10** (2011) 110, `arXiv:1103.2771 [hep-ph]`.

[88] H. Iminniyaz, M. Drees, and X. Chen, "Relic Abundance of Asymmetric Dark Matter," *JCAP* **1107** (2011) 003, arXiv:1104.5548 [hep-ph].

[89] N. F. Bell, S. Horiuchi, and I. M. Shoemaker, "Annihilating Asymmetric Dark Matter," *Phys. Rev.* **D91** no. 2, (2015) 023505, arXiv:1408.5142 [hep-ph].

[90] I. Baldes and K. Petraki, "Asymmetric thermal-relic dark matter: Sommerfeld-enhanced freeze-out, annihilation signals and unitarity bounds," *JCAP* **1709** no. 09, (2017) 028, arXiv:1703.00478 [hep-ph].

[91] I. Baldes, M. Cirelli, P. Panci, K. Petraki, F. Sala, and M. Taoso, "Asymmetric dark matter: residual annihilations and self-interactions," arXiv:1712.07489 [hep-ph].

[92] **Planck** Collaboration, P. A. R. Ade *et al.*, "Planck 2015 results. - XIII. Cosmological parameters," *Astron. Astrophys.* **594** (2016) A13, arXiv:1502.01589 [astro-ph.CO].

[93] K. Saikawa and S. Shirai, "Primordial gravitational waves, precisely: The role of thermodynamics in the Standard Model," *JCAP* **1805** no. 05, (2018) 035, arXiv:1803.01038 [hep-ph].

[94] E. D. Carlson, M. E. Machacek, and L. J. Hall, "Self-interacting dark matter," *Astrophys. J.* **398** (1992) 43–52.

[95] M. Escudero, "Neutrino decoupling beyond the Standard Model: CMB constraints on the Dark Matter mass with a fast and precise N_{eff} evaluation," *JCAP* **02** (2019) 007, arXiv:1812.05605 [hep-ph].

[96] G. Mangano, G. Miele, S. Pastor, T. Pinto, O. Pisanti, and P. D. Serpico, "Relic neutrino decoupling including flavor oscillations," *Nucl. Phys.* **B729** (2005) 221–234, arXiv:hep-ph/0506164 [hep-ph].

[97] P. F. de Salas and S. Pastor, "Relic neutrino decoupling with flavour oscillations revisited," *JCAP* **1607** no. 07, (2016) 051, arXiv:1606.06986 [hep-ph].

[98] J. H. Chang, R. Essig, and S. D. McDermott, "Revisiting Supernova 1987A Constraints on Dark Photons," *JHEP* **01** (2017) 107, arXiv:1611.03864 [hep-ph].

[99] J. H. Chang, R. Essig, and S. D. McDermott, "Supernova 1987A Constraints on Sub-GeV Dark Sectors, Millicharged Particles, the

QCD Axion, and an Axion-like Particle," `arXiv:1803.00993`
`[hep-ph]`.

[100] M. Bauer, P. Foldenauer, and J. Jaeckel, "Hunting All the Hidden
Photons," `arXiv:1803.05466 [hep-ph]`.

[101] M. Ibe, S. Kobayashi, Y. Nakayama, and S. Shirai, "Cosmological
constraint on dark photon from N_{eff}," *JHEP* **04** (2020) 009,
`arXiv:1912.12152 [hep-ph]`.

[102] R. Foot and R. R. Volkas, "Was ordinary matter synthesized from
mirror matter? An Attempt to explain why $\Omega_B \approx 0.2\Omega_{dark}$," *Phys.
Rev.* **D68** (2003) 021304, `arXiv:hep-ph/0304261 [hep-ph]`.

[103] H. An, S.-L. Chen, R. N. Mohapatra, and Y. Zhang, "Leptogenesis
as a Common Origin for Matter and Dark Matter," *JHEP* **03** (2010)
124, `arXiv:0911.4463 [hep-ph]`.

[104] M. Farina, "Asymmetric Twin Dark Matter," *JCAP* **1511** no. 11,
(2015) 017, `arXiv:1506.03520 [hep-ph]`.

[105] S. J. Lonsdale and R. R. Volkas, "Comprehensive asymmetric dark
matter model," *Phys. Rev.* **D97** (2018) 103510, `arXiv:1801.05561`
`[hep-ph]`.

[106] H. Fukuda, S. Matsumoto, and S. Mukhopadhyay, "Asymmetric dark
matter in early Universe chemical equilibrium always leads to an
antineutrino signal," *Phys. Rev.* **D92** no. 1, (2015) 013008,
`arXiv:1411.4014 [hep-ph]`.

[107] **Super-Kamiokande** Collaboration, K. Frankiewicz, "Indirect
searches for dark matter particles with the Super-Kamiokande
detector," *Nuovo Cim. C* **38** no. 4, (2016) 125.

[108] K. Frankiewicz, *Indirect Search for Dark Matter with the
Super-Kamiokande Detector.* PhD thesis, Warsaw, Inst. Nucl.
Studies, 2018.

[109] L. Covi, M. Grefe, A. Ibarra, and D. Tran, "Neutrino Signals from
Dark Matter Decay," *JCAP* **1004** (2010) 017, `arXiv:0912.3521`
`[hep-ph]`.

[110] G. Krnjaic and K. Sigurdson, "Big Bang Darkleosynthesis," *Phys.
Lett.* **B751** (2015) 464–468, `arXiv:1406.1171 [hep-ph]`.

[111] W. Detmold, M. McCullough, and A. Pochinsky, "Dark Nuclei I:
Cosmology and Indirect Detection," *Phys. Rev.* **D90** no. 11, (2014)
115013, `arXiv:1406.2276 [hep-ph]`.

[112] W. Detmold, M. McCullough, and A. Pochinsky, "Dark nuclei. II. Nuclear spectroscopy in two-color QCD," *Phys. Rev.* **D90** no. 11, (2014) 114506, `arXiv:1406.4116 [hep-lat]`.

[113] M. B. Wise and Y. Zhang, "Yukawa Bound States of a Large Number of Fermions," *JHEP* **02** (2015) 023, `arXiv:1411.1772 [hep-ph]`. [Erratum: JHEP10,165(2015)].

[114] E. Hardy, R. Lasenby, J. March-Russell, and S. M. West, "Big Bang Synthesis of Nuclear Dark Matter," *JHEP* **06** (2015) 011, `arXiv:1411.3739 [hep-ph]`.

[115] M. I. Gresham, H. K. Lou, and K. M. Zurek, "Early Universe synthesis of asymmetric dark matter nuggets," *Phys. Rev.* **D97** no. 3, (2018) 036003, `arXiv:1707.02316 [hep-ph]`.

[116] M. I. Gresham, H. K. Lou, and K. M. Zurek, "Nuclear Structure of Bound States of Asymmetric Dark Matter," *Phys. Rev.* **D96** no. 9, (2017) 096012, `arXiv:1707.02313 [hep-ph]`.

[117] E. Del Nobile, M. Kaplinghat, and H.-B. Yu, "Direct Detection Signatures of Self-Interacting Dark Matter with a Light Mediator," *JCAP* **1510** no. 10, (2015) 055, `arXiv:1507.04007 [hep-ph]`.

[118] **XENON** Collaboration, E. Aprile *et al.*, "Physics reach of the XENON1T dark matter experiment," *JCAP* **1604** no. 04, (2016) 027, `arXiv:1512.07501 [physics.ins-det]`.

[119] B. J. Mount *et al.*, "LUX-ZEPLIN (LZ) Technical Design Report," `arXiv:1703.09144 [physics.ins-det]`.

[120] **DARWIN Consortium** Collaboration, **DARWIN** Consortium, L. Baudis, "DARWIN dark matter WIMP search with noble liquids," *J. Phys. Conf. Ser.* **375** (2012) 012028, `arXiv:1201.2402 [astro-ph.IM]`.

[121] J. B. Dent, B. Dutta, J. L. Newstead, and L. E. Strigari, "Dark matter, light mediators, and the neutrino floor," *Phys. Rev.* **D95** no. 5, (2017) 051701, `arXiv:1607.01468 [hep-ph]`.

[122] M. Markevitch, A. H. Gonzalez, D. Clowe, A. Vikhlinin, L. David, W. Forman, C. Jones, S. Murray, and W. Tucker, "Direct constraints on the dark matter self-interaction cross-section from the merging galaxy cluster 1E0657-56," *Astrophys. J.* **606** (2004) 819–824, `arXiv:astro-ph/0309303 [astro-ph]`.

[123] S. W. Randall, M. Markevitch, D. Clowe, A. H. Gonzalez, and M. Bradac, "Constraints on the Self-Interaction Cross-Section of

Dark Matter from Numerical Simulations of the Merging Galaxy Cluster 1E 0657-56," *Astrophys. J.* **679** (2008) 1173–1180, `arXiv:0704.0261 [astro-ph]`.

[124] F. Kahlhoefer, K. Schmidt-Hoberg, M. T. Frandsen, and S. Sarkar, "Colliding clusters and dark matter self-interactions," *Monthly Notices of the Royal Astronomical Society* **437** no. 3, (Nov, 2013) 2865–2881. `http://dx.doi.org/10.1093/mnras/stt2097`.

[125] D. Harvey, R. Massey, T. Kitching, A. Taylor, and E. Tittley, "The nongravitational interactions of dark matter in colliding galaxy clusters," *Science* **347** no. 6229, (Mar, 2015) 1462–1465. `http://dx.doi.org/10.1126/science.1261381`.

[126] A. Robertson, R. Massey, and V. Eke, "What does the bullet cluster tell us about self-interacting dark matter?" *Monthly Notices of the Royal Astronomical Society* **465** no. 1, (Oct, 2016) 569–587. `http://dx.doi.org/10.1093/mnras/stw2670`.

[127] D. Wittman, N. Golovich, and W. A. Dawson, "The mismeasure of mergers: Revised limits on self-interacting dark matter in merging galaxy clusters," *The Astrophysical Journal* **869** no. 2, (Dec, 2018) 104. `http://dx.doi.org/10.3847/1538-4357/aaee77`.

[128] D. Harvey, A. Robertson, R. Massey, and I. G. McCarthy, "Observable tests of self-interacting dark matter in galaxy clusters: Bcg wobbles in a constant density core," *Monthly Notices of the Royal Astronomical Society* **488** no. 2, (Jul, 2019) 1572–1579. `http://dx.doi.org/10.1093/mnras/stz1816`.

[129] K. Bondarenko, A. Sokolenko, A. Boyarsky, A. Robertson, D. Harvey, and Y. Revaz, "From dwarf galaxies to galaxy clusters: Self-Interacting Dark Matter over 7 orders of magnitude in halo mass," `arXiv:2006.06623 [astro-ph.CO]`.

[130] L. Sagunski, S. Gad-Nasr, B. Colquhoun, A. Robertson, and S. Tulin, "Velocity-dependent Self-interacting Dark Matter from Groups and Clusters of Galaxies," `arXiv:2006.12515 [astro-ph.CO]`.

[131] K. Hayashi, M. Ibe, S. Kobayashi, Y. Nakayama, and S. Shirai, "Probing dark matter self-interaction with ultrafaint dwarf galaxies," *Phys. Rev. D* **103** no. 2, (2021) 023017, `arXiv:2008.02529 [astro-ph.CO]`.

[132] S. L. Zoutendijk, J. Brinchmann, N. F. Bouché, M. Den Brok, D. Krajnović, K. Kuijken, M. V. Maseda, and J. Schaye, "The MUSE-Faint survey. II. The dark matter-density profile of the

ultra-faint dwarf galaxy Eridanus 2," `arXiv:2101.00253` `[astro-ph.GA]`.

[133] Y. Cai, M. A. Luty, and D. E. Kaplan, "Leptonic Indirect Detection Signals from Strongly Interacting Asymmetric Dark Matter," `arXiv:0909.5499 [hep-ph]`.

[134] M. R. Buckley and S. Profumo, "Regenerating a Symmetry in Asymmetric Dark Matter," *Phys. Rev. Lett.* **108** (2012) 011301, `arXiv:1109.2164 [hep-ph]`.

[135] M. Cirelli, P. Panci, G. Servant, and G. Zaharijas, "Consequences of DM/antiDM Oscillations for Asymmetric WIMP Dark Matter," *JCAP* **1203** (2012) 015, `arXiv:1110.3809 [hep-ph]`.

[136] S. Tulin, H.-B. Yu, and K. M. Zurek, "Oscillating Asymmetric Dark Matter," *JCAP* **1205** (2012) 013, `arXiv:1202.0283 [hep-ph]`.

[137] N. Okada and O. Seto, "Originally Asymmetric Dark Matter," *Phys. Rev.* **D86** (2012) 063525, `arXiv:1205.2844 [hep-ph]`.

[138] E. Hardy, R. Lasenby, and J. Unwin, "Annihilation Signals from Asymmetric Dark Matter," *JHEP* **07** (2014) 049, `arXiv:1402.4500 [hep-ph]`.

[139] S.-L. Chen and Z. Kang, "Oscillating asymmetric sneutrino dark matter from the maximally $U(1)_L$ supersymmetric inverse seesaw," *Phys. Lett.* **B761** (2016) 296–302, `arXiv:1512.08780 [hep-ph]`.

[140] T. R. Slatyer and C.-L. Wu, "General Constraints on Dark Matter Decay from the Cosmic Microwave Background," *Phys. Rev. D* **95** no. 2, (2017) 023010, `arXiv:1610.06933 [astro-ph.CO]`.

[141] **Super-Kamiokande** Collaboration, K. Frankiewicz, "Dark matter searches with the Super-Kamiokande detector," *J. Phys. Conf. Ser.* **888** no. 1, (2017) 012210.

[142] T. Asaka, K. Hamaguchi, M. Kawasaki, and T. Yanagida, "Leptogenesis in inflaton decay," *Phys. Lett. B* **464** (1999) 12–18, `arXiv:hep-ph/9906366`.

[143] M. Ibe, T. Moroi, and T. Yanagida, "Dark matter and baryon asymmetry of the universe in large-cutoff supergravity," *Phys. Lett.* **B620** (2005) 9–16, `arXiv:hep-ph/0502074 [hep-ph]`.

[144] J. E. Gunn, B. W. Lee, I. Lerche, D. N. Schramm, and G. Steigman, "Some Astrophysical Consequences of the Existence of a Heavy Stable Neutral Lepton," *Astrophys. J.* **223** (1978) 1015–1031. [,190(1978)].

[145] L. Bergstrom, "Dark Matter Evidence, Particle Physics Candidates and Detection Methods," *Annalen Phys.* **524** (2012) 479–496, `arXiv:1205.4882 [astro-ph.HE]`.

[146] G. Gilmore, M. I. Wilkinson, R. F. G. Wyse, J. T. Kleyna, A. Koch, N. W. Evans, and E. K. Grebel, "The Observed properties of Dark Matter on small spatial scales," *Astrophys. J.* **663** (2007) 948–959, `arXiv:astro-ph/0703308 [ASTRO-PH]`.

[147] A. W. McConnachie, "The observed properties of dwarf galaxies in and around the Local Group," *Astron. J.* **144** (2012) 4, `arXiv:1204.1562 [astro-ph.CO]`.

[148] J. Mardon, Y. Nomura, D. Stolarski, and J. Thaler, "Dark Matter Signals from Cascade Annihilations," *JCAP* **0905** (2009) 016, `arXiv:0901.2926 [hep-ph]`.

[149] G. Elor, N. L. Rodd, and T. R. Slatyer, "Multistep cascade annihilations of dark matter and the Galactic Center excess," *Phys. Rev.* **D91** (2015) 103531, `arXiv:1503.01773 [hep-ph]`.

[150] G. Elor, N. L. Rodd, T. R. Slatyer, and W. Xue, "Model-Independent Indirect Detection Constraints on Hidden Sector Dark Matter," *JCAP* **1606** no. 06, (2016) 024, `arXiv:1511.08787 [hep-ph]`.

[151] Y. Gao, A. V. Gritsan, Z. Guo, K. Melnikov, M. Schulze, and N. V. Tran, "Spin Determination of Single-Produced Resonances at Hadron Colliders," *Phys. Rev.* **D81** (2010) 075022, `arXiv:1001.3396 [hep-ph]`.

[152] J. Liu, N. Weiner, and W. Xue, "Signals of a Light Dark Force in the Galactic Center," *JHEP* **08** (2015) 050, `arXiv:1412.1485 [hep-ph]`.

[153] S. J. Orfanidis and V. Rittenberg, "Nucleon-antinucleon annihilation into pions," *Nucl. Phys.* **B59** (1973) 570–582.

[154] **BROOKHAVEN-HOUSTON-PENNSYLVANIA STATE-RICE** Collaboration, T. Armstrong *et al.*, "Measurement of Anti-neutron Proton Total and Annihilation Cross-sections From 100-MeV/c to 500-MeV/c," *Phys. Rev.* **D36** (1987) 659–673.

[155] **OBELIX** Collaboration, A. Bertin *et al.*, "anti-n p annihilation in flight in two mesons in the momentum range between 50-MeV/c and 400-MeV/c with OBELIX," *Nucl. Phys. Proc. Suppl.* **56** (1997) 227–233. [,227(1997)].

[156] R. Huo, S. Matsumoto, Y.-L. Sming Tsai, and T. T. Yanagida, "A scenario of heavy but visible baryonic dark matter," *JHEP* **09** (2016) 162, `arXiv:1506.06929 [hep-ph]`.

[157] T.-G. Lee and C.-Y. Wong, "Nuclear annihilation by antinucleons," *Phys. Rev.* **C93** no. 1, (2016) 014616, `arXiv:1509.06031` `[nucl-th]`. [Erratum: Phys. Rev.C95,no.2,029901(2017)].

[158] A. Geringer-Sameth, S. M. Koushiappas, and M. Walker, "Dwarf galaxy annihilation and decay emission profiles for dark matter experiments," *Astrophys. J.* **801** no. 2, (2015) 74, `arXiv:1408.0002` `[astro-ph.CO]`.

[159] **Fermi-LAT** Collaboration, M. Ackermann *et al.*, "Searching for Dark Matter Annihilation from Milky Way Dwarf Spheroidal Galaxies with Six Years of Fermi Large Area Telescope Data," *Phys. Rev. Lett.* **115** no. 23, (2015) 231301, `arXiv:1503.02641` `[astro-ph.HE]`.

[160] L. A. Fisk, "Solar Modulation and a Galactic Origin for the Anomalous Component Observed in Low-Energy Cosmic Rays," *Astrophys. J.* **206** (1976) 333–341.

[161] M. Boudaud, J. Lavalle, and P. Salati, "Novel cosmic-ray electron and positron constraints on MeV dark matter particles," *Phys. Rev. Lett.* **119** no. 2, (2017) 021103, `arXiv:1612.07698` `[astro-ph.HE]`.

[162] M. Cirelli, G. Corcella, A. Hektor, G. Hutsi, M. Kadastik, P. Panci, M. Raidal, F. Sala, and A. Strumia, "PPPC 4 DM ID: A Poor Particle Physicist Cookbook for Dark Matter Indirect Detection," *JCAP* **1103** (2011) 051, `arXiv:1012.4515` `[hep-ph]`. [Erratum: JCAP1210,E01(2012)].

[163] J. Buch, M. Cirelli, G. Giesen, and M. Taoso, "PPPC 4 DM secondary: A Poor Particle Physicist Cookbook for secondary radiation from Dark Matter," *JCAP* **1509** (2015) 037, `arXiv:1505.01049` `[hep-ph]`.

[164] F. Donato, N. Fornengo, D. Maurin, and P. Salati, "Antiprotons in cosmic rays from neutralino annihilation," *Phys. Rev.* **D69** (2004) 063501, `arXiv:astro-ph/0306207` `[astro-ph]`.

[165] A. Burkert, "The Structure of dark matter halos in dwarf galaxies," *IAU Symp.* **171** (1996) 175, `arXiv:astro-ph/9504041` `[astro-ph]`. [Astrophys. J.447,L25(1995)].

[166] D. Maurin, F. Melot, and R. Taillet, "A database of charged cosmic rays," *Astron. Astrophys.* **569** (2014) A32, `arXiv:1302.5525` `[astro-ph.HE]`.

[167] **Fermi-LAT, DES** Collaboration, A. Albert *et al.*, "Searching for Dark Matter Annihilation in Recently Discovered Milky Way Satellites with Fermi-LAT," *Astrophys. J.* **834** no. 2, (2017) 110, `arXiv:1611.03184 [astro-ph.HE]`.

[168] **e-ASTROGAM** Collaboration, M. Tavani *et al.*, "Science with e-ASTROGAM: A space mission for MeV–GeV gamma-ray astrophysics," *JHEAp* **19** (2018) 1–106, `arXiv:1711.01265 [astro-ph.HE]`.

[169] **thee-ASTROGAM** Collaboration, R. Rando, A. De Angelis, and M. Mallamaci, "e-ASTROGAM: a space mission for MeV-GeV gamma-ray astrophysics," *J. Phys. Conf. Ser.* **1181** no. 1, (2019) 012044.

[170] T. Sawano, K. Hattori, and N. Higashi, "SMILE: A Balloon-Borne sub-MeV/MeV Gamma-ray Compton Camera Using an Electron-TrackingGaseous TPC and a Scintillation Camera," in *Proceedings, 32nd International Cosmic Ray Conference (ICRC 2011): Beijing, China, August 11-18, 2011*, vol. 9, p. 183.

[171] S. Aoki *et al.*, "Balloon-borne gamma-ray telescope with nuclear emulsion : overview and status," `arXiv:1202.2529 [astro-ph.IM]`.

[172] T. Aramaki, P. Hansson Adrian, G. Karagiorgi, and H. Odaka, "Dual MeV Gamma-Ray and Dark Matter Observatory - GRAMS Project," `arXiv:1901.03430 [astro-ph.HE]`.

[173] **PFS Team** Collaboration, R. Ellis *et al.*, "Extragalactic science, cosmology, and Galactic archaeology with the Subaru Prime Focus Spectrograph," *Publ. Astron. Soc. Jap.* **66** no. 1, (2014) R1, `arXiv:1206.0737 [astro-ph.CO]`.

[174] H. Ruegg and M. Ruiz-Altaba, "The Stueckelberg field," *Int. J. Mod. Phys. A* **19** (2004) 3265–3348, `arXiv:hep-th/0304245`.

[175] K. Kamada and A. J. Long, "Evolution of the Baryon Asymmetry through the Electroweak Crossover in the Presence of a Helical Magnetic Field," *Phys. Rev. D* **94** no. 12, (2016) 123509, `arXiv:1610.03074 [hep-ph]`.

[176] C. Vafa and E. Witten, "Restrictions on Symmetry Breaking in Vector-Like Gauge Theories," *Nucl. Phys. B* **234** (1984) 173–188.

[177] O. Antipin, M. Redi, A. Strumia, and E. Vigiani, "Accidental Composite Dark Matter," *JHEP* **07** (2015) 039, `arXiv:1503.08749 [hep-ph]`.

[178] S. Bottaro, M. Costa, and O. Popov, "Asymmetric accidental composite dark matter," `arXiv:2104.14244 [hep-ph]`.

[179] A. Manohar and H. Georgi, "Chiral Quarks and the Nonrelativistic Quark Model," *Nucl. Phys. B* **234** (1984) 189–212.

[180] T. P. Cheng and L. F. Li, *GAUGE THEORY OF ELEMENTARY PARTICLE PHYSICS*. Oxford University Press, U.S.A., 1984.

[181] T. Das, G. S. Guralnik, V. S. Mathur, F. E. Low, and J. E. Young, "Electromagnetic mass difference of pions," *Phys. Rev. Lett.* **18** (1967) 759–761.

[182] **CMB-S4** Collaboration, K. N. Abazajian *et al.*, "CMB-S4 Science Book, First Edition," `arXiv:1610.02743 [astro-ph.CO]`.

[183] M. Ibe, S. Matsumoto, and T. T. Yanagida, "The GeV-scale dark matter with B–L asymmetry," *Phys. Lett.* **B708** (2012) 112–118, `arXiv:1110.5452 [hep-ph]`.

[184] G. D. Moore, "Do we understand the sphaleron rate?," in *4th International Conference on Strong and Electroweak Matter.* 6, 2000. `arXiv:hep-ph/0009161`.

[185] **Super-Kamiokande** Collaboration, S. Desai *et al.*, "Search for dark matter WIMPs using upward through-going muons in Super-Kamiokande," *Phys. Rev. D* **70** (2004) 083523, `arXiv:hep-ex/0404025`. [Erratum: Phys.Rev.D 70, 109901 (2004)].

[186] **XENON** Collaboration, E. Aprile *et al.*, "Projected WIMP sensitivity of the XENONnT dark matter experiment," *JCAP* **11** (2020) 031, `arXiv:2007.08796 [physics.ins-det]`.

[187] D. P. Finkbeiner, S. Galli, T. Lin, and T. R. Slatyer, "Searching for dark matter in the cmb: A compact parametrization of energy injection from new physics," *Physical Review D* **85** no. 4, (Feb, 2012) . `http://dx.doi.org/10.1103/PhysRevD.85.043522`.

[188] T. R. Slatyer, "Indirect dark matter signatures in the cosmic dark ages. I. Generalizing the bound on s-wave dark matter annihilation from Planck results," *Phys. Rev.* **D93** no. 2, (2016) 023527, `arXiv:1506.03811 [hep-ph]`.

[189] E. Laermann and O. Philipsen, "The Status of lattice QCD at finite temperature," *Ann. Rev. Nucl. Part. Sci.* **53** (2003) 163–198, `arXiv:hep-ph/0303042`.

[190] P. de Forcrand and O. Philipsen, "The Chiral critical line of N(f) = 2+1 QCD at zero and non-zero baryon density," *JHEP* **01** (2007) 077, `arXiv:hep-lat/0607017`.

[191] P. Schwaller, "Gravitational Waves from a Dark Phase Transition," *Phys. Rev. Lett.* **115** no. 18, (2015) 181101, `arXiv:1504.07263 [hep-ph]`.

[192] Y. Nakai, M. Suzuki, F. Takahashi, and M. Yamada, "Gravitational Waves and Dark Radiation from Dark Phase Transition: Connecting NANOGrav Pulsar Timing Data and Hubble Tension," *Phys. Lett. B* **816** (2021) 136238, `arXiv:2009.09754 [astro-ph.CO]`.

[193] W.-C. Huang, M. Reichert, F. Sannino, and Z.-W. Wang, "Testing the Dark Confined Landscape: From Lattice to Gravitational Waves," `arXiv:2012.11614 [hep-ph]`.

[194] M. Ibe, A. Kamada, S. Kobayashi, T. Kuwahara, and W. Nakano, "Baryon-Dark Matter Coincidence in Mirrored Unification," *Phys. Rev.* **D100** no. 7, (2019) 075022, `arXiv:1907.03404 [hep-ph]`.

[195] A. Walker-Loud, "Nuclear Physics Review," *PoS* **LATTICE2013** (2014) 013, `arXiv:1401.8259 [hep-lat]`.

[196] V. Poulin, J. Lesgourgues, and P. D. Serpico, "Cosmological constraints on exotic injection of electromagnetic energy," *JCAP* **1703** no. 03, (2017) 043, `arXiv:1610.10051 [astro-ph.CO]`.

[197] C. Kouvaris, I. M. Shoemaker, and K. Tuominen, "Self-Interacting Dark Matter through the Higgs Portal," *Phys. Rev.* **D91** no. 4, (2015) 043519, `arXiv:1411.3730 [hep-ph]`.

[198] P. F. Bedaque, M. I. Buchoff, and R. K. Mishra, "Sommerfeld enhancement from Goldstone pseudo-scalar exchange," *JHEP* **11** (2009) 046, `arXiv:0907.0235 [hep-ph]`.

[199] Z.-P. Liu, Y.-L. Wu, and Y.-F. Zhou, "Sommerfeld enhancements with vector, scalar and pseudoscalar force-carriers," *Phys. Rev.* **D88** (2013) 096008, `arXiv:1305.5438 [hep-ph]`.

[200] B. Bellazzini, M. Cliche, and P. Tanedo, "Effective theory of self-interacting dark matter," *Phys. Rev.* **D88** no. 8, (2013) 083506, `arXiv:1307.1129 [hep-ph]`.

[201] A. Sommerfeld, " Über die beugung und bremsung der elektronen (in German)," *Ann. d. Phy* **11** (1931) 257.

[202] J. Hisano, S. Matsumoto, and M. M. Nojiri, "Unitarity and higher order corrections in neutralino dark matter annihilation into two photons," *Phys. Rev.* **D67** (2003) 075014, arXiv:hep-ph/0212022 [hep-ph].

[203] J. Hisano, S. Matsumoto, and M. M. Nojiri, "Explosive dark matter annihilation," *Phys. Rev. Lett.* **92** (2004) 031303, arXiv:hep-ph/0307216 [hep-ph].

[204] J. Hisano, S. Matsumoto, M. M. Nojiri, and O. Saito, "Non-perturbative effect on dark matter annihilation and gamma ray signature from galactic center," *Phys. Rev.* **D71** (2005) 063528, arXiv:hep-ph/0412403 [hep-ph].

[205] K. Blum, R. Sato, and T. R. Slatyer, "Self-consistent Calculation of the Sommerfeld Enhancement," *JCAP* **1606** no. 06, (2016) 021, arXiv:1603.01383 [hep-ph].

[206] B. Bellazzini, R. Franceschini, F. Sala, and J. Serra, "Goldstones in Diphotons," *JHEP* **04** (2016) 072, arXiv:1512.05330 [hep-ph].

[207] S. Weinberg, *Cosmology*. Oxford, UK: Oxford Univ. Pr., 2008.